COMPOSITE AT ELEVATED TEMPERATURE

THESIS

Robert N. Pittman
1st Lieutenant, USAF
AFIT/GAE/ENY/95D-20

DEPARTMENT OF THE AIR FORCE
AIR UNIVERSITY
AIR FORCE INSTITUTE OF TECHNOLOGY

Wright-Patterson Air Force Base, Ohio

DISCLAIMER NOTICE

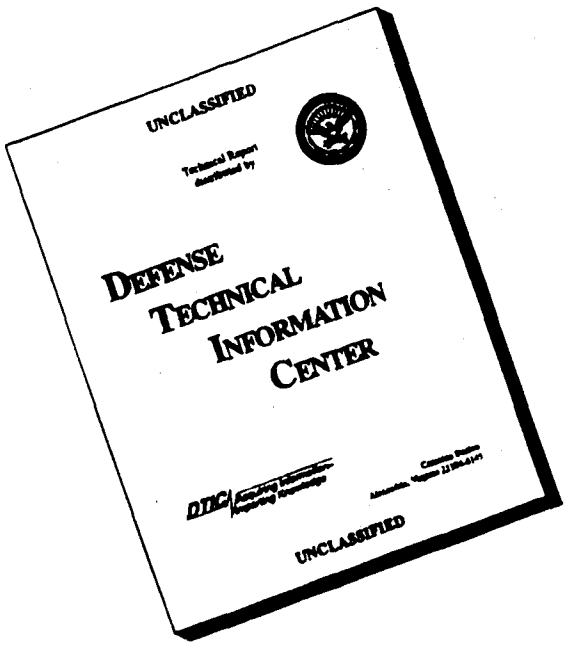

THIS DOCUMENT IS BEST QUALITY AVAILABLE. THE COPY FURNISHED TO DTIC CONTAINED A SIGNIFICANT NUMBER OF PAGES WHICH DO NOT REPRODUCE LEGIBLY.

AFIT/GAE/ENY/95D-20

FREQUENCY EFFECTS ON FATIGUE BEHAVIOR OF A UNIDIRECTIONAL METAL MATRIX COMPOSITE AT ELEVATED TEMPERATURE

THESIS

Robert N. Pittman
1st Lieutenant, USAF
AFIT/GAE/ENY/95D-20

AFIT/GAE/ENY/95D-20

FREQUENCY EFFECTS ON FATIGUE BEHAVIOR OF A UNIDIRECTIONAL METAL MATRIX COMPOSITE AT ELEVATED TEMPERATURE

THESIS

Presented to the Faculty of the Graduate School of

Engineering of the Air Force Institute of Technology

Air University

In Partial Fulfillment of the

Requirements for the Degree of

Master of Science in Aeronautical Engineering

Robert N. Pittman, B.S.

1st Lieutenant, USAF

December 1995

Acknowledgments

The accomplishment of this thesis would not have been possible were it not for the generous support of several individuals. Dr. Mall, thank you for your patience and direction as my advisor. I think it was remarkable that you were able to juggle the rough drafts of five students! Capt. Brian Sanders, thanks for all your advice and looking at drafts long distance. Thanks also to my sponsor at the Wright Laboratory Materials Directorate, Dr. Ted Nicholas, and to Dr. Andy Rosenberger: I've enjoyed the spontaneous MMC lectures you both have given me! To my committee members, Dr. Torvik and Maj. Robertson, I appreciate the time you have put in reading my report. Jay, Mark, Sean, Andy and Dan—thanks for putting up with meltdowns, leaky hoses and lots of questions (Andy, siphoning the water from the recirculation tank the old fashioned way was definitely beyond the call of duty). Finally, and most importantly, thank you Shauna for being my chief editor, cheerleader, and best friend.

Rob Pittman

Table of Contents

List of Figures

Page

List of Tables

Page

Abstract

MMCs have great potential in a variety of aerospace applications, but they must be better understood before they can be employed. Despite the many studies that have contributed to characterizing the fatigue response of titanium alloy MMCs, few have researched the effects of cyclic load frequency. This research examined the fatigue response and life of unidirectional SCS-6/Ti-6-4 under tension-tension, load-controlled conditions at elevated temperatures and different frequencies. Specimens were fatigued at frequencies of 0.01, 0.1, 1 and 10 Hz, and at three stress levels with a stress ratio of 0.05. Isothermal tests at 427°C were compared with tests at room temperature, 370°C and 538°C. Fatigue lives were compared using S-N diagrams and plots of test frequency and temperature versus cycles to failure. Macromechanical fatigue responses at different frequencies and temperatures were compared using stress-strain plots, modulus histories and strain histories, while microscopy and fractography revealed the micromechanical behavior and damage mechanisms.

Plots of cycles to failure versus maximum stress and test frequency showed that fatigue life was more cycle-dependent at higher frequencies and more time-dependent at lower frequencies. Comparisons of tests at 427°C with their counterparts at 370°C and 538°C showed that these frequency effects were magnified as temperature increased: lower frequency tests at 538°C exhibited greater time-dependence than tests at 427°C, which was due to poorer creep and environmental resistance at the higher temperature.

Macroscopic analysis of tests conducted at lower stress levels and higher frequencies revealed decreasing laminate stiffnesses with cycling, typical of matrix-dominated responses, while increasing strain and constant modulus histories during fatigue indicated that tests conducted at higher stress levels and lower frequencies were fiber-dominated. Microscopic observations revealed that matrix cracks initiated at flaws and fiber breaks on the specimen edges, and the extent of matrix cracking increased at lower stress levels and higher frequencies.

FREQUENCY EFFECTS ON FATIGUE BEHAVIOR OF A UNIDIRECTIONAL METAL MATRIX COMPOSITE AT ELEVATED TEMPERATURE

1 Introduction

Initiatives such as the research and development of a hypersonic flight vehicle have articulated the need for materials that can withstand extreme environments. The few monolithic metals that can endure high temperature environments do not have the specific strengths and stiffnesses necessary for such a vehicle. Polymeric composites exhibit better strength to weight and stiffness to weight ratios, but would not perform well at elevated temperatures. This has driven the National Aeronautics and Space Administration (NASA) and Department of Defense (DoD) to emphasize materials research in the area of Metal Matrix Composites (MMCs) [14].

By reinforcing high temperature, light weight metal alloys with high strength and high stiffness continuous ceramic fibers, MMCs provide the fatigue endurance and strength to survive high temperature and high stress environments. Other applications of these composites include energy efficient aircraft engine concepts such as the DoD/NASA Integrated High Performance Turbine Engine Technology (IHPTET) Initiative and the High Temperature Engine Technology Program (HITEMP). Since structural components must perform under a wide range of mechanical and thermal loading conditions, much research has been performed in the last decade to characterize the performance of MMCs.

Titanium MMCs such as SCS-6/Ti-15-3 and SCS-6/Ti-6-4 have been studied extensively because the titanium alloy matrix may be used at high temperatures and has the highest specific strength of any of the common structural materials. The thermal expansion coefficients of the titanium matrix and boron fibers are more compatible than those of the titanium matrix and silicon carbide fibers. However, since boron reacts excessively with titanium, silicon carbide fibers such as SCS-6 have become the best candidates to reinforce the titanium matrix [27]. The difference in thermal expansion coefficients between silicon carbide fibers and the titanium alloy matrix and unique properties of the fiber/matrix interface zone make the prediction of fatigue behavior complex in titanium MMCs.

Research in recent years has focused on damage and fracture mechanisms of titanium MMCs under various loading conditions. Tension-tension fatigue experiments under the load controlled mode at room temperature have provided the baseline understanding of their fatigue behavior and damage mechanisms which consist of fiber-dominated, progressive fatigue damage, and matrix dominated modes [2,7,13]. Elevated temperature effects have also been studied in isothermal tests and in thermomechanical fatigue tests to better simulate the environment in which these materials would be used. These effects included relief of residual stresses, but accelerated damage progression and reduced fatigue life. Studying the behavior of laminates with different lay-ups, such as angle-ply [±45] and cross-ply [0/90], helped to characterize effects of fiber orientation [3,6,19], and strain-controlled testing has also been accomplished since most engineering applications subject materials to this condition [6,7,26]. Recent tension-compression

research has also added to the knowledge base of MMC fatigue characterization [3,15], showing that the influence of the matrix and fiber/matrix interfaces on fatigue life is also important.

One area that has not received much attention is the effect that cyclic loading frequency has on damage mechanisms and fatigue life of MMCs. If the composite's life at a particular load level were totally dependent on the number of loading cycles to which it is subjected, one would not expect to see any variation with respect to frequency. On the other hand, if fatigue life were strictly time-dependent we would expect the number of cycles to failure to increase in proportion to the reduction in frequency (i.e., decreasing frequency by a factor of ten would result in ten times as many cycles to failure). Since titanium alloys exhibit some time-dependent fatigue behavior, it is not surprising that a previous study by Mall and Portner has shown titanium-based MMCs to have a frequency dependence [19]. A study by Jeng et al. evaluating the effects of high temperature oxidation on damage mechanisms has also helped to establish that fatigue life is neither a strictly cycle-dependent nor time-dependent phenomenon [9]. The present study will probe this area further to evaluate fully the effects of frequency on damage mechanisms and fatigue life of MMCs at elevated temperatures.

This research investigates the behavior of a unidirectional laminate of SCS-6/Ti-6-4 composite system consisting of Ti-6Al-4V (%wt) titanium alloy reinforced with continuous silicon-carbide fibers (SCS-6). Load-controlled, isothermal fatigue tests were conducted at several frequencies and maximum stress levels to determine their effects on this composite's various damage mechanisms and fatigue life. Although most specimens

were tested at 427°C, a few tests at other temperatures were also conducted to investigate how frequency effects varied with test temperature. Fracture surfaces and specimen sections were then examined microscopically to study the damage and fracture mechanisms. Coupling this information with macroscopically measured stress-strain data during cycling helped to determine which deformation mechanisms led to specimen failure. Finally, plots of maximum stress versus fatigue life (S-N curves), and fatigue life versus test frequency (N-f curves) were established to illustrate how changes in cyclic frequency and test temperature affected fatigue life.

The following chapters will fully describe this study. Following a discussion of significant contributions in MMC research from previous studies, a description of the experimental equipment and procedures will be given. Microscopic and macroscopic observations, analyses and results will precede the research summary, and recommendations for further exploration.

2 Previous Works

2.1 Introduction

Although not exhaustive, this chapter provides a review of the research that influenced the direction of the current work and aided in the analysis of test results of the present study. Monotonic studies are included to give a general understanding of damage mechanisms, interface properties and the effects of high temperature processing on MMCs. Results from room temperature fatigue research provide baseline information for the expected mechanical behavior of the MMC in this study. Thermal fatigue tests show the isolated effects of temperature changes, while thermomechanical fatigue tests more closely simulate the environment that MMCs will be expected to endure. Finally, previous works that sought to determine effects of frequency variations on damage mechanisms are presented to provide expected composite behavior in the current study.

2.2 Monotonic Testing

Tensile fracture mechanisms in titanium alloy MMCs were investigated by Jeng et al. [11]. They found that fiber strength, matrix toughness and interfacial shear strength all influence fracture behavior as well as the initiation and growth of damage. They also reported that the strength of the interfacial reaction zone decreases as its thickness increases. Damage mechanisms in the interfacial region were found to be a function of both matrix toughness and the ratio of fiber strength to interfacial shear strength.

Majumdar and Newaz [17] used mechanical measurements and microstructural analysis to study the deformation mechanisms of SCS-6/Ti-15-3. Plasticity dominated matrix deformation in the 0° MMC, but reaction-zone cracks aided in nucleating plasticity. Inelastic deformation of the 90° composite, on the other hand, was caused by damage in the medium stress region (Stage II) and plasticity in the high stress region (Stage I). Damage mechanisms included fiber and matrix cracking, fiber-matrix reaction zone cracking and interfacial debonding. Evidence of plasticity included a change in dislocation densities and slip band formation.

Sun et al. [28] performed off-axis tension tests of SCS-6/Ti-6-4 and developed both a one-parameter plasticity model and a micromechanical model. The macromechanical plasticity model characterized the composite as an orthotropic elastic-plastic solid and could predict matrix yielding as well as initial separation of the fiber and matrix. The micromechanical model predicted the normal interfacial bonding strength and the nonlinear stress-strain curves under on- and off-axis loading.

Jeng et al. studied interfacial [10] and toughening behavior [12] in SCS-6 fiber reinforced Ti-6-4, Ti-15-3 and Ti-25-10. They used indentation and fragmentation tests to measure interfacial shear strength and frictional stress and found that the properties were greatly influenced by fiber surface chemistry, matrix alloy composition and residual stresses at the interface. Also, high temperature fabrication and extended thermal exposure was found to decrease SCS-6 fiber strength. In order to study toughening, three-point bending was applied to notched specimens and damage mechanisms were evaluated. The composite formed a crack tip damage zone where matrix cracking, plastic

deformation, interfacial debonding and multiple fiber failure acted as damage mechanisms. Fiber strength, matrix stiffness and shear strength influenced the crack initiation energy, while matrix plastic deformation and fiber pull-out affected crack propagation. They concluded that composite toughness could be enhanced by optimizing processing conditions.

Transverse tensile behavior and the effects of fiber-matrix interface strength were investigated by Nimmer, et al. [22]. Residual stresses due to the fiber-matrix mismatch in the coefficients of thermal expansion were measured experimentally and estimated analytically. Predictions of transverse stress-strain behavior were compared with experimental results at room temperature, 315°C and 427°C. The study found that residual stresses due to high-temperature fabrication could be as high as the matrix yield stress in Ti-6-4.

Lerch et al. [16] compared oxidation and aging behavior of SCS-6/Ti-15-3 and unreinforced titanium alloy. Hardness measurements, room-temperature tensile tests and optical microscopy were used to evaluate and compare age-hardening between the two materials. They reported that unprotected Ti-15-3 forms a thick surface oxide at temperatures greater than 550°C. Maximum hardness for both materials occurred at an aging temperature of 450°C, and maximum room-temperature elastic modulus and ultimate tensile strength of the titanium alloy were attained after the material was aged for 24 hr at temperatures between 350 and 550°C.

2.3 Mechanical Fatigue Research

To study the effects of a cyclic mechanical load on a material, fatigue testing is accomplished at a constant temperature. Since no environmental effects are expected at room temperature, this often serves as a baseline for further high temperature isothermal fatigue (IF) or thermomechanical fatigue (TMF) testing.

Room temperature load-controlled fatigue testing of three titanium alloy MMCs was accomplished by Jeng et al. [13]. The behavior of SCS-6 reinforced Ti-15-3, Ti-6-4 and Ti-25-10 composites was evaluated at 10 Hz, R = 0.1 in a maximum applied stress range 470-1400 MPa. They found that heat treatment made little difference in the fatigue life of SCS-6/Ti-15-3 at maximum stress levels above 860 MPa, but heat treated specimens withstood a higher maximum stress at 10^6 cycles (690 MPa compared with 470 MPa). Also, well-polished specimens had longer fatigue lives at all stress levels.

Damage mechanisms for all three composites were classified into three regions. In the fiber breakage dominated region (high stress levels and non-progressive failure), existing flaws on fiber surfaces initiated instantaneous crack growth which led to random fiber breaks early in the fatigue life. Stress concentrations in the region surrounding the broken fibers caused damage in adjacent fibers and eventually fracture of the specimen due to stress overload. Although ductile matrix failure often includes matrix necking and fiber pull-out, post-mortem microscopic observation of specimens stressed greater than 1255 MPa showed flat fracture surfaces without significant fiber pull-out. Fatigue damage was randomly distributed and located at the interfacial region, but little matrix cracking was evident.

At the medium stress levels (630 to 1100 MPa), progressive fatigue damage included interfacial cracking, matrix cracking and fiber breakage. Stresses in this range were not high enough to cause as many fiber breaks, but were higher than the cracking stress of the interfacial reaction layer. Examined SCS-6/Ti-15-3 specimens had irregular fracture surfaces with flat fatigue cracking regions adjacent to overload regions, and specimens exhibited more fiber pull-out as the applied stress decreased. Metallographic observation showed severe matrix cracks which initiated from broken fibers and the interfacial reaction zone near the specimens' edges, or from interfacial zones within the specimens. Fiber bridging revealed that the matrix cracked prior to fiber breakage. The SCS-6/Ti-6-4 damage was similar, but fatigue cracking was not observed around broken fibers in the overload region and cracks were found to initiate only at the specimen edges. Well-polished Ti-15-3 specimens fatigued at 945 MPa had less crack initiation from the edges, which implied that the polishing procedure suppressed cracks due to surface defects.

At the stress levels below 630 MPa, the response of Ti-15-3 fell into the matrix-dominated region, where stresses were not high enough to initiate cracks in the fibers or interface regions. Multiple cracks initiated at the specimen edges, and steadily propagated through the matrix, perpendicular to the loading direction. Fibers either bridged the progressively growing cracks or arrested them if the crack tip stress intensities were not great enough. At these stress levels, fibers and interfacial reaction zones within the specimens failed only after the matrix had cracked.

2.4 Thermal and Thermomechanical Fatigue Research

Thermal fatigue research reveals the effects of temperature changes while either mechanical stress or strain remains constant. Isolating thermal loading in this way provides an understanding of its particular effects on a material. Then, when a complex thermal and mechanical condition is applied to the material, the effects of the thermal loading may be distinguished from the effects of the mechanical loading.

Thermal cycling of the $[0]_6$, SCS-6/Ti-15-3 composite material was investigated by Mall and Ermer [20]. Temperatures ranged from 149°C to 427°C and 149°C to 649°C. The interfacial reaction zone began to degrade after 500 cycles. Material properties such as Young's modulus, Poisson's ratio, the coefficient of thermal expansion and residual tensile strength did not change up to 15000 cycles for either temperature range. Also, stress-strain curves from monotonic testing were more linear for the thermally cycled specimens than for uncycled specimens which was likely due to the relaxation of residual stresses that were incurred during specimen processing. During thermal cycling, cracks that initiate and grow in the reaction zone relieve some of the laminate's residual stress.

Gabb et al. [8] tested SCS-6/Ti-15-3 under isothermal and bithermal cycling. Isothermal tests were conducted at 300°C and 550°C, and in their bithermal tests, each loading cycle was preceded by a thermal cycle between 300°C and 550°C. Not true thermomechanical conditions, bithermal loading cycles are easier to analyze, and fatigue response may be directly compared to isothermal tests. As a result of their tests it was concluded that the fiber-matrix interface of the composite was weaker than the fiber or matrix. Fatigue resistance was reduced by surface and internal cracking in isothermal

tests, but bithermal tests showed even less fatigue resistance. Under load-control conditions, the mean strain remained relatively constant for the 300°C isothermal and bithermal out-of-phase tests but steadily increased for the 500°C isothermal and in-phase bithermal tests.

In order to isolate thermal cycling effects, longitudinal and transverse tensile strength test results were compared with equivalent mechanical tests run after 10000 thermal cycles (300-550°C) at zero load. Strengths were virtually the same. Isothermal fatigue tests run with and without prior thermal cycling had a negligible difference in cycles to failure, so it was concluded that thermal cycling at zero load did not degrade mechanical response.

Under thermomechanical fatigue, both temperature and stress (or strain) are cycled. This complex condition best approximates the loading environment in many aerospace and general engineering applications. The thermal and mechanical loads are typically cycled at the same frequency, but may be cycled out-of-phase or even at different frequencies.

Castelli et al. [5] researched thermomechanical fatigue (TMF) testing of SCS-6/Ti-15-3 MMCs. They extended newly developed TMF techniques of testing monolithic alloys to the testing of this composite system. Fatigue lives were found to be shorter under TMF than under isothermal or bithermal fatigue conditions, and damage mechanisms were compared for isothermal and TMF tests (in-phase and out-of-phase). The load-controlled isothermal tests were run at 0.17 Hz and 427°C at maximum stress levels of 896, 965 and 1034 MPa (R=0.05). TMF tests had three minute temperature

cycles from 93°C to 538°C and were mechanically fatigued to maximum stresses of 827 to 1241 MPa.

The isothermal tests resulted in extensive matrix cracking and fiber damage throughout the cross-section. Higher stressed specimens displayed more fiber pull-out and ductile matrix failure. Out-of-phase TMF produced very little fiber cracking, but extensive matrix cracking. Fracture surfaces showed an outer "ring" of oxidized cracking with a ductile region in the center. In-phase TMF resulted in extensive fiber pull-out and cracking and ductile matrix failure instead of fatigue cracking. This was evident even at the lowest stress levels.

2.5 Isothermal Fatigue Research

Bhatt and Grimes investigated composite fatigue properties at a temperature of 650°C [1]. In a previous study at room temperature [2], they had reported that fiber reinforcement of the Ti-6-4 alloy did not substantially improve fatigue resistance. Crack growth initiated by fractured fibers at the composite surface, and matrix residual stresses from high temperature processing negated any fatigue life benefit from the silicon carbide fiber reinforcement.

At 650°C, the authors found significant improvement in the composite's life over the alloy's life. They discovered that the elevated temperature reduced the modulus of the monolithic alloy and matrix of the composite, so the unreinforced alloy strained more with the applied stress. In the composite, however, the fibers experienced no reduction in strength and since they controlled the strain of the matrix, the composite specimens lasted longer than the monolithic specimens. Another reason the composite performed better

than the alloy at 650°C is that the residual stresses in the composite were relieved. As with room temperature testing, all cracks initiated on the specimen surfaces at broken and fragmented fibers, while interior fibers only failed near advancing cracks.

Especially pertinent to the present study, Mall and Portner [19] investigated the frequency effects of isothermal fatigue behavior for the $[0/90]_{2s}$ SCS-6/Ti-15-3 system. Their test matrix included frequencies of 2.0 and 0.02 Hz and maximum stress levels ranged from 375 to 625 MPa (R=0.1) at 427°C. At stress levels above 438 MPa, the specimens tested at 2.0 Hz endured 15 to 25 times as many cycles as the 0.02 Hz specimens. This indicated a mixed time- and cycle-dependent phenomenon. Comparisons with 10 Hz data at room temperature and 650°C revealed that fatigue life decreased with both increasing temperature and decreasing frequency. However, all the S-N curves converged at the 420 MPa stress level where temperature and frequency did not seem to have an effect.

Fatigue damage at the low stress levels initiated at the 90° fiber reaction zones and progressed toward the 0° fibers. Fatigue failure in the matrix was followed by failure of 90° and 0° fibers. At high stresses, 0° fibers fractured first, then matrix cracking initiated at the reaction zone of fractured fibers. Specimens stressed at intermediate levels exhibited fiber damage as well as matrix cracking initiated at the 90° fibers. Low frequency tests at this level resulted in degradation of the fiber-matrix interface and therefore more fractured 0° fibers than the high frequency tests. Presumably this was due to longer exposure at the elevated temperature. The authors also observed that the higher

frequency specimens became more brittle due to strain hardening, while the lower frequency specimens showed ductile failure and less matrix cracking.

Nicholas et al. [21] studied frequency and stress ratio effects on fatigue of the unidirectional SCS-6/Ti-24Al-llNb system tested isothermally at 650°C. Time-dependent and cycle-dependent effects on fatigue life were found by testing at frequencies of 0.003, 0.08, 3 and 200 Hz and at stress ratios of 0.1, 0.5 and 0.8. In addition, a linear summation model was developed and employed to predict fatigue life based on frequency, $\Delta\sigma$ and R. An electrodynamic shaker apparatus was used to produce the high sinusoidal load frequencies. Their results showed that the fatigue lives were neither purely time-dependent nor purely cycle-dependent, therefore, the linear life fraction modeling required an interaction term where both creep and fatigue were active. Their model has the form:

$$\frac{N}{N_c} + \frac{N}{N_t} + \frac{N}{N_m} = 1 \qquad (2.1)$$

where N_c, N_t and N_m are the number of cycles to failure due to cyclic, time-dependent and mixed-mode effects, respectively. This model predicted the general trends for fatigue life across their test matrix.

2.6 Summary

This chapter has provided an overview of MMC research, including both monotonic and fatigue testing. Although fatigue testing is of greater interest, monotonic loading of a material to failure provides tensile parameters such as the Young's modulus of each of the composite's constituents, the coefficients of thermal expansion and tensile strength. Previous studies showed that fracture behavior was influenced by fiber strength,

matrix toughness and interfacial shear strength. Plasticity was found to dominate matrix deformation (aided by reaction-zone cracking) and high temperature composite fabrication decreased SCS-6 fiber strength and weakened the interface zone strength.

Fracture mechanisms in fatigue testing included non-progressive fiber breakage at the higher stress levels, progressive matrix and interface cracking at intermediate stress levels and matrix-cracking dominated failure at the lower stress levels. Figure 2.1 illustrates these damage mechanisms.

Effects of temperature in thermal, isothermal, bithermal and thermomechanical fatigue research were also reviewed [1,5,8,20]. Thermal fatigue at zero load did not degrade the mechanical response of the composite, and at constant tensile loads, cracks that initiated and grew in the reaction zone relieved laminate residual stresses. Damage mechanisms of isothermal testing were similar but accelerated compared to the mechanisms of room temperature fatigue. Thermomechnical research resulted in even greater damage but was more fiber-dominated for in-phase fatigue, and matrix-dominated for out-of-phase fatigue.

Most applicable to the present study were two studies that focused on the effects of cyclic frequency on fatigue response and damage mechanisms of titanium alloy MMCs [19,21]. Comparisons of fatigue life at two frequencies showed that the composite behaved in neither a strictly cycle- nor time-dependent manner. More interfacial damage was observed at the lower frequencies, but the matrix tended to fracture in a more ductile manner. A linear summation model of fatigue life was also developed which accounted for failure due to cyclic, time-dependent, and mixed-mode tendencies.

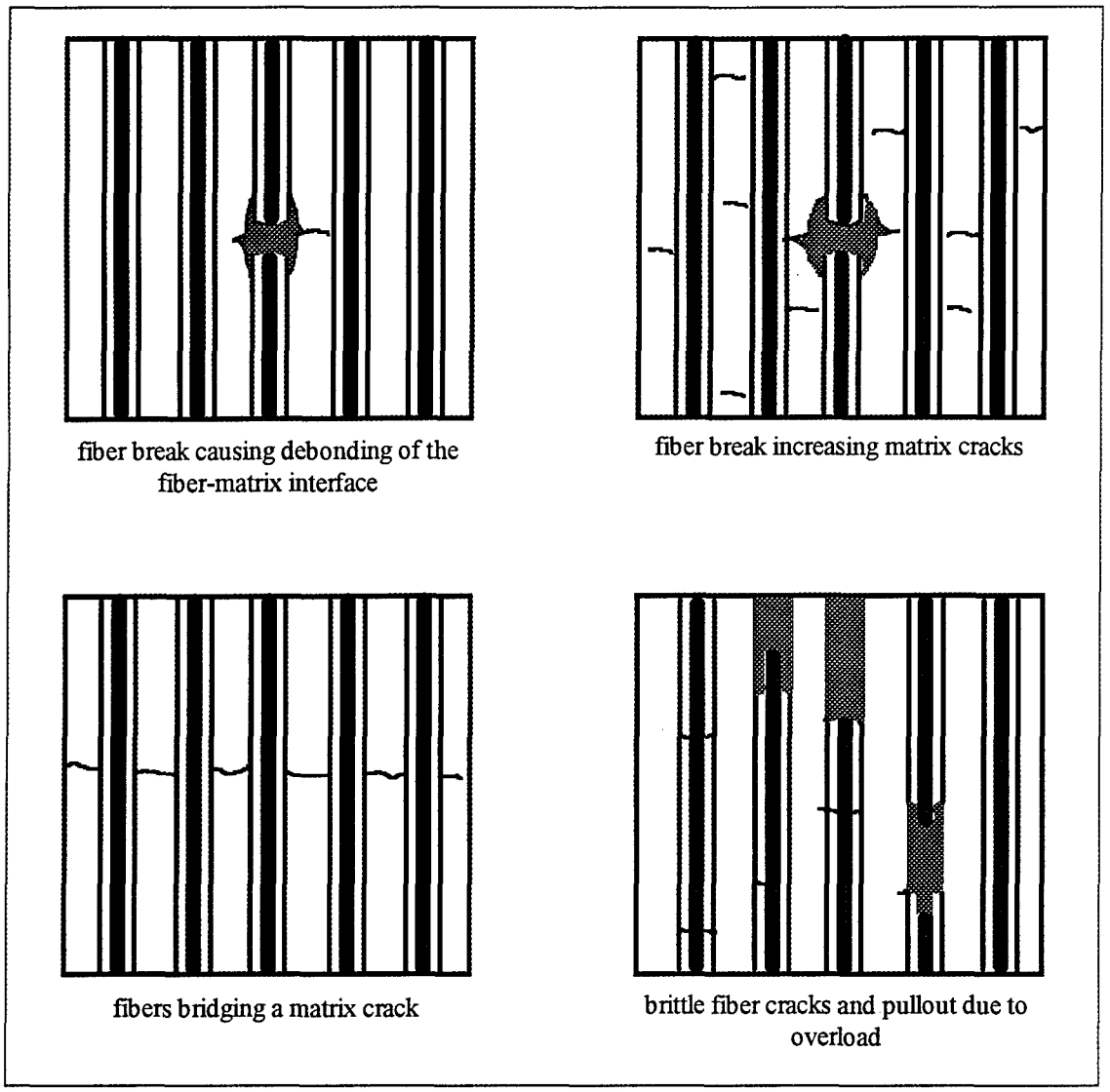

Figure 2.1 Fatigue Damage Mechanisms

3 Test Procedures

This chapter describes the material under investigation, equipment and procedures used in the experiments, and the post-test observation tools and processes. First, the physical and material properties of the composite specimens, as well as the methods of fabrication and preparation are discussed. Next, the experimental setup and testing procedures are presented. Lastly, the tools and techniques used to perform microscopic specimen preparation and analysis are described.

3.1 Material Description and Processing

Several MMCs have been studied for use in high temperature aerospace applications. Comonly available titanium based MMCs are SCS-6/Ti-15-3, SCS-6/Ti-6-4, SCS-6/Ti-25-10 and SCS-6/TIMETAL®21S. SCS-6/Ti-15-3 has been studied extensively under load- and strain-controlled modes, isothermal and thermomechanical conditions, and in tension-tension and tension-compression fatigue [5,6,8,13,15,16,17,23,26]. Interest in SCS-6/Ti-6-4 has been growing recently because of its greater strength and stiffness and near term application to gas turbine engine components. This system is much more expensive to process because the Ti-6-4 matrix requires annealing as it is rolled into foils, whereas Ti-15-3 may be coldworked with no annealing (Ti-15-3 is a metastable beta phase alloy, while Ti-6-4 is primarily an alpha phase alloy). The current work investigated frequency effects on fatigue behavior of SCS-6/Ti-6-4, but other titanium MMCs are expected to exhibit similar trends.

The composition of the Ti-6-4 alloy is: 90% titanium, 6% aluminum and 4% vanadium (by weight). The composite of this study consists of nine (9) plies of Ti-6-4 reinforced with eight (8) plies of silicon carbide fibers (SCS-6). Each fiber has a carbon core which acts as a substrate for surrounding layers of silicon carbide. Measurement of the average fiber volume fraction was approximately 0.35. Table 3.1 shows the room tempertature Young's modulus (E), coefficient of thermal expansion (α), and yield stress (σ_{ys}) of the composite's constituents [14]. Properties of the composite were calculated using rule of mixtures approximation [18]. For example, the composite's longitudinal modulus (E_C) can be written:

$$E_C = E_f v_f + E_m (1 - v_f) \tag{3.1}$$

where E_f and E_m are the moduli of elasticity of the fiber and matrix, respectively, and v_f is the fiber volume fraction. The volume fraction is given by:

$$v_f = \frac{w_f}{\rho_f}\left(\frac{1}{\frac{w_f}{\rho_f} + \left(\frac{1 - w_f}{\rho_m}\right)}\right) \tag{3.2}$$

where w_f is the fiber weight fraction, $(1 - w_f)$ represents the matrix weight fraction, and ρ_f and ρ_m are the fiber and matrix densities, respectively.

Table 3.1 SCS-6/Ti-6-4 Constituent Properties

Constituent	E (GPa)	α (10^{-6} /°C)	σ_{ys} (MPa)
SCS-6 fiber	400	4.9	1300
Ti-6-4 matrix	110	7.5	1089
Laminate	212	6.6	1163

A unique loading condition that MMCs experience arises from the large difference in coefficient of thermal expansion between the fiber and matrix. After cool down from high temperature processing, large residual shear stresses along the fiber/matrix interface can be a source of damage in as-received composite plates, and can accelerate interfacial cracking during fatigue testing.

3.2 Specimen Description and Preparation

Textron Specialty Materials Division, Textron Inc. supplied the MMC plates. Each plate was produced by their patented hot isostatic pressing (HIP) method, in which layers of fibers and sheets of alloy foil are alternated and then pressed at 35 MPa and 815°C. The final laminate was nominally 1.89 mm thick. Non-destructive inspection of the plates revealed no internal fiber damage, matrix cracks or ply delamination.

The composite plates were first cut into rectangular coupons with a low-speed diamond saw, and most specimens were further machined into "dogbone" shapes as shown

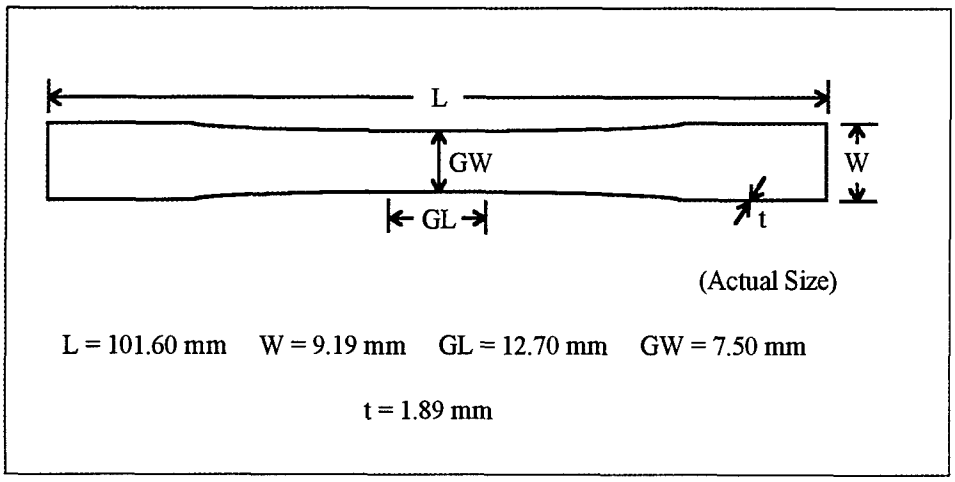

Figure 3.1 Specimen Geometry

in Figure 3.1. This design was implemented because of the servohydraulic test machine's load limitation. Its maximum load capability was 22 kN (5 kip), which required a gage section area of less than 18.3 mm^2 to achieve a 1200 MPa tensile stress (the highest stress in the test matrix). The cross-sectional area of the rectangular specimens was nominally 23.2 mm^2. Gabb et al. found that the mechanical response and fatigue life of SCS-6/Ti-15-3 was independent of specimen design, noting that rectangular and reduced section specimens have the same material properties [8]. The nominal dimensions of the rectangular specimens were 101.60 mm x 12.70 mm, and the dogbone width was 9.2 mm at the ends and 7.5 mm in the gage section. A large shoulder radius was required to minimize the shear stress in the shoulder region [3].

Next, specimens were heat treated to simulate a secondary processing cycle that this composite would be expected to undergo in an aerospace application. The specimens were wrapped in Tantalum foil and placed in a 0.0133 Pa vacuum environment. Chamber temperature was increased to 677°C at 10°C/min. and held constant for 60 min. Temperature was then ramped to 843°C at 10°C/min and held constant for 120 min. Next, temperature was decreased to 316°C at 3°C/min. where power was cut and the specimens cooled to room temperature at 1.6°C/min. Finally, specimen edges were ground and polished in order to remove burs and damage from cutting.

3.3 Experimental Equipment

Isothermal, load-controlled fatigue tests required a mechanical actuator, load and temperature controllers and a data acquisition system. This section describes each of these subsystems. Figure 3.2 is a photograph of the entire test system, including the test stand,

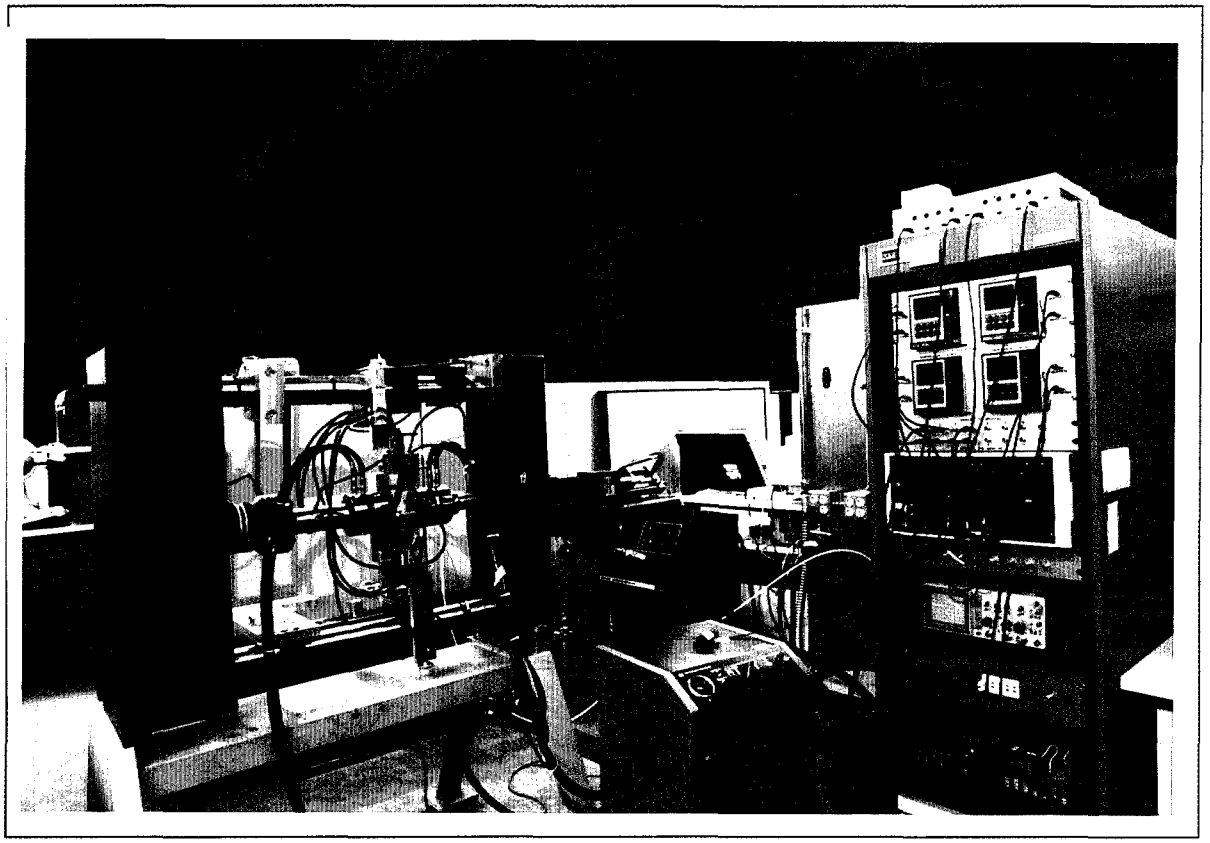

Figure 3.2 Test Setup

load and temperature controller unit, and personal computer. Figure 3.3 is a photograph of a dogbone specimen in the hydraulic grips, upper and lower parabolic lamps and an extensometer.

The specimen was aligned longitudinally in the hydraulic grips of a Material Test System (MTS) hydraulic actuator, so all stresses would act in the fiber direction. The grips held 19 mm (0.75 in) of the specimen at each end. The load actuator was rated for 24.5 kN, and 18 MPa grip pressure was applied. The loading cycle was generated and

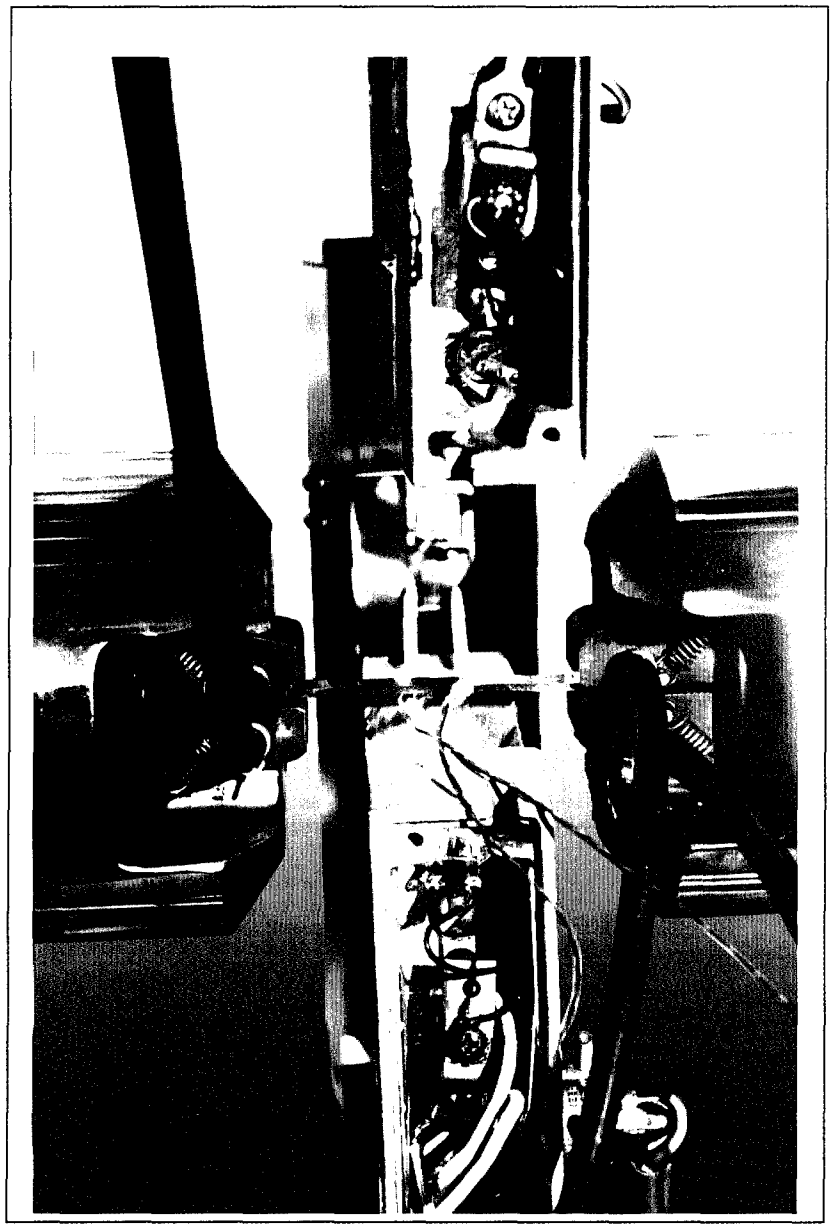

Figure 3.3 Specimen in Grips

controlled by an MTS Microprofiler and DC Controller. These components were commanded by the LABoratory Material Analysis and Testing Enviornment (MATE, developed by University of Dayton Research Institute) data acquisition software on a

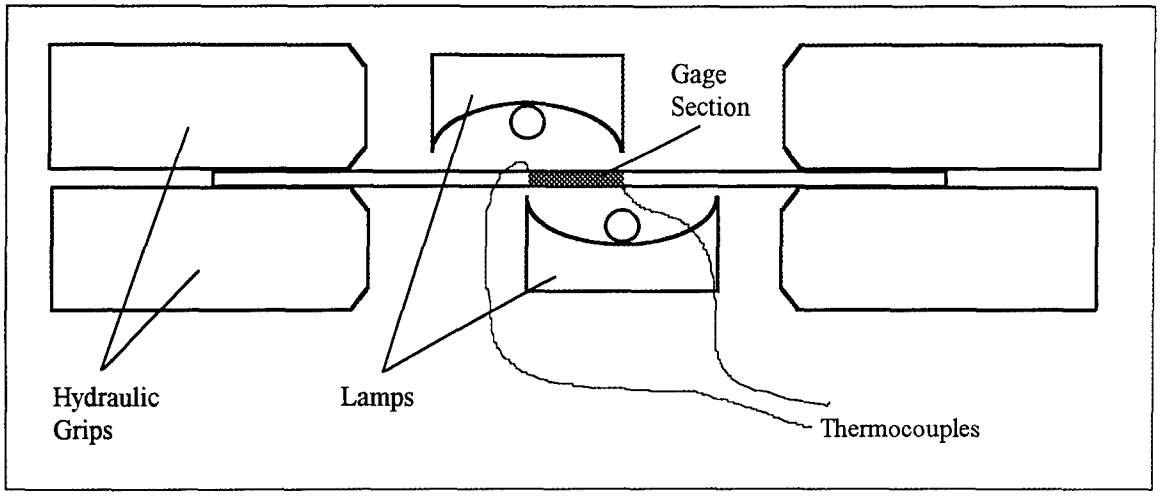

Figure 3.4 Heating Lamp Setup

Zenith 386DX, 16 MHz personal computer. A ±22.2 kN load cell was employed for the controller's ±10 volt range.

Test temperature was controlled with two 1000 watt, tungsten filament parabolic lamps--one positioned above, and one below the test specimen (Figure 3.4). The lamps were offset so that each was centered on an end of the gage section, which provided a uniform temperature throughout the section. Chromel-alumel thermocouples, used as temperature feedback transducers, were spot welded to the specimen surface directly below the lamps so that the temperature of each lamp could be independently controlled. The Micricon controller maintained a temperature in the gage section of 12.7 mm within 2°C of the target level. The hydraulic grips and the parabolic lamps were cooled with water circulating at a reservoir temperature of 17°C.

Data acquisition was accomplished with a combination of hardware and software. An air-cooled MTS extensometer with ceramic rods measured specimen displacement in

the 12.7 mm gage section. A Techmar Labmaster analog-to-digital converter and the MATE software completed the data acquisition equipment. Software input parameters included: specimen dimensions, gage length, fatigue waveform type, frequency, maximum stress, stress ratio and data acquisition interval. Data collection intervals were usually logarithmic (cycles 1, 2, 5, 10, 20, 50, 100, etc.), but could be adjusted during the test if necessary. MATE created output files at the specified cycles which included modulus measurements and load-displacement data.

3.4 Experimental Procedures

The experimental procedure for testing each SCS-6/Ti-6-4 specimen included: measuring coefficient of thermal expansion and initial Young's modulus before cycling at room- and elevated-temperatures, performing the fatigue test, examining collected data and finally, inspecting the fractured specimen microscopically.

3.4.1 Physical and Material Measurements

Minimum cross-sectional dimensions were determined by measuring the width at the specimen's center, and calculating the average thickness in the gage section. The product was recorded as the cross-sectional area.

Young's modulus at room temperature was determined by performing a monotonic tensile test. Figure 3.5 shows stress strain curves for tensile tests of the composite at room temperature and at 427°C. Both curves are linear up to about 0.5% strain (1050 MPa for the room temperature test and 950 MPa for the 427°C test), so loading the specimen from 0 MPa to 600 MPa was well within the elastic region of the composite's

room temperature stress-strain curve, and therefore no permanent deformation or damage was expected.

Next, the temperature in the gage section was ramped to the desired level in two to three minutes with no mechanical load applied. The extensometer displacement was then recorded in order to calculate thermal strain and coefficient of thermal expansion (α):

$$\varepsilon_T = \frac{\delta}{GL} \tag{3.3}$$

$$\alpha = \frac{\varepsilon_T}{\Delta T} \tag{3.4}$$

where ε_T is thermal strain, δ is extensometer displacement, GL is gage length and ΔT is the

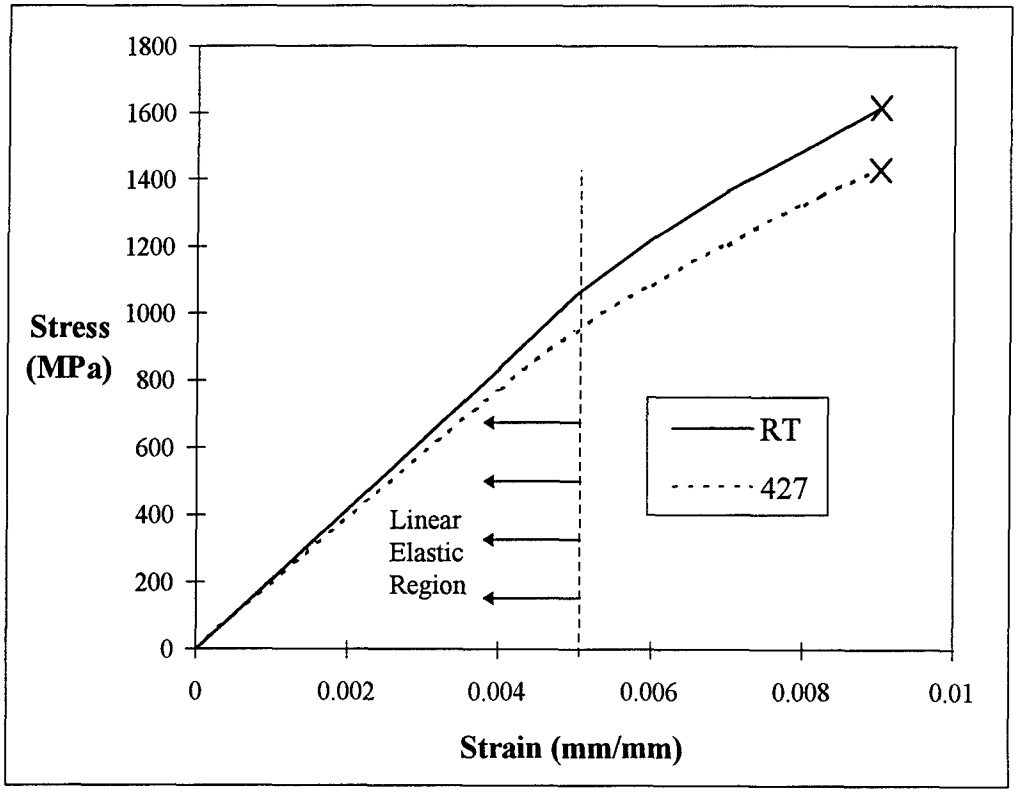

Figure 3.5 SCS-6/Ti-6-4 Tensile Response

change from room to test temperature.

After about three minutes, the first cycle was applied to determine the high temperature modulus and verify that the waveform's maximum and minimum loads were accurate. MATE determined the modulus by calculating the slope of the stress-strain curve in the region between 15% and 45% of the maximum stress. This range was used to calculate modulus for all subsequent cycles.

3.4.2 Fatigue Testing

The fatigue test commenced with the second cycle. During the test, periodic checks were made of the load waveform, test temperature, lamp operation, and water hoses to ensure proper operation. The DAC interval was also adjusted to collect data more frequently as the test neared its anticipated completion. Fatigue tests were considered complete when the specimen fractured into two pieces or when the number of cycles exceeded 10^6 (an "infinite" life), but none of the tests lasted longer than 10^6 cycles. Table 3.2 summarizes the test plan. Fourteen tests were performed by the author at the Air Force Institute of Technology, with the remaining eleven by the Materials Directorate of Wright Laboratory located at Wright-Patterson AFB.

Maximum stress levels from 800 MPa to 1200 MPa were selected so that both matrix-dominated and fiber-dominated fatigue responses would be studied. The lower stress level was expected to be less than both the fiber strength and interfacial shear strength, while fiber strength was anticipated to be exceeded by the highest stress level.

Table 3.2 Fatigue Test Plan

Specimen Number	Plate Number & Specimen Location	Test Temperature (°C)	Frequency (Hz)	Maximum Stress (MPa)
95-726 ML	25-6L	23	10	800
95-728 ML	25-8L	23	10	1050
95-696	18-6L	370	1	800
95-699	18-9L	370	1	1050
95-727 ML	25-7L	370	10	800
95-722 ML*	25-2L	370	10	1050
95-716	24-9L	370	10	1050
95-712	24-5L	427	0.01	900
95-729 ML*	25-9L	427	0.01	1050
95-702	18-12L	427	0.01	1050
95-701	18-11L	427	0.01	1200
95-708	24-1L	427	0.1	800
95-700	18-10L	427	0.1	1050
95-730 ML	25-10L	427	0.1	1200
95-695*	18-5L	427	1	800
95-697	18-7L	427	1	800
95-698	18-8L	427	1	1050
95-725 ML	25-5L	427	10	800
95-724 ML	25-4L	427	10	900
95-723 ML	25-3L	427	10	1050
95-711	24-4L	427	10	1200
95-709	24-2L	538	0.1	800
95-710	24-3L	538	0.1	1050
95-737 ML	26-4L	538	10	800
95-738 ML	26-5L	538	10	1050

* invalid test

ML: test performed by WL/ML

Under load-control, the minimum stress of tension-tension tests is usually slightly higher than zero to prevent compression of the specimen. The stress ratio, R is defined by:

$$R = \frac{\sigma_{min}}{\sigma_{max}} \tag{3.5}$$

and was selected to be 0.05. The broad frequency range of 0.01 Hz to 10 Hz was chosen to well characterize the time- and cycle-dependence of the composite. Although most tests were conducted at 427°C, a few were performed at room temperature (23°C), 370°C and 538°C to evaluate the influence of environmental temperature on frequency effects.

3.4.3 Post-mortem Observations and Analysis

Much information can be gained from microscopic observations of the fractured specimens. It is important to combine observations from data reduction with physical observations in order to conclude how the composite behaved during the fatigue test and what mechanisms caused its final failure.

FORTRAN programs were written to create stress-strain data files from load-displacement data files. The programs also produced maximum, minimum and mean strain, and modulus histories during cycling to investigate the macro-mechanical response of specimens. Modulus values were normalized by the specimen's initial modulus and cycle number was normalized by the number of cycles to failure. This was done to better compare the modulus history curves among different test conditions. For strain history comparisons, cycle number was again normalized by the number of cycles to failure.

Microscopic observation included sectioning several test specimens and examining fracture surfaces under a scanning electron microscope (SEM) and studying polished specimen surfaces up to the first fiber layer with an optical microscope. Figure 3.6 shows sectioning locations for the fractography and microscopy samples. A low speed diamond saw was used to transversely cut one side of the broken specimen about 5 mm from the fracture surface. This piece was ultrasonically cleansed and mounted on a small pedestal with conductive paint adhesive (SEM analysis required that both the paint and pedestal be conductive). The sample was then placed in a SEM where its fracture surface features were observed. This fractographic analysis provided much information about both damage and fracture mechanisms.

Microscopy was accomplished by studying the polished specimen face surface under an optical microscope. First, another transverse cut in the specimen was made with the low speed diamond saw about 8 mm below the location of the first cut. This sample was then mounted in a conductive molding compound (Beuhler's Konductomet II), which facilitated automated and hand polishing. The goal was to grind and polish the sample down to its first fiber layer. When sufficient polishing produced a clean surface free of

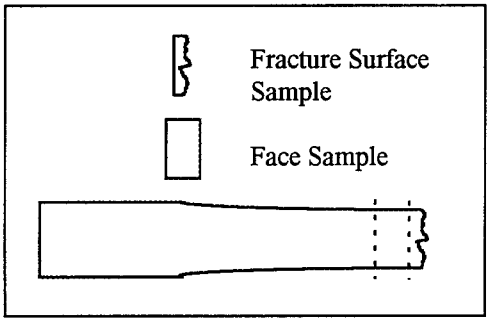

Figure 3.6 Specimen Sectioning

scratches and pitting, the sample could be examined for matrix cracking, fiber/matrix interface debonding and fiber damage. Since the sample was only about 8 mm long, its damage was representative of damage in the gage section.

Rough lapping was completed automatically using a Bueller Maximet with a 45 micron diamond slurry. Lapping with 9 micron slurry and a number 8 platen removed enough material to produce an even surface at the first layer of fibers. Lapping with 6 micron and 3 micron diamond slurries on nylon and silk platens removed surface scratches and most pits in the matrix. Final polishing was accomplished with 1 micron and 0.5 micron slurries in a Beuhler Vibromet for 24 hours and 45 minutes, respectively. Specimens were then ultrasonically cleansed in distilled water, and then with acetone. At this point they were ready for observation under an optical microscope.

4 Results and Discussion

In this section the results from experimental work are presented. First, the response under monotonic loading showing specimen stiffness and coefficient of thermal expansion is discussed. Trends and comparisons among strain and modulus histories during fatigue loading follow, and the chapter concludes with post-mortem microscopic observations of fracture surfaces and lamina layers inside the tested specimens. These comparisons and observations reveal the dominant damage mechanisms under various test conditions and the effects of cyclic frequency variations.

4.1 Monotonic Loading Response

As stated in the previous chapter, monotonic loading tests were necessary to determine the Young's modulus at room temperature and elevated temperature. These tests were performed for all specimens in order to determine variations of moduli among them. At room temperature, specimens were loaded and unloaded in the elastic range so that they would receive no permanent deformation or damage. The heat lamps set the desired test temperature, and the coefficient of thermal expansion (α) was determined. The modulus during the first cycle as recorded by the data acquisition program was also determined.

Table 4.1 shows the monotonic test results. The coefficient of thermal expansion varied nonlinearly as temperature increased, ranging from an average of 6.13×10^{-6} /°C at 370°C to 6.35×10^{-6} /°C at 538°C. The maximum variance from the mean value at each

Table 4.1 Summary of Modulus Data

Specimen Number	Test Temp (°C)	HT* Modulus (GPa)	α (10^{-6} /°C)	RT** Modulus (GPa)
95-696	370	196	6.2	205
95-699	370	197	6.1	211
95-716	370	197	6.1	213
Average		196.7	6.13	
95-697	427	195	6.6	214
95-698	427	196	6.5	205
95-700	427	190	6.6	212
95-701	427	197	6.3	219
95-702	427	196	6.1	218
95-708	427	202	6.0	223
95-711	427	197	6.2	215
95-712	427	189	6.3	205
Average		195.3	6.33	
95-709	538	181	6.4	214
95-710	538	177	6.3	211
Average		179.0	6.35	
* HT: High Temperature		**Average RT Modulus**		212.7
** RT: Room Temperature				

temperature was 4.3% (specimen #95-700). The average modulus at room temperature was 212.7 GPa and the maximum variance was 4.8% (specimen #95-708). The average modulus was 196.7 GPa at 370°C, 195.3 GPa at 427°C, and 179.0 GPa at 538°C. The maximum variance for a test temperature modulus was 4.3% (specimen #95-712). This shows that all specimens tested had consistent thermal expansions and stiffness values.

4.2 Fatigue Response: Macroscopic Observations

For the purposes of this discussion, the macroscopic response is defined as the change in maximum, minimum, and mean cyclic strain for a given maximum cyclic stress, and the change in modulus over the fatigue life of the specimen. Figures of stress-strain responses, mean strain history comparisons and modulus history comparisons are

presented to illustrate how varying test frequency affected fatigue response. Comparisons are made in three maximum stress categories: fiber-dominated mode (1200 MPa), matrix-dominated mode (800 MPa and 900 MPa), and mixed-mode (1050 MPa). It will be pointed out, however, that the degree of fiber- or matrix-dominance varies within each category. Test parameters included maximum stress (σ_{max}), frequency (f) and temperature (T). All tests were performed under the load-controlled mode and isothermal condition with a stress ratio, R = 0.05.

In all tests, the specimens fractured in two pieces, and the break was either in the 12.7 mm gage section or within 5.5 mm (the cooler shoulders) of the gage section. None of the specimens fractured in the hydraulic grips. Table 4.2 lists the specimens that fractured outside the gage length. Figure 4.1 is a photograph of two fractured specimens, and other such photographs are located in Appendix B. Crack growth outside the gage length may have resulted in inaccurate strain and modulus histories which will be pointed out in the following sections.

Table 4.2 Specimens Fractured Outside Gage Section

Specimen Number	Temperature (°C)	Frequency (Hz)	Maximum Stress (MPa)	Distance Outside Gage Section
95-699	370	1	1050	5.0 mm
95-722	370	10	1050	1.5 mm
95-708	427	0.1	800	5.0 mm
95-700	427	0.1	1050	1.5 mm
95-730	427	0.1	1200	4.0 mm
95-738	538	10	1050	5.5 mm

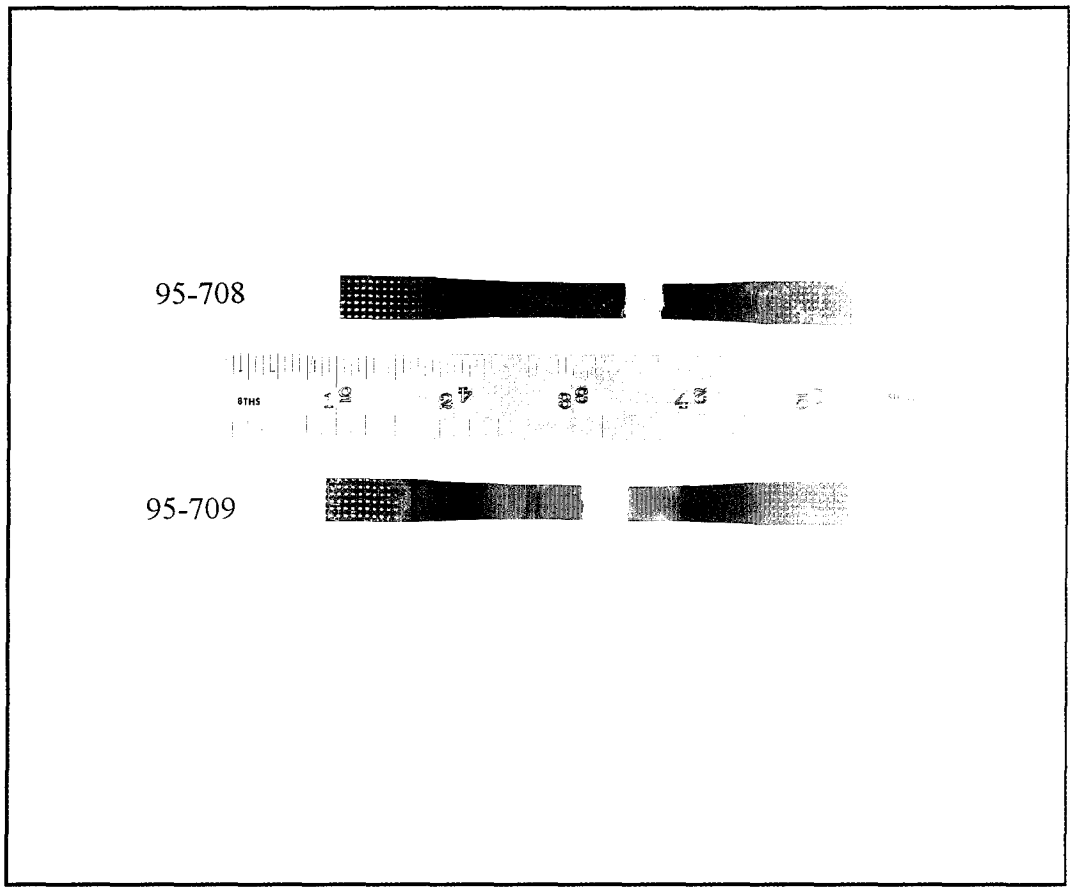

Figure 4.1 Fractured Specimens, Nos. 95-708 and 95-709

4.2.1 Fiber-Dominated Failure Mode (σ_{max} = 1200 MPa)

Figure 4.2 is the stress-strain response for a specimen tested at a maximum stress of 1200 MPa, frequency of 0.01 Hz, and temperature of 427°C (only mechanical strain is plotted). The stress-strain curve during the first cycle shows yielding beginning at about 0.40% strain, but the unloading portion of the cycle is parallel to the loading portion, indicating that no damage occurred. The curves for the remaining cycles are linear and parallel, but shift to the left throughout the specimen's life.

In general, the fatigue responses of all specimens tested at the 1200 MPa maximum stress level were fiber-dominated. In studying the behavior of unidirectional SCS-6/Ti-15-3, both Sanders and Kraabel noted that at high maximum stress values (or maximum strain for strain-controlled tests), failure was dominated by random, progressive fiber failure [15,26]. For this class of tests, maximum and minimum strains steadily increase at the same rate throughout the life of the specimen, resulting in a constant modulus. During

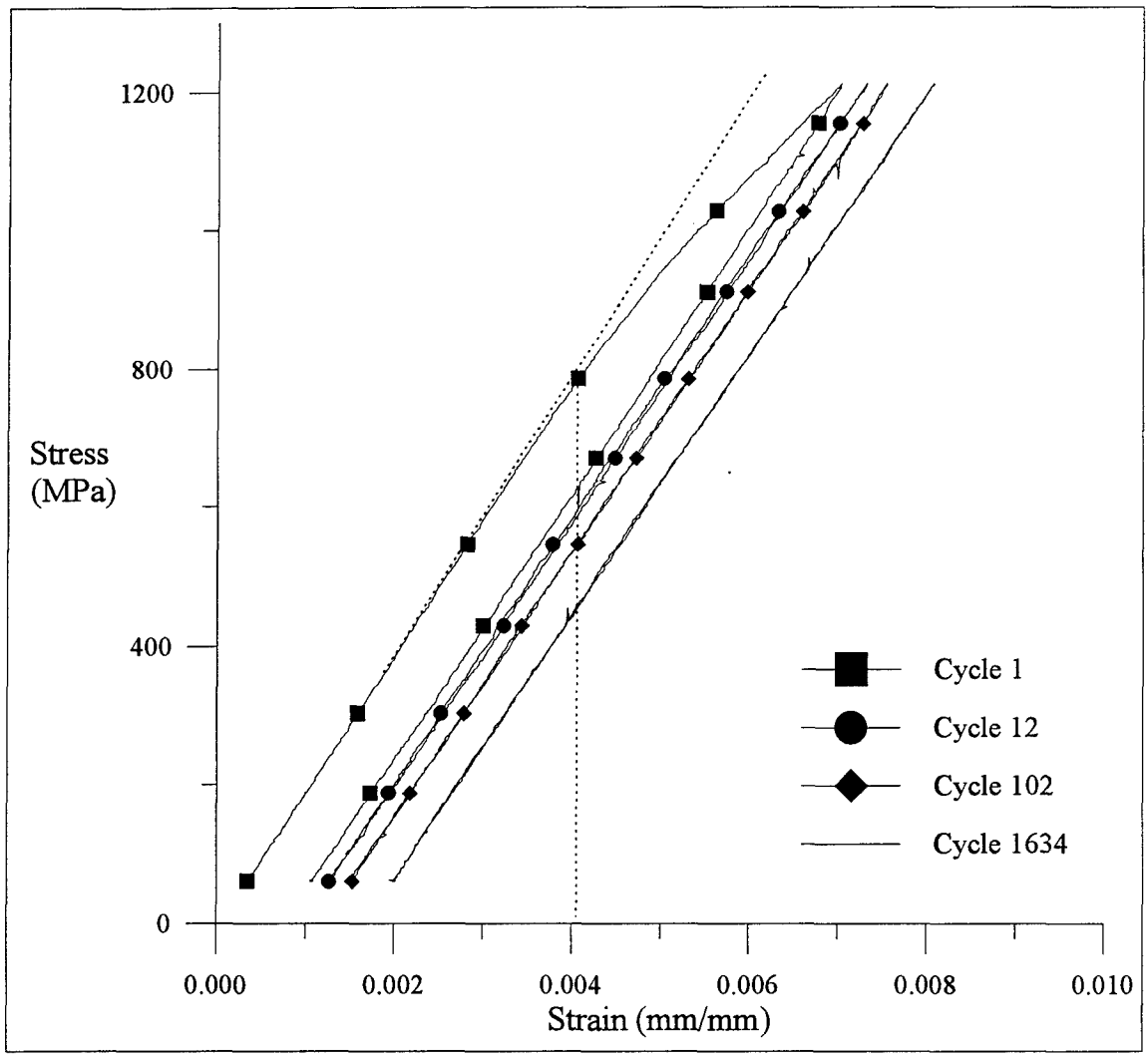

Figure 4.2 Stress-Strain Response (1200 MPa, 0.01 Hz, 427°C)

fatigue, fibers strain elastically and control the strain of the matrix which deforms plastically. As the test progresses, the creeping matrix material relaxes and stress transfers to the fibers. Since the elastic fibers maintain their modulus, the increased stress they bear causes them (and the laminate as a whole) to strain more. This accounts for the parallel increase in maximum and minimum strain throughout life.

Figure 4.3 illustrates the influence of frequency variations on the macroscopic response of specimens tested at 1200 MPa maximum stress and 427°C. Fatigue cycles are normalized by dividing the current cycle number (N) by the number of cycles to failure (N_f). Young's modulus is normalized by dividing the secant modulus of the current test

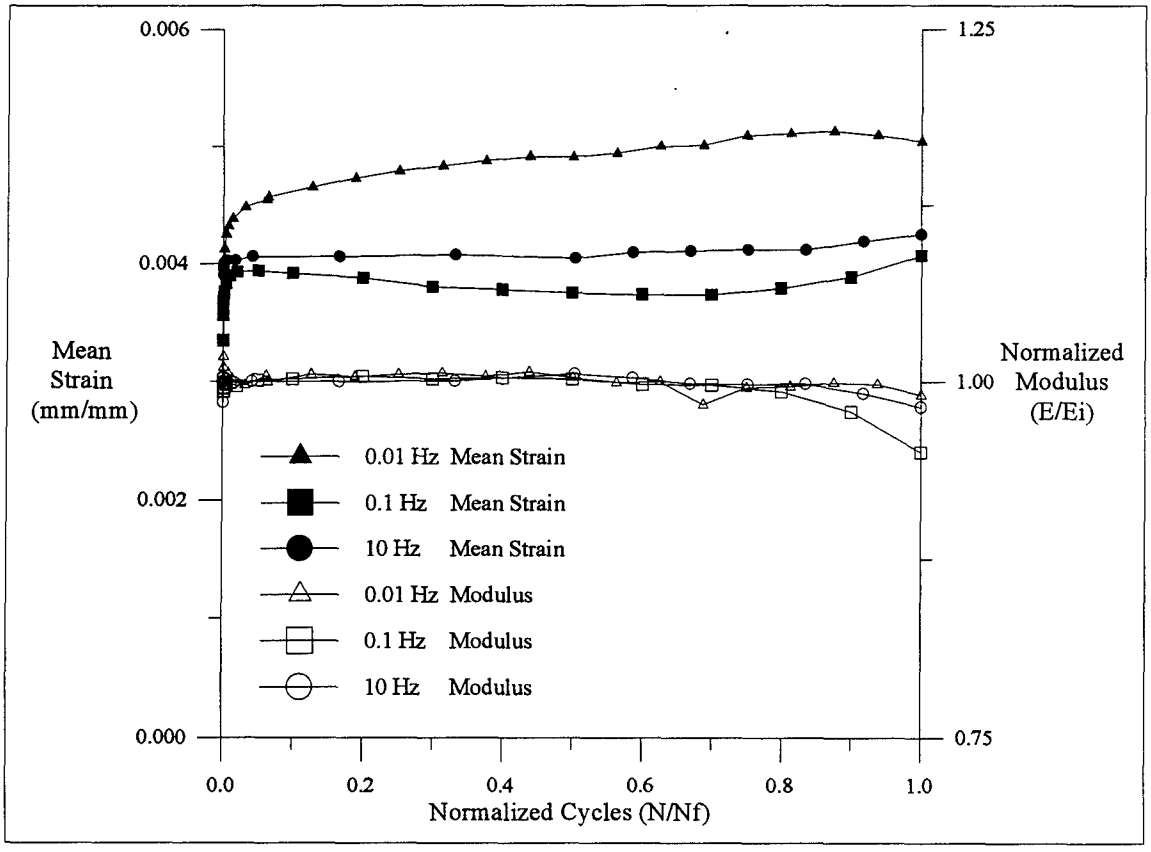

Figure 4.3 Strain and Modulus History Comparisons (1200 MPa, 427°C)

cycle (E) by the initial modulus (E_i). Mean strain is defined as the average of the minimum and maximum mechanical strains for the test cycle, and is not normalized.

The modulus was relatively constant at all three test frequencies, which illustrates a classical fiber-dominated response of MMCs. The mean strain of the specimen cycled at 0.01 Hz steadily increased throughout life, while the other two tests (f = 0.1 Hz and 10 Hz) exhibited a fairly constant mean strain. At the lowest test frequency, the long fatigue cycle (100 sec) provided the matrix sufficient opportunity to creep, relax and transfer its stress to the fibers. This did not occur as much in the specimens tested at the higher frequencies. The specimen cycled at 0.1 Hz fractured 4 mm outside the gage section, which may account for its fairly constant strain history.

At all frequencies, the increased tensile stress in the fibers eventually caused them to randomly break at their weakest points. Despite this creep-induced fiber damage, the modulus remained constant. When a fiber breaks during a fiber-dominated fatigue test, the surrounding bonded matrix receives the fiber's load and distributes the stress among the adjacent fibers and also back to the broken fiber a distance from the crack. Thus, there is little or no loss of laminate stiffness. Sometimes a broken fiber can be an initiation site for an internal crack, and this will be discussed in Section 4.3.

4.2.2 Matrix-Dominated Failure Mode (σ_{max} = 800 and 900 MPa)

Figure 4.4 illustrates the stress-strain response at a few selected cycles for a specimen tested at 800 MPa maximum stress, 10 Hz and 427°C. At this stress level, the laminate did not deform plastically and there was very little increase in strain for two-thirds of the fatigue test. The stress-strain curve for the final cycle exhibited a reduced

modulus and a hysteresis gap between the loading and unloading portions, which is indicative of laminate damage.

All specimens tested at maximum stress levels of 800 MPa and 900 MPa had matrix-dominated responses, but to varying degrees. In a matrix dominated response, the maximum strain rises at a greater rate than the minimum strain throughout the life, and therefore the modulus decreases. Although the stress level is not high enough to break fibers or crack the interface, cracks can develop in the matrix. As these cracks propagate,

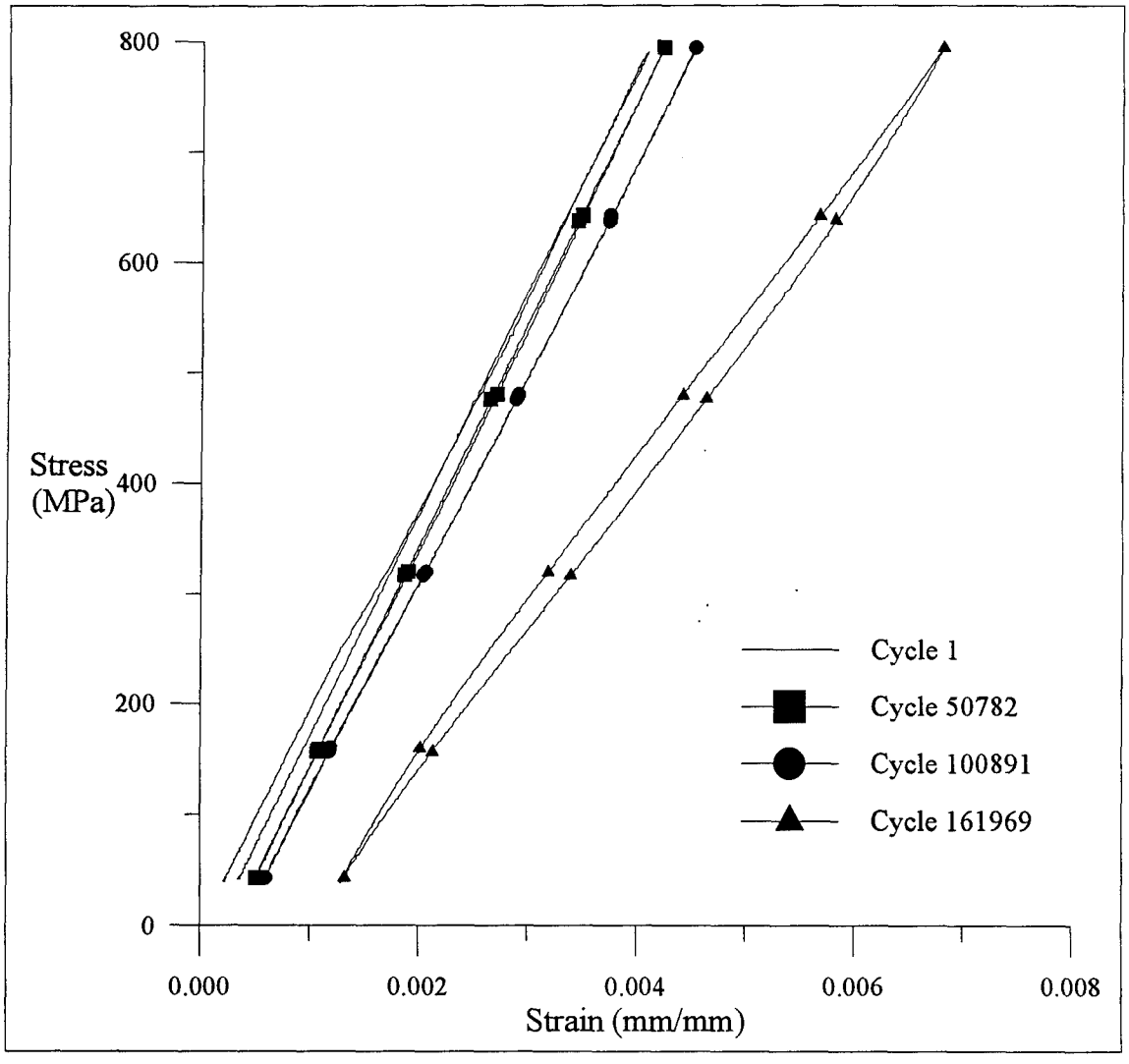

Figure 4.4 Stress-Strain Response (800 MPa, 10 Hz, 427°C)

stress is transferred to the rest of the intact laminate, but unlike the damage in the fiber-dominated response, matrix cracking results in the reduced stiffness of the entire laminate (modulus decreases). Some fibers crack early in life due to stress concentrations, while others crack later due to overload. Microscopic evidence of these damage mechanisms will be further discussed in Sections 4.3 and 4.4.

Figure 4.5 illustrates the influence of frequency on the macroscopic response of specimens tested at stress levels of 800 MPa and 900 MPa and 427°C. The maximum damage occurred during the life of the specimen cycled at the highest frequency. The modulus of specimen cycled at 10 Hz began to decrease after half of its life, while the

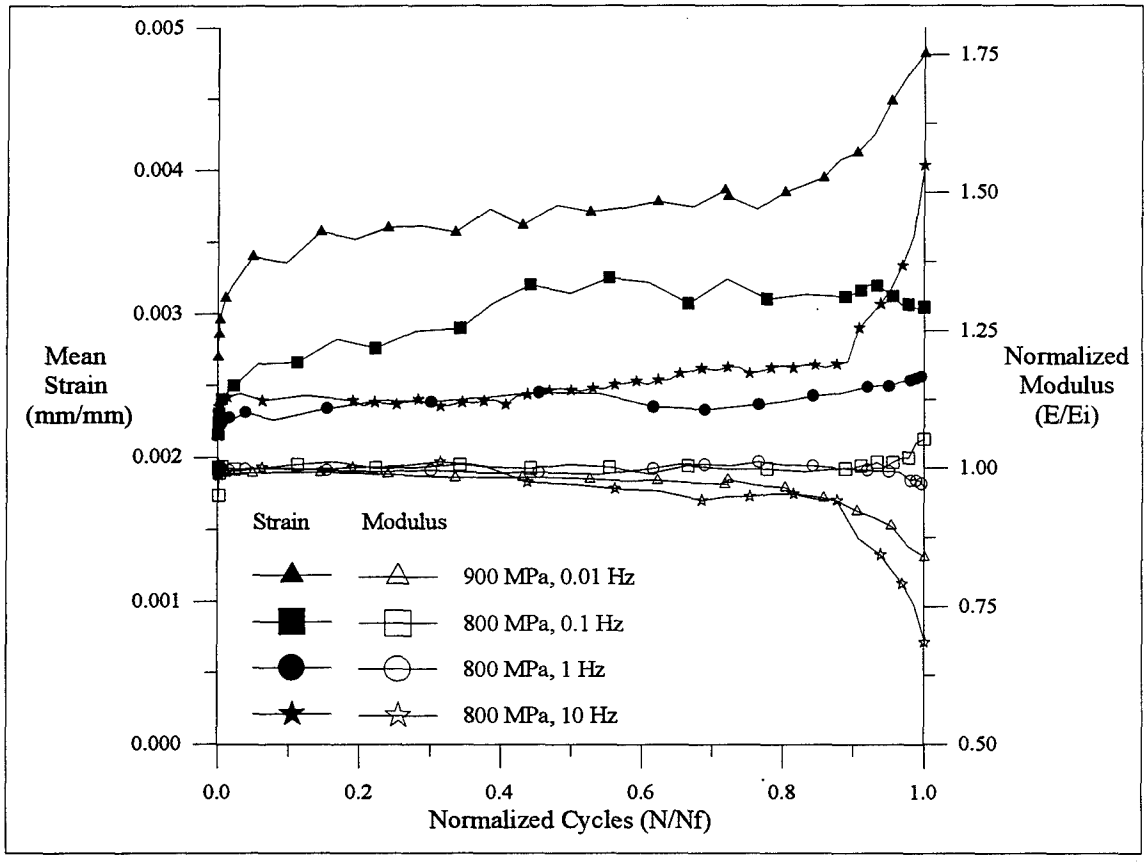

Figure 4.5 Strain and Modulus History Comparisons (800 and 900 MPa, 427°C)

specimens cycled at the 0.1 Hz and 1 Hz frequencies had fairly constant modulus histories. The modulus of the specimen tested at 900 MPa and 0.01 Hz also dropped in the latter portion of its life, suggesting that the 100 MPa increase in maximum stress initiated more damage than would have occurred in a specimen tested at 800 MPa and 0.01 Hz.

The increasing strain histories for the three specimens in this group tested at 800 MPa maximum stress almost mirror the decreasing modulus histories (mean strains increased in the same way that the moduli decreased). This reveals that the rise in strain was primarily due to matrix crack growth. However, the specimen cycled at 0.01 Hz at a maximum stress of 900 MPa, experienced a greater strain increase, which suggests an

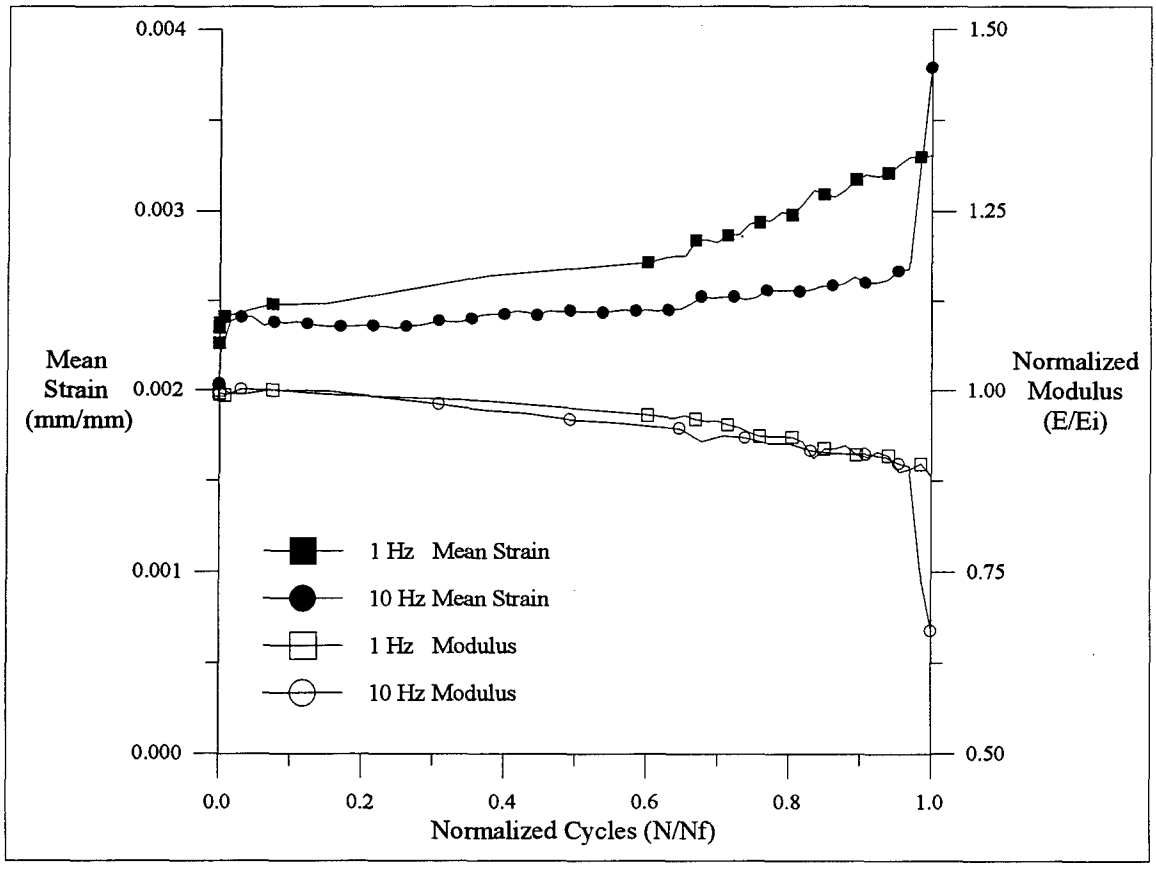

Figure 4.6 Strain and Modulus History Comparisons (800 MPa, 370°C)

added influence of creep. Microscopic examination of this specimen's fracture surface (reported in Section 4.3) also revealed the effects of increased creep. The specimen cycled at 0.1 Hz fractured 5 mm outside the gage section, which may account for its strain history showing a slight drop during the second half of its life.

Figure 4.6 shows how the frequency change from 1 Hz to 10 Hz affected the fatigue behavior of the MMC at 370°C. Both specimens experienced nearly identical damage up to 95% of their fatigue life, but the strain histories were different: the mean strain of the specimen cycled at 1 Hz increased throughout its life at a greater rate than the

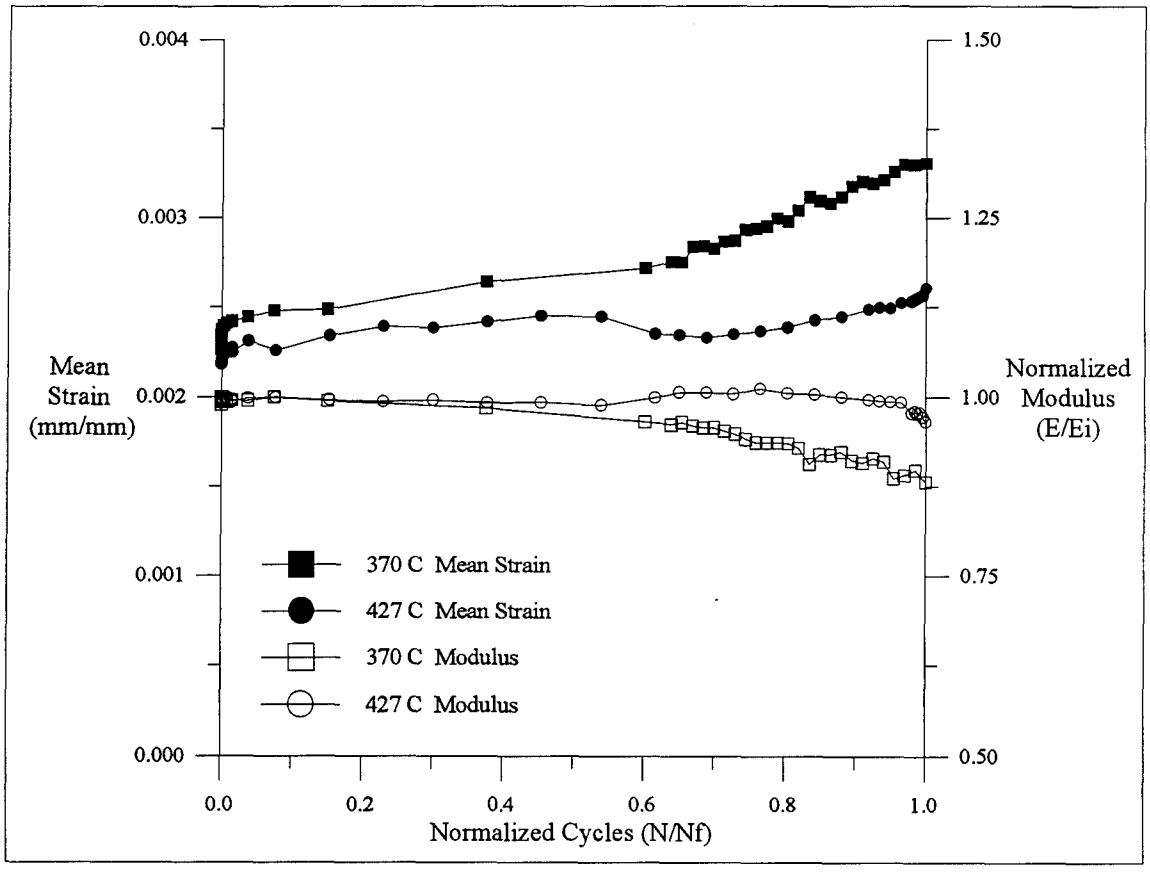

Figure 4.7 Strain and Modulus History Comparisons (800 MPa, 1 Hz)

mean strain of the specimen cycled at 10 Hz. This may have been due to greater creep in the specimen tested at the lower frequency, or more cracking within the gage section.

Figures 4.7 and 4.8 illustrate the effects of temperature on the fatigue response for matrix-dominated tests. Figure 4.7 compares 370°C and 427°C tests of specimens cycled at 1 Hz, and shows that the modulus of the specimen tested at the lower temperature decreased gradually throughout life, while the modulus of the specimen tested at the higher temperature remained fairly constant. Again, the mean strain histories mirrored the modulus histories, suggesting that most of the strain increase was primarily due to matrix cracking. Figure 4.8 compares 427°C and 538°C tests of specimens cycled at 0.1 Hz. In

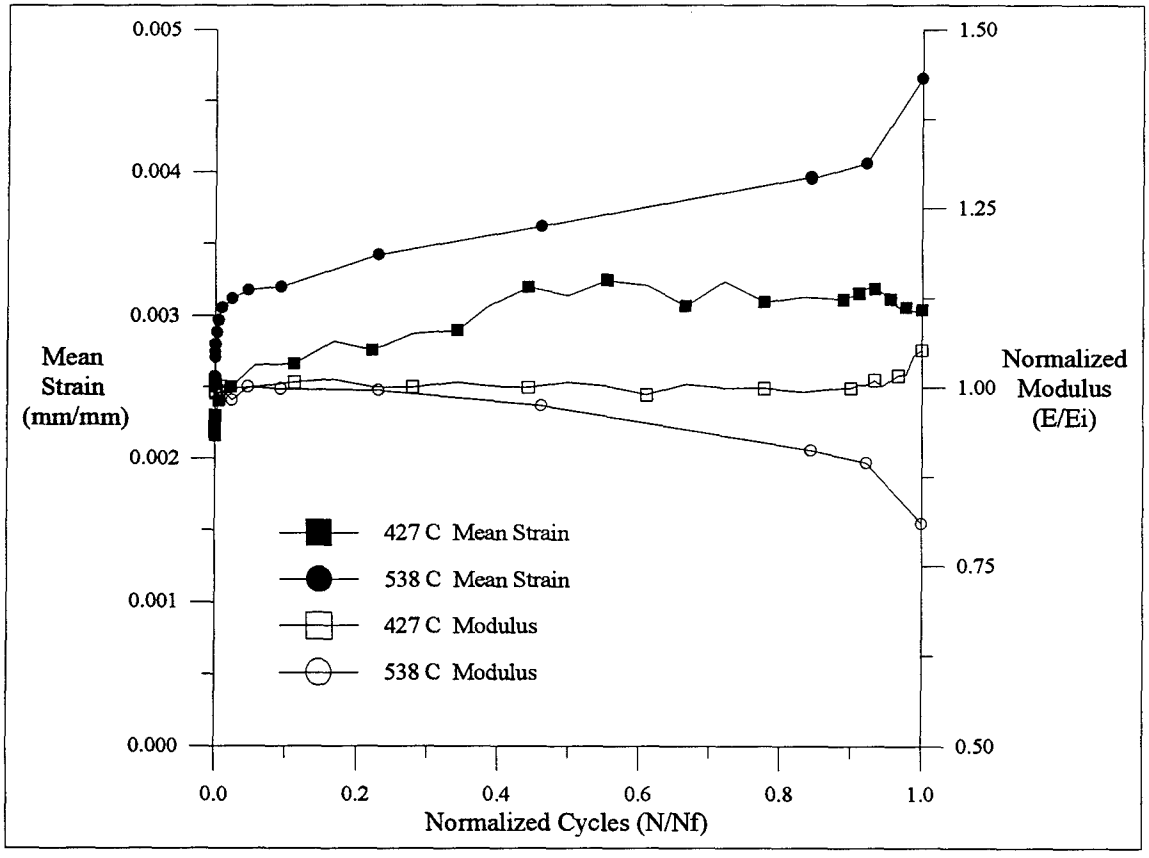

Figure 4.8 Strain and Modulus History Comparisons (800 MPa, 0.1 Hz)

this comparison, the higher temperature appeared to increase damage and mean strain. The rise in strain at 538°C may have been due in part to creep, but the increased damage at this temperature conflicts with the observations in Figure 4.7, where damage decreased. Therefore, the effect of temperature on the matrix-dominated fatigue response is inconclusive.

This section has described how the matrix-dominated response at the stress levels of 800 MPa and 900 MPa was significantly influenced by test frequency. Modulus and mean strain histories suggest that the greatest amount of laminate cracking occurred at the highest frequencies, but as frequency decreased, specimens incurred less cracking and more creep effects. Increased test temperature also seemed to diminish the dominance of matrix cracking at test frequencies of 1 Hz, but it increased matrix cracking as well as creep at test frequencies of 0.1 Hz.

4.2.3 Mixed-Mode Failure (σ_{max} = 1050 MPa)

At the maximum stress level of 1050 MPa, the fatigue response was highly dependent on test frequency and temperature and therefore was neither purely fiber- or matrix-dominated. Figures 4.9, 4.10 and 4.11 are stress-strain curves plotted for selected cycles of fatigue tests at 1050 MPa maximum stress, at temperatures of 427°C, 427°C and 538°C, and at frequencies of 1 Hz, 0.01 Hz, and 0.1 Hz, respectively. The stress-strain curves in Figure 4.9 (the higher frequency test), have gradually decreasing slopes throughout life, and only the last cycle shows nonlinearity. However, Figure 4.10 shows

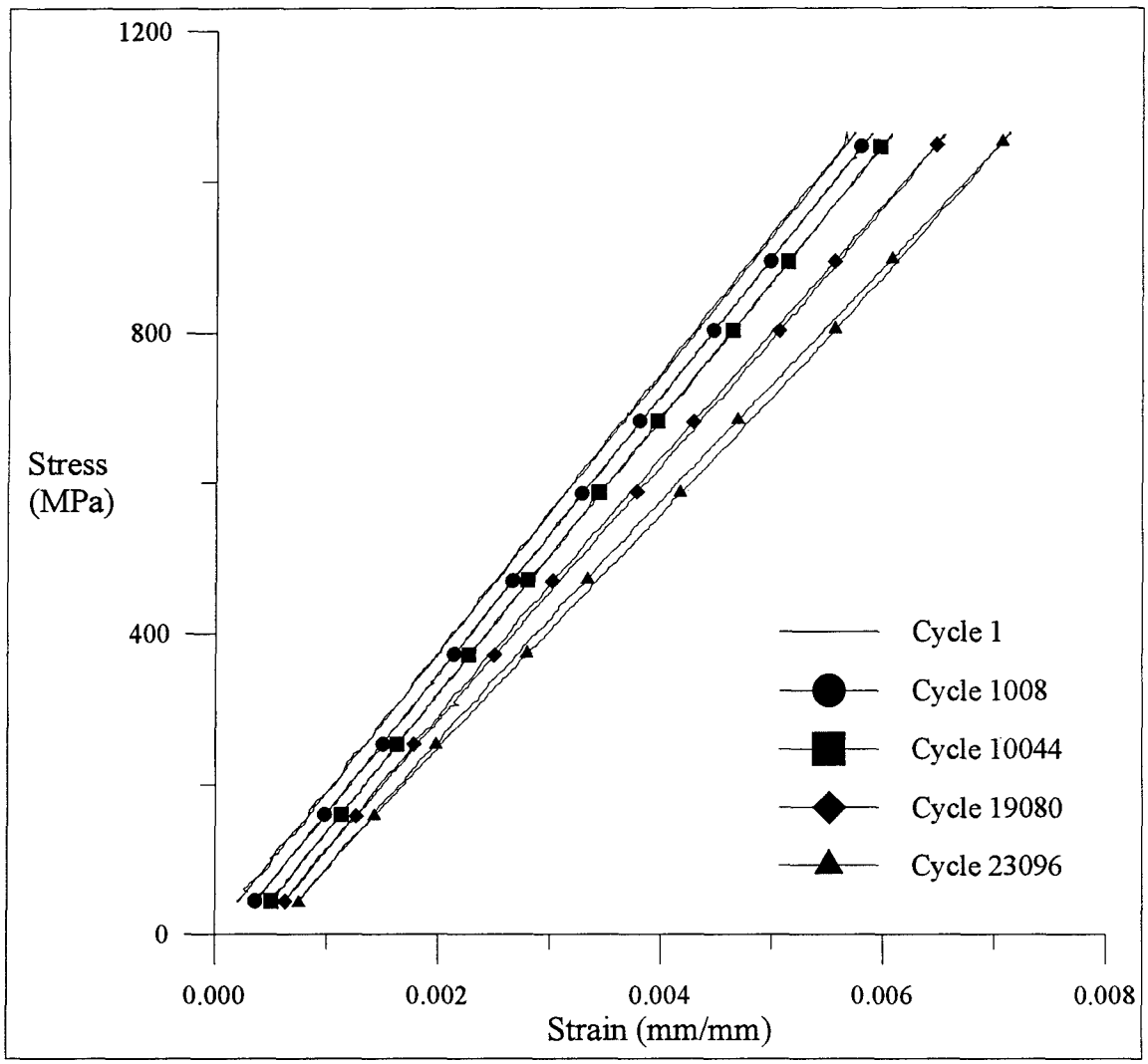

Figure 4.9 Stress-Strain Response (1050 MPa, 1 Hz, 427°C)

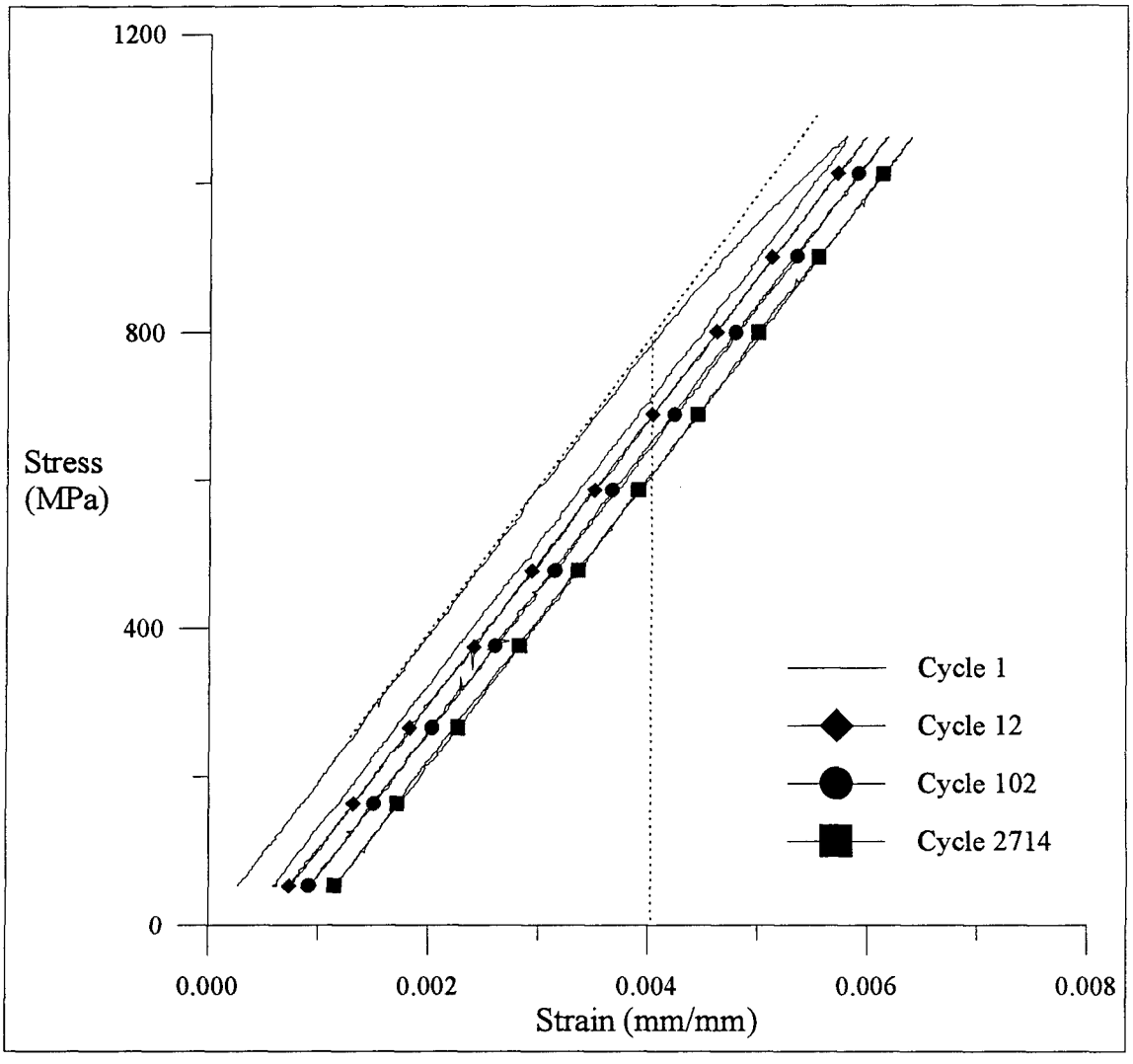

Figure 4.10 Stress-Strain Response (1050 MPa, 0.01 Hz, 427°C)

that the specimen tested at the lowest frequency (0.01 Hz) retained stiffness and stress-strain linearity for its entire life, and the first cycle stress-strain curve exhibited plastic yielding at 0.41% strain. This apparent plasticity at the lower stress rate may be due to the material's viscoplastic effects. Finally, Figure 4.11 shows the response at the higher temperature, where plastic yielding existed in the first cycle at about 0.27% strain and the average stiffness (slope of the curves) remained constant throughout the test. Like the

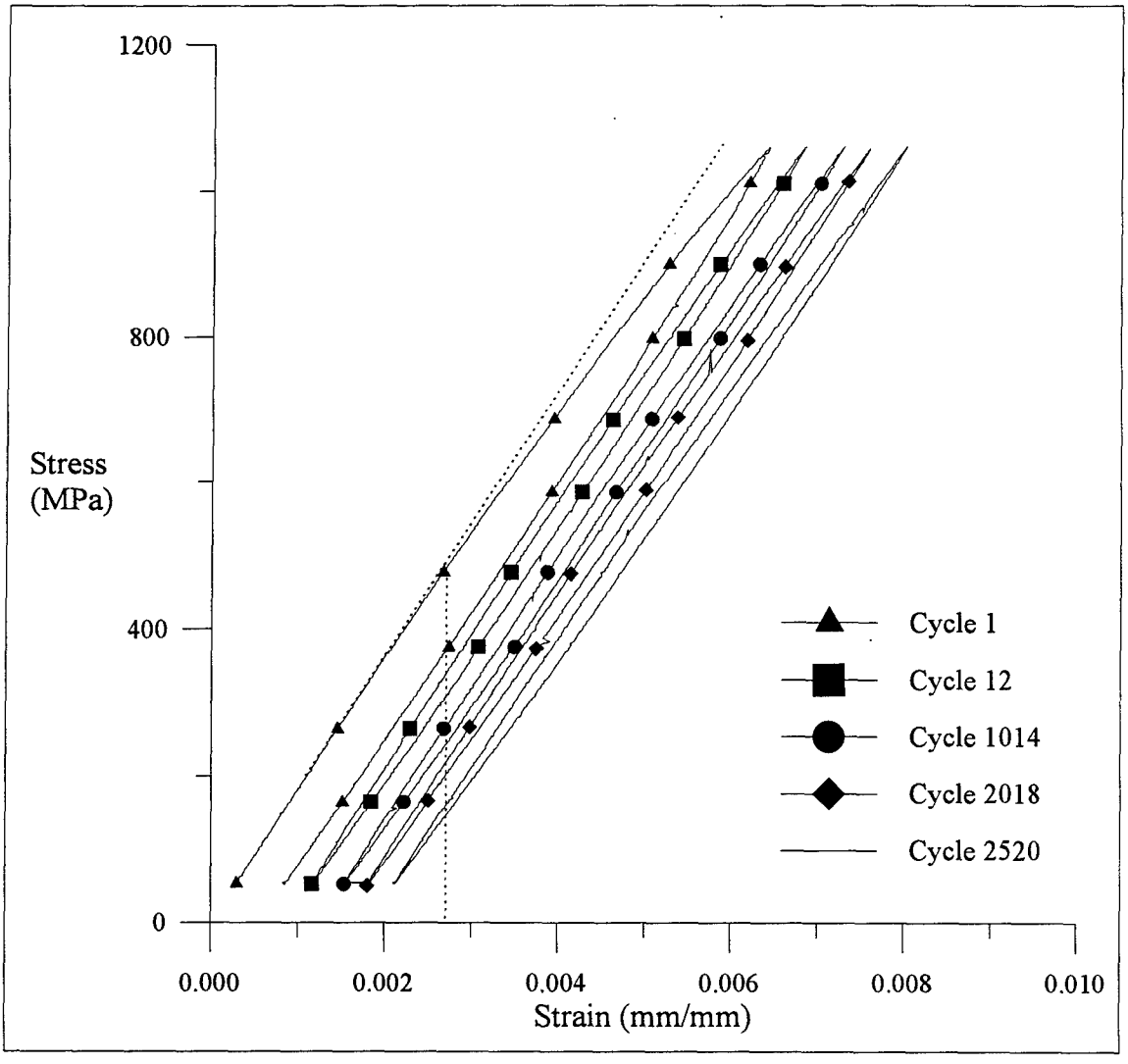

Figure 4.11 Stress-Strain Response (1050 MPa, 0.1 Hz, 538°C)

response in Figure 4.10, this response was fiber-dominated. The differences between the two responses are that at 538°C, the curves exhibit significant hysteresis (gaps) between the loading and unloading portions (evidence of a greater amount of creep), and laminate yielding occurred at a lower mechanical strain.

Figure 4.12 illustrates the effects of frequency on mean strain and modulus histories of specimens tested at 427°C. The modulus histories indicate that very little laminate damage occurred during the lower frequency tests, while the stiffness of the specimen cycled at the higher frequency began to drop after 60% of its life. The mean strain histories of the specimens tested at the lower frequencies showed a slight rise in the

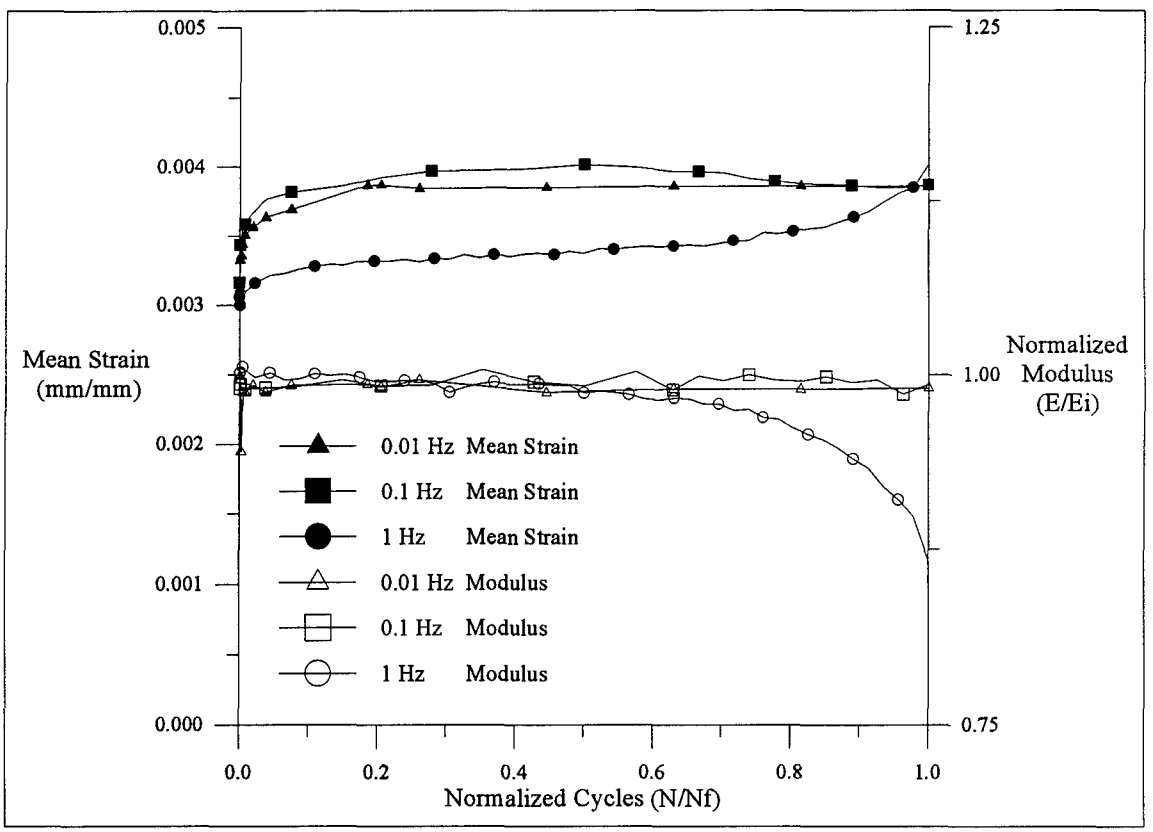

Figure 4.12 Strain and Modulus History Comparisons (1050 MPa, 427°C)

first 25% of life but then appeared to remain fairly constant for the remainder of life. In contrast, the mean strain of the specimen cycled at the higher frequency remained constant for 60% of life and then began to rise, mirroring the modulus drop. These histories seem to indicate that the response at the maximum stress of 1050 MPa was matrix-dominated at higher frequencies and fiber-dominated at lower frequencies.

Fatigue behavior at the 1050 MPa maximum stress level was also influenced by test temperature. Figure 4.13 presents modulus and strain histories for specimens cycled at 1 Hz and temperatures of 370°C and 427°C. At the higher temperature the laminate's modulus dropped after 60% of life, while modulus began to drop after 85% of life at the

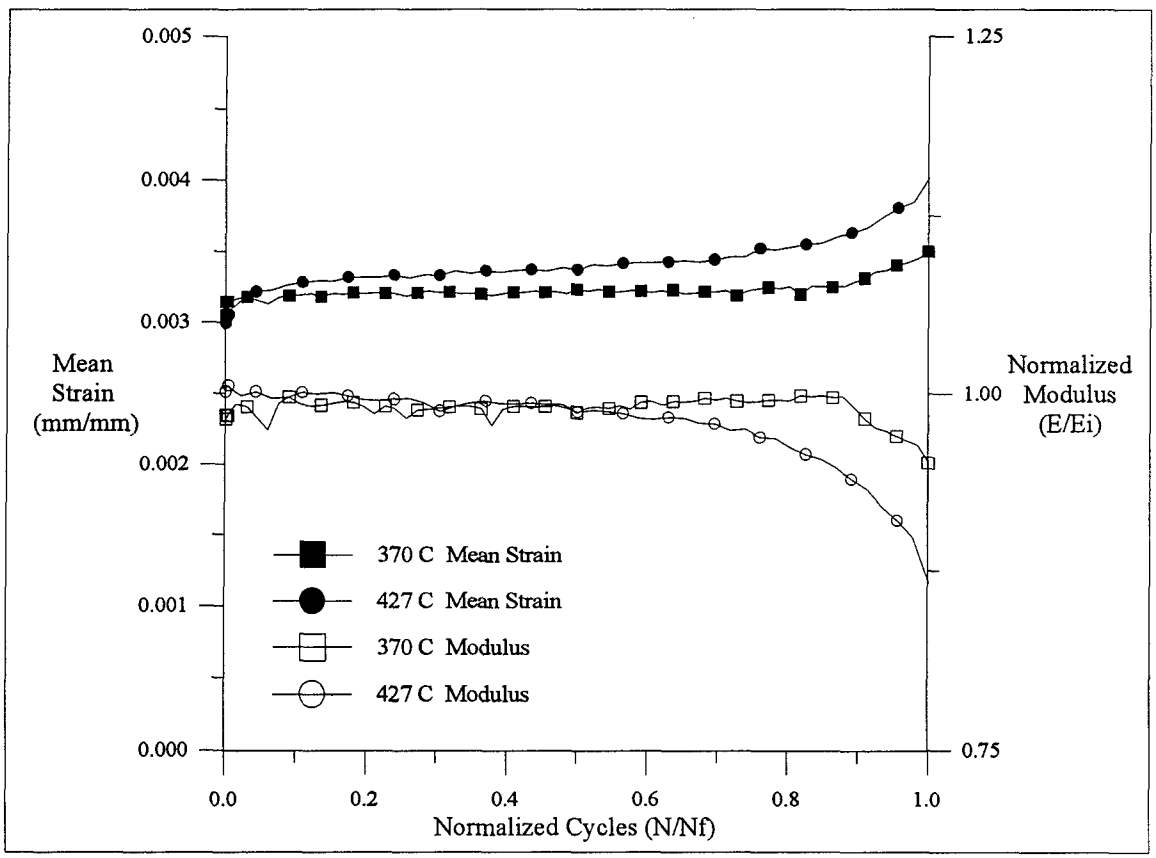

Figure 4.13 Strain and Modulus History Comparisons (1050 MPa, 1 Hz)

lower temperature. Likewise, mean strain rose earlier in life for the specimen tested at the higher temperature. Figure 4.14 shows a similar trend when comparing specimens cycled at 0.1 Hz at temperatures of 427°C and 538°C. Laminate modulus remained relatively constant during the fatigue life of the specimen tested at the lower temperature, but the modulus of the specimen tested at the higher temperature decreased after 60% of life and then increased after 80% of life, which could indicate either matrix cracking damage or poor data. The mean strain of the specimen tested at 427°C remained constant throughout life, but the mean strain of the specimen tested at 538°C steadily increased. Figure 4.11 indicated that the specimen tested at 538°C exhibited a fiber-dominated

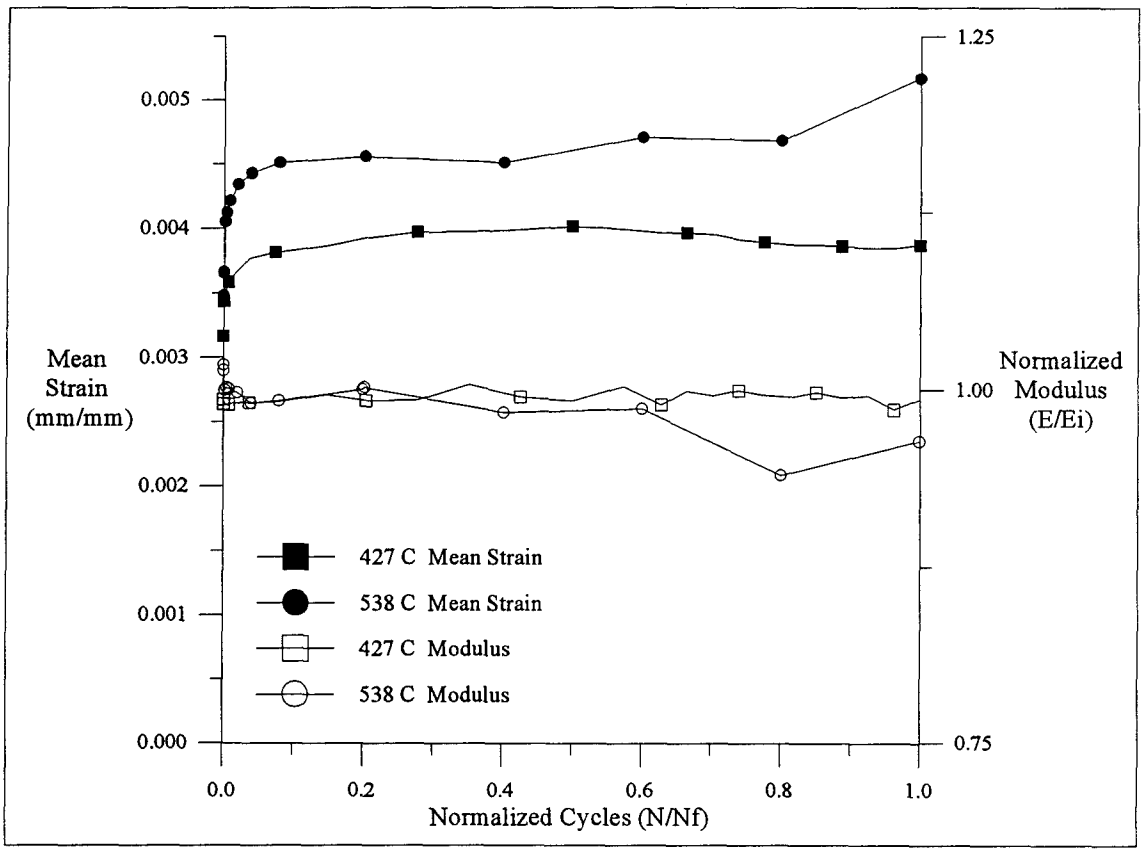

Figure 4.14 Strain and Modulus History Comparisons (1050 MPa, 0.1 Hz)

response with much creep, so it appears that at 1050 MPa, specimens tested at higher temperatures experience a greater amount of creep than specimens tested at lower temperatures.

4.2.4 Summary of Macroscopic Observations

Tables 4.3 and 4.4 show the summary of the qualitative changes in mean strain and modulus histories among several test sets. Table 4.3 describes how the fatigue response varied with frequency. In each set, maximum stress and test temperature were held constant while cyclic frequency ranged from 0.01 Hz to 10 Hz.

Fatigue responses were generally matrix-dominated at the lowest stress level, particularly at the highest test frequency (10 Hz) where the laminate's stiffness decreased throughout life due to matrix-cracking damage. Laminate damage diminished with decreasing test frequency, with the exception of the specimen cycled at the frequency of 0.01 Hz, which exhibited more damage than the specimens tested at 0.1 Hz and 1 Hz.

Table 4.3 Effects of Varying Frequency on Strain and Modulus Histories

σ_{max} (MPa)	T (°C)	**Strain History Trends**	**Modulus History Trends**
800	370	increases more at lower f	steady drop entire life at all f
800	427	increases at lower f, constant at higher f	decreases early in life at higher f, constant at lower f
800	538	increases at lower f, constant at higher f	possibly decreases more at lower f (bad data at 10 Hz)
1050	427	fairly constant at all f (but bad data at 10 Hz)	decreases more at high f, constant at lower f
1050	538	increases at about same rate for all f	constant for all f
1200	427	increases entire life at lower f, slight increase at higher f	constant for all f

f: frequency

The greater amount of laminate damage at 0.01 Hz was likely due to the higher maximum stress level (900 MPa).

Fiber-dominated behavior was most evident in the test run at 1200 MPa maximum stress and cycled at 0.01 Hz, which could be considered an "inefficient creep test" rather than a fatigue test. In a true creep test, a constant stress would be applied to a specimen and its strain would increase. Only a portion of the triangular stress waveform near its peak is sufficient to cause the specimen to creep, so any fiber breakage due to creep occurs during that fraction of the cycle. Since failure in creep tests is by nature more time-dependent than cycle-dependent, failure in low frequency fatigue tests would also be expected to exhibit a certain amount of time-dependence. In fact, this observation is detailed in Chapter 5.

At 1050 MPa maximum stress, the fatigue responses were found to be mixed-mode, that is, the degree to which they were fiber- or matrix-dominated depended on test frequency and temperature. At 427°C, specimens cycled at 0.01 Hz and 0.1 Hz exhibited fiber-dominance, while specimens cycled at higher frequencies exhibited matrix-dominance.

Table 4.4 summarizes the temperature effects observed. In general, tests run at higher temperatures seemed to exhibit less matrix cracking and more creep. The actual change in the macroscopic response was dependent on the maximum stress and frequency. For tests conducted at high frequencies and low maximum stress levels, cracking damage was inversely proportional to temperature. For the fiber-dominated tests (high maximum stress and low frequency), the amount of creep increased as temperature increased. The

Table 4.4 Effects of Varying Test Temperature on Strain and Modulus Histories

f (Hz)	σ_{max} (MPa)	Strain History Trends	Modulus History Trends
0.1	800	increases slightly more at higher T than medium T	decreases early at higher T, constant at medium T
0.1	1050	increases slightly more at higher T than medium T	constant at all T
1	800	increases at lower T, constant at medium T	decreases early at lower T, constant at medium T
1	1050	increases at medium T, constant at lower T	decreases earlier at medium T, constant at lower T
10	800	increases most at RT, constant at lower, medium & higher T	decreases most at RT, decreases less as T increases
10	1050	bad data at medium T (possibly increases), constant at higher T	bad data at medium T (possibly decreases) constant at higher T

T: temperature
RT: room temperature

trend differed under the "mixed-mode" conditions (1050 MPa maximum stress and high frequency), where both matrix cracking and creep appeared to increase at higher temperatures. More strain and modulus history comparisons are located in Appendix A.

4.3 Microscopic Observations--Fractography

The previous section discussed observations from macroscopic data trends that helped to determine the factors that influenced fatigue behavior during testing. This section supports those conclusions by presenting evidence from physical examination of fracture surfaces of tested specimens. Physical evidence from microscopy observations, also supporting macroscopic conclusions, will be given in Section 4.4.

A scanning electron microscope (SEM) was used to view the fracture surfaces in detail and determine which mechanisms were involved in initiating and leading to failure of the laminate. Comparisons are made in three maximum stress categories: fiber-dominated mode (1200 MPa), matrix-dominated mode (800 MPa and 900 MPa), and mixed-mode

mode (1200 MPa), matrix-dominated mode (800 MPa and 900 MPa), and mixed-mode (1050 MPa). This section compares specimens cycled at different frequencies at each stress level and discusses inferences of failure mechanisms. Most microscopic observations were of specimens tested at 427°C, but the effect of increased temperature on fracture mechanisms will be shown by observations of two specimens tested at 538°C. Photographs of surface morphology are also included.

4.3.1 Fiber-Dominated Failure Mode (σ_{max} = 1200 MPa)

In order to determine fracture mechanisms of specimens cycled at high maximum stress levels, three specimens were analyzed microscopically. They were tested at a maximum stress of 1200 MPa and frequencies of 10 Hz, 0.1 Hz and 0.01 Hz. Macroscopic analysis in Section 4.2.1 suggested that responses were fiber-dominated at this stress level, so creep and ductile matrix failure was expected in microscopic observations of these fractured specimens.

Figure 4.15 is a SEM photograph of the entire fracture surface of the specimen cycled at a frequency of 10 Hz. Most of the surface was very irregular and fibers were pulled out of the surrounding matrix, which is evidence of fiber-dominated failure. Matrix material pulled away from the fibers, and close examination revealed "dimpling," or coalescence of microvoids. A predominantly ductile surface results from fiber dominated failure, where matrix relaxation causes fibers to overload and then randomly break.

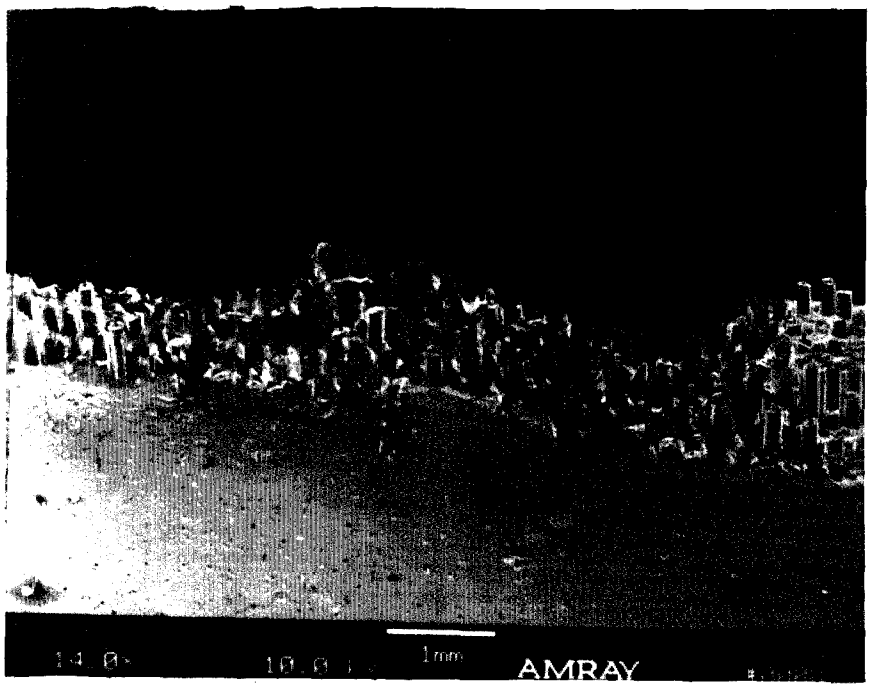

Figure 4.15 Fracture Surface. 1200 MPa, 10 Hz, 427°C (14x)

Figure 4.16 shows an area of the same surface that transitioned from a ductile fracture to a flat region where fibers cleaved at or close to the matrix. This was evidence of fatigue cracking: there were no gaps between the fibers and the surrounding matrix material and the dimple pattern was not present. The largest matrix crack measured 0.7 mm along one of the specimen edges and 0.4 mm into the width, and it likely initiated from fibers along the edge that were broken during the machining process. Three cracks grew from the other edge of the specimen, each on its own surface plane. The equivalent through-the-thickness crack growth was measured to be about 11% of the cross-sectional area.

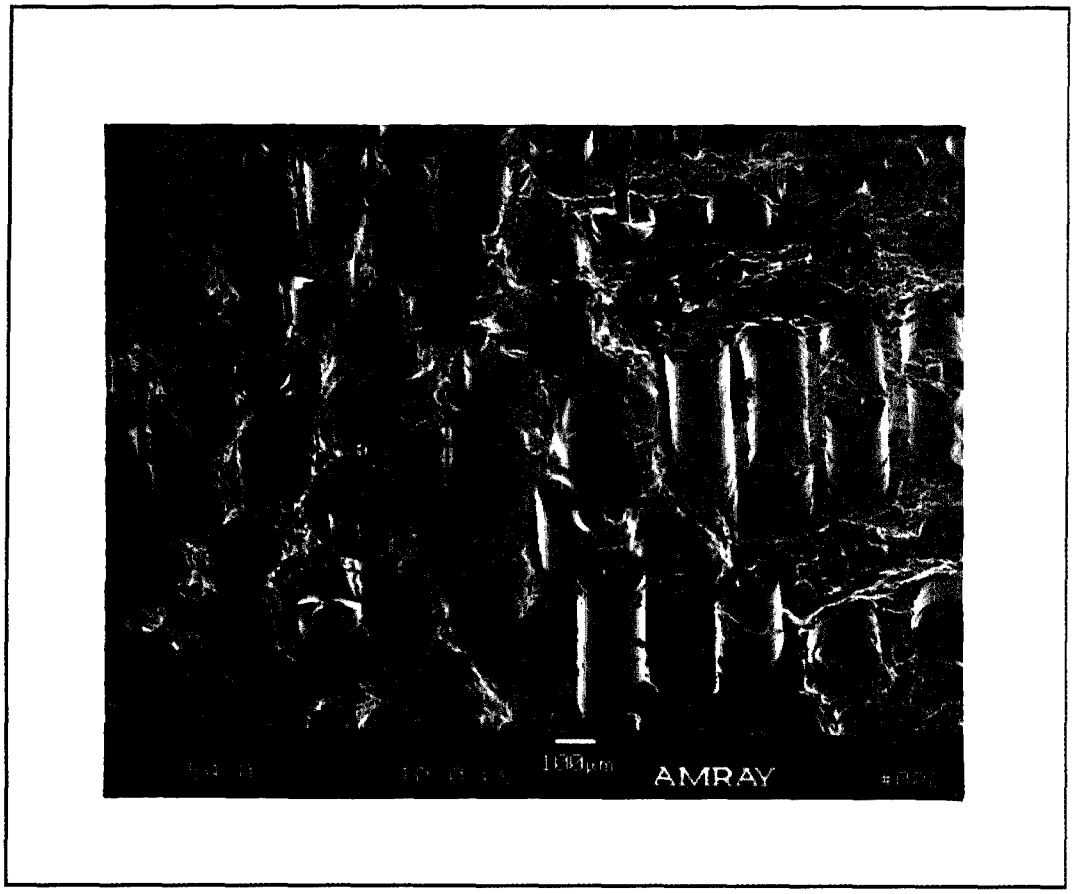

Figure 4.16 Ductile and Matrix Cracking Regions. 1200 MPa, 10 Hz, 427°C (54x)

Figures 4.17 and 4.18 show the ductile fracture surface of the specimen cycled at 0.1 Hz. In this specimen, the predominant crack was observed in one corner of the fracture surface, and measured about 0.7 mm in both directions (about 4% of the surface area). As expected, the remaining fracture surface experienced fiber-dominated failure.

The fracture surface of the specimen cycled at 0.01 Hz and 1200 MPa maximum stress was expected to show fiber-dominated failure. In fact, the fracture surface exhibited much ductility with dimpling, but had one corner crack measuring 0.55 mm x 0.65 mm and a 1 mm edge crack which extended 0.8 mm into the specimen width. The total crack

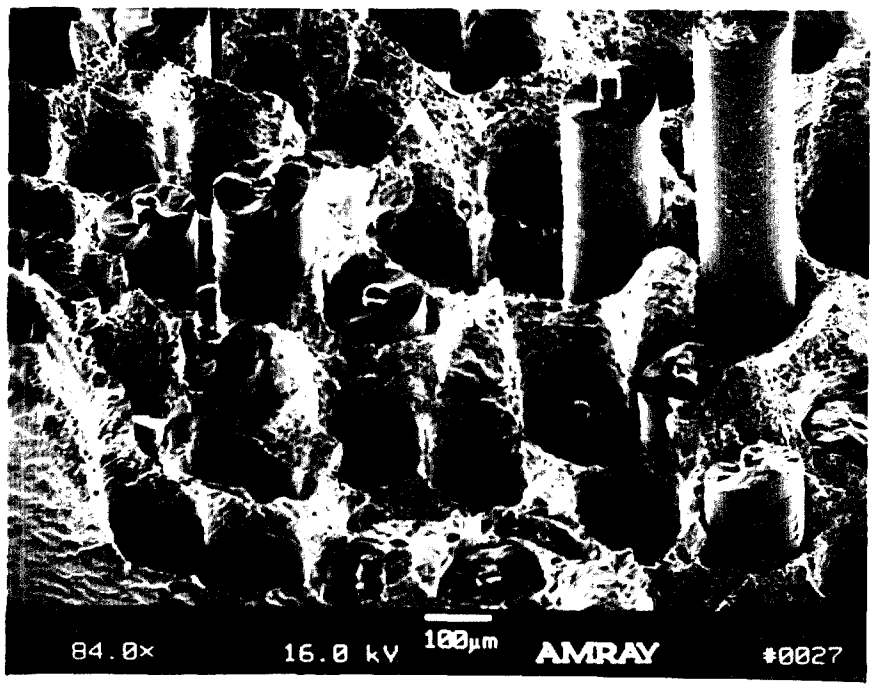

Figure 4.17 Matrix Ductility. 1200 MPa, 0.1 Hz, 427°C (84x)

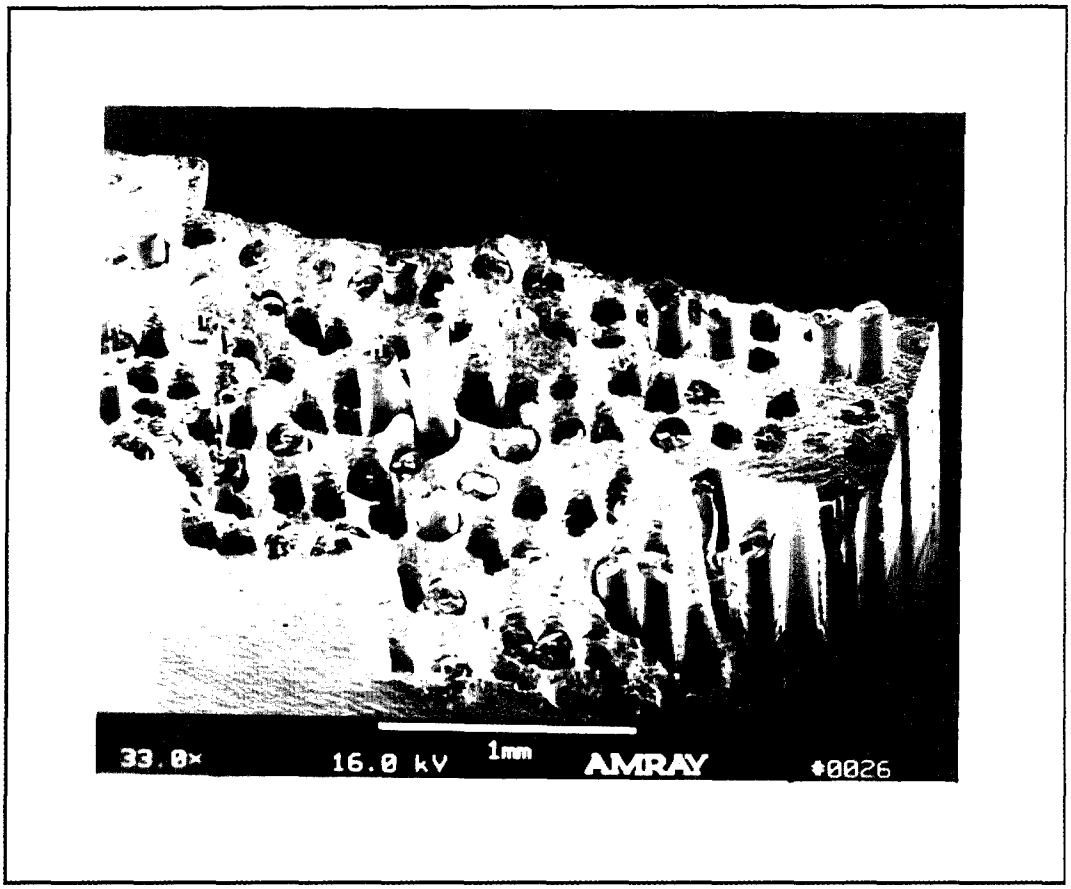

Figure 4.18 Corner Fatigue Crack. 1200 MPa, 0.1 Hz, 427°C (33x)

growth area covered approximately 8% of the fracture surface. Figure 4.19 exhibits the dimpling effect of microvoid coalescence in a ductile region.

Observations under 1000X to 3000X magnification revealed matrix cracking due to three different mechanisms. Figure 4.20 shows one region where probable striations or slip bands were visible on the grain surfaces. These ridges were parallel, but changed direction at each new grain. In other parts of the fatigue region, the matrix cracked by transgranular cleavage, which was evidenced by smooth, flat surfaces where the grains fractured along well-defined crystallographic planes. Technically speaking, only body-

Figure 4.19 Ductile Microvoid Coalescence. 1200 MPa, 0.01 Hz, 427°C (392x)

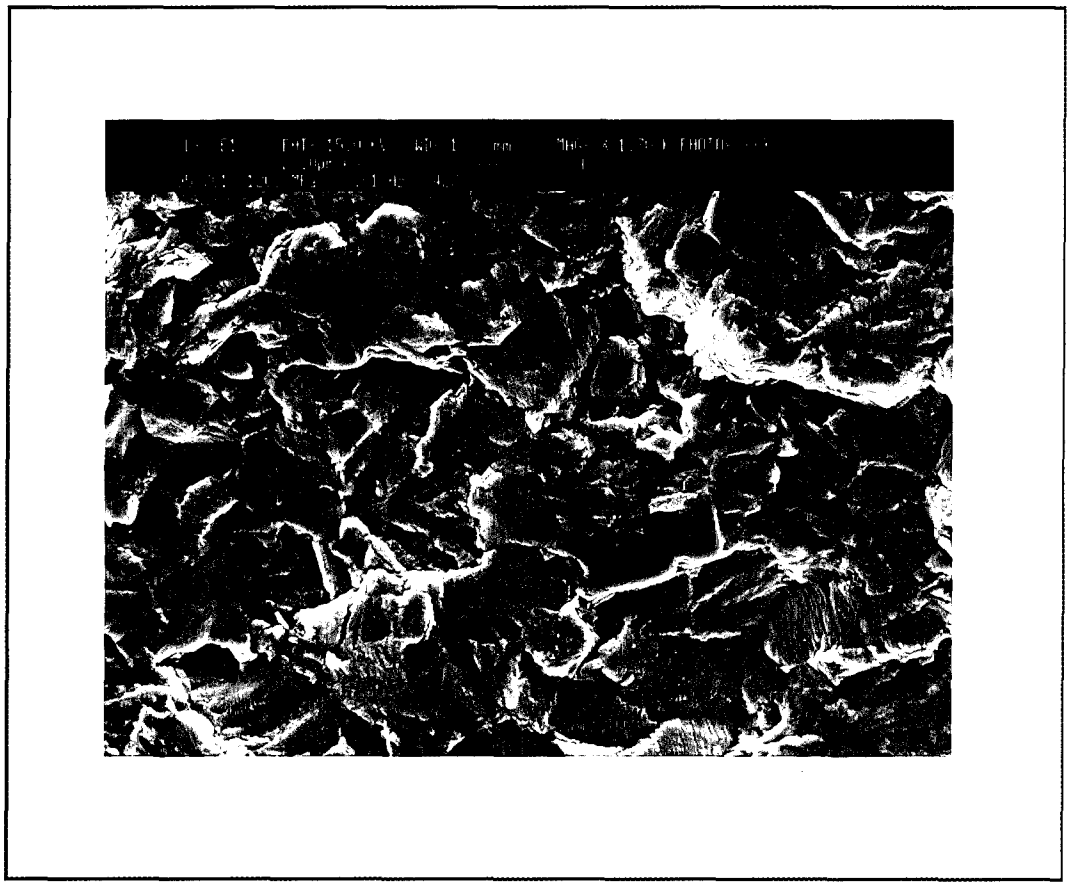

Figure 4.20 Striations on Grains. 1200 MPa, 0.01 Hz, 427°C (1700x)

centered cubic materials like β-titanium alloys and some hexagonal-close packed materials (like Ti-6-4) can cleave; face-centered cubic structures do not normally cleave [4].

A third cracking mechanism observed was intergranular decohesion, which is prevalent in high oxidation and creep environments. This mechanism is evidenced by gaps between the grains and well-defined, faceted grain boundaries. Figure 4.21 depicts intergranular decohesion observed in a ring around a fiber, and a transition to transgranular cleavage further from the fiber, and Figure 4.22 shows a region in an edge crack where transgranular cracking is present with oxidation precipitates visible on some

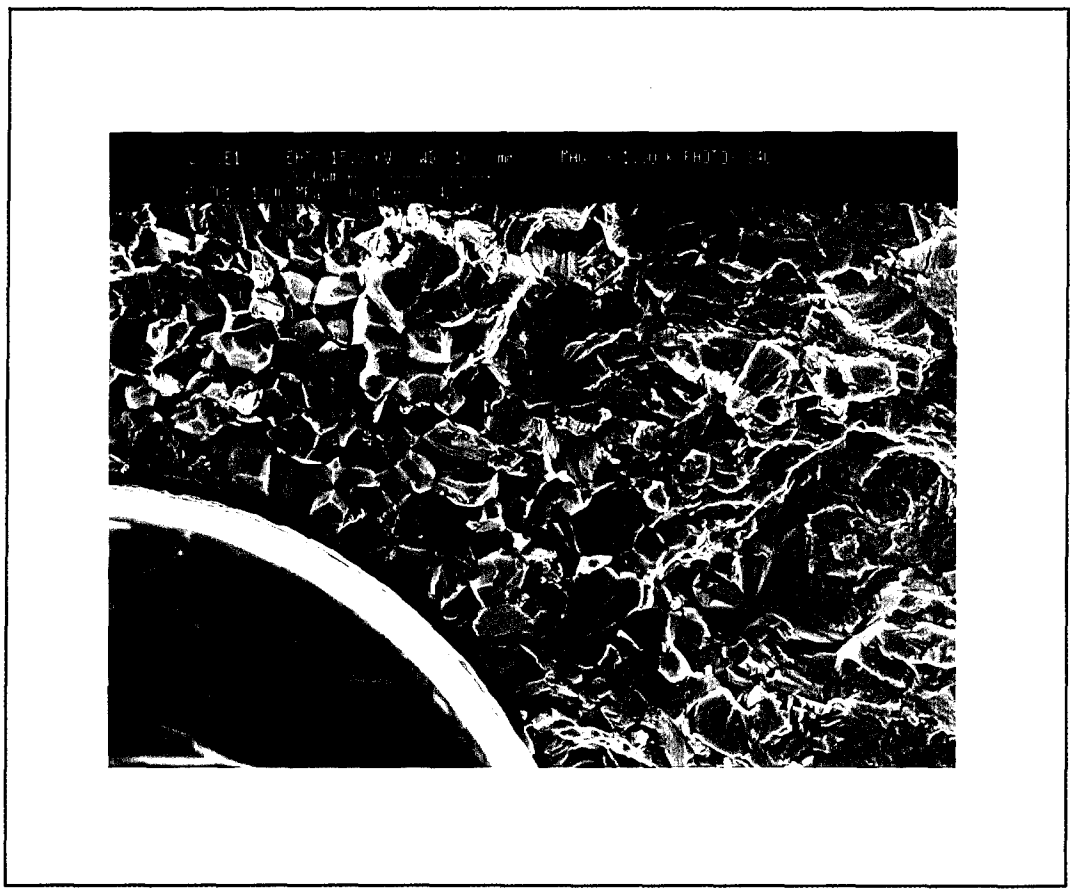

Figure 4.21 Intergranular Decohesion and Granular Cleavage.
1200 MPa, 0.01 Hz, 427°C (1000x)

of the grains. In the specimen cycled at 0.01 Hz, intergranular decohesion was only observed in rings around a few fibers, which was possibly caused by carbon from the fibers that diffused into the matrix during laminate fabrication.

Test frequency affected the amount of matrix cracking at the 1200 MPa maximum stress level, but all of the fracture surfaces showed fiber-dominated failure. The amount of matrix cracking ranged from 4% of the fracture surface of the specimen cycled at 1 Hz to 11% of the fracture surface of the specimen cycled at 10 Hz.

Figure 4.22 Oxidation Precipitates on Grains. 1200 MPa, 0.01 Hz, 427°C (3000x)

4.3.2 Matrix-Dominated Failure Mode (σ_{max} = 800 MPa and 900 MPa)

Four specimens were analyzed at the low maximum stress levels. Three were cycled at frequencies of 10 Hz, 1 Hz and 0.1 Hz, respectively, and 800 MPa maximum stress, and the fourth was cycled at 0.01 Hz and 900 MPa maximum stress. The higher maximum stress level was used to reduce the length of the test (800 MPa at 0.01 Hz would have probably taken more than one month).

Figure 4.23 depicts a flat matrix-cracking region on the fracture surface of the specimen cycled at a frequency of 10 Hz. Fibers in this region cleaved at or near the

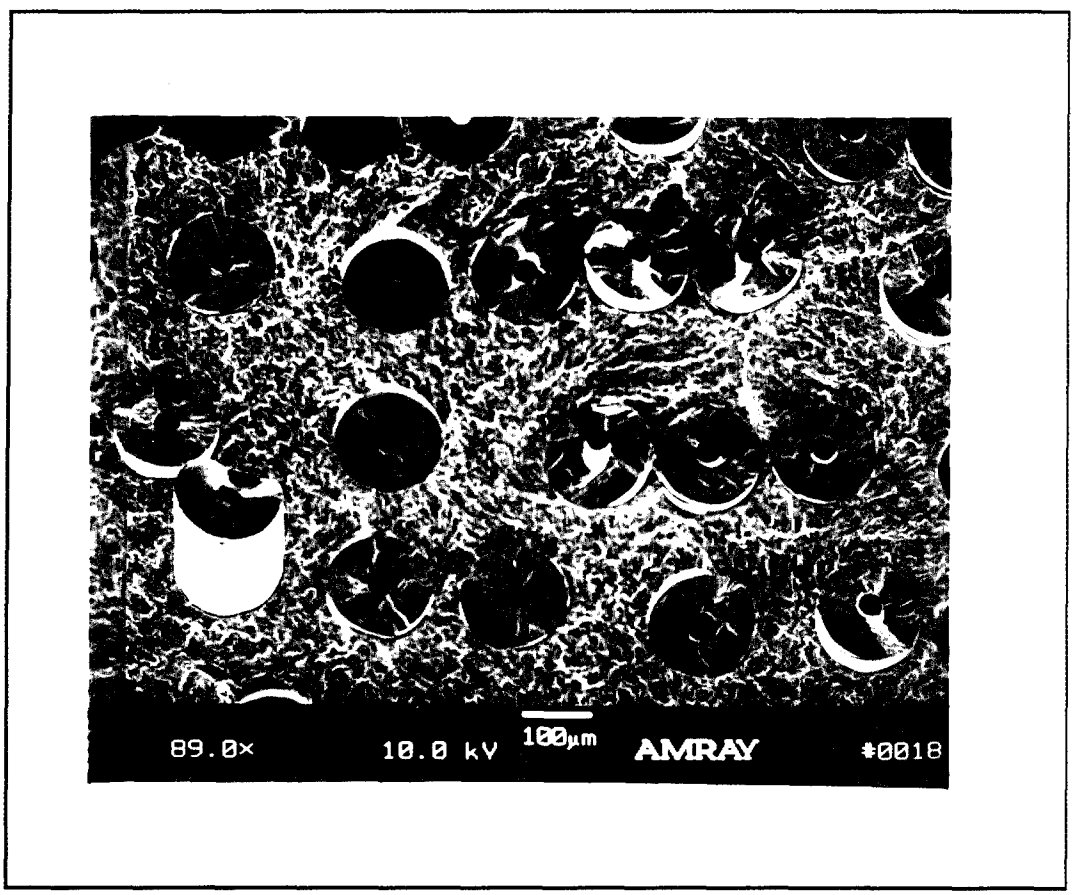

Figure 4.23 Matrix Cracking Region. 800 MPa, 10 Hz, 427°C (89x)

matrix surface and no necking or ductility was present. The entire fracture surface was very flat but consisted of three matrix cracking planes, each extending about one-third the length of the fracture surface. The second plane was offset about 0.2 mm from the first plane and the third plane was offset about 2.0 mm from the second plane. Figure 4.24 shows a triangular-shaped ductile region between the second and third planes, where the surface was very irregular and fibers pulled out from the surrounding matrix. Another ductile region, the width of two fiber rows, extended the length of the first two fracture planes (about 5 mm).

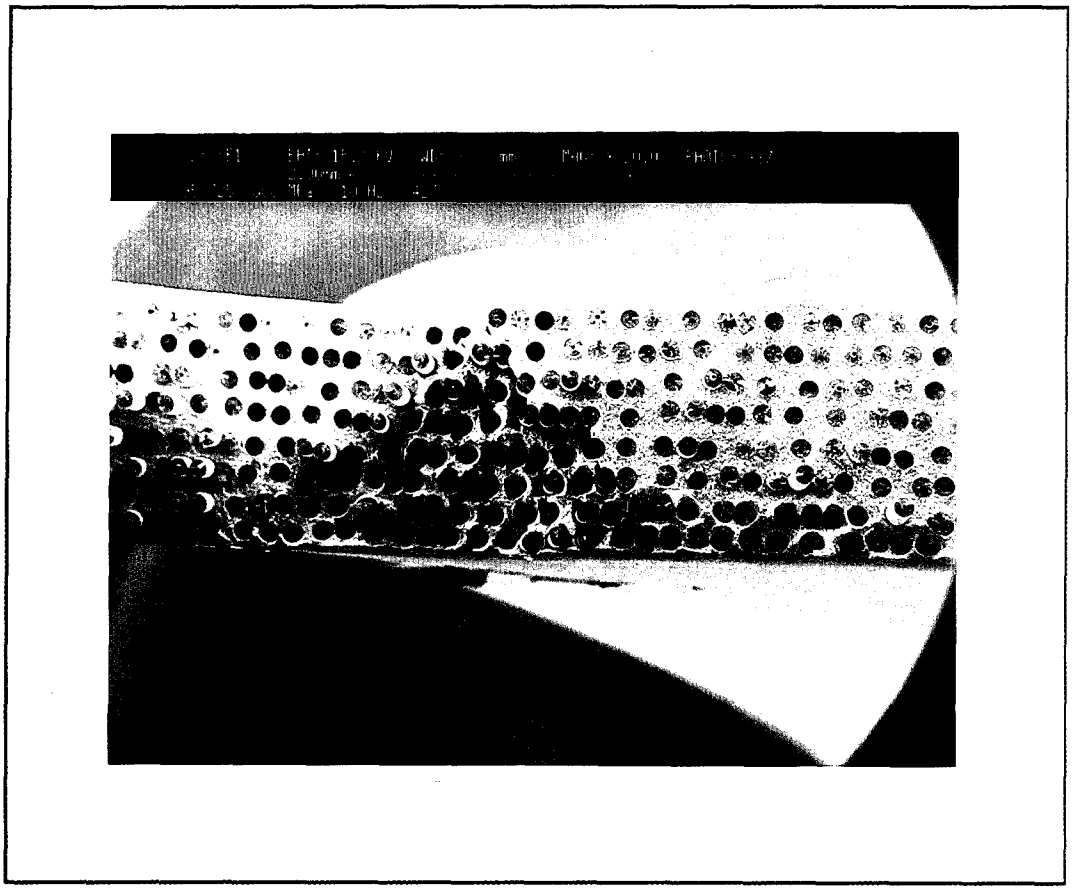

Figure 4.24 Ductile Region Between Two Cracking Planes.
800 MPa, 10 Hz, 427°C (20x)

Macroscopic analysis concluded that this specimen, tested at the lowest stress level and highest frequency of this study (σ_{max} = 800 MPa and f = 10 Hz), experienced the most matrix fatigue cracking of all the specimens tested at 427°C (see Section 4.2.2). About 77% of the fracture surface exhibited laminate cracking. Two or possibly three cracks developed (probably from the edges) and worked their way inward. Fibers began cracking as more and more of the stress was transferred from the matrix. Finally, when crack tips neared each other, the overloaded interior portion fractured, leaving the triangular-shaped ductile region. It is likely that the ductile region along the edge of the first two planes tore when the central triangular region fractured.

The fracture surface of the specimen cycled at 1 Hz was very flat and had only one cracking plane. Matrix cracking was the dominant failure mechanism, and only one small region of ductility was observed along the surface (0.8 mm long). Therefore, almost 100% of the fracture surface consisted of matrix crack growth. Several fibers pulled out of the matrix, but no necking was evident. Normally, the fibers bridge the crack as it advances, but the matrix stress is transferred to the fibers and causes them to break. The presence of fibers broken above and below the cracking surface indicates that the advancing crack caused the fiber/matrix interface to fail first, and then the fiber cracked at a point along the interface separation. Observations from microscopy show that sometimes the fibers cracked at one end of the damaged interface zone, above or below the matrix crack.

Figure 4.25 shows the fracture surface of the specimen cycled at 0.1 Hz. The dominant matrix crack extended about 2.3 mm into the specimen from one edge (or 31% of the specimen surface area), but most of the rest of the specimen experienced ductile failure. Figure 4.26 shows three interior crack regions completely surrounded by ductile matrix failure, and Figure 4.27 shows the transition from matrix cracking to ductile failure in one of these regions. High magnification observations revealed no oxidation damage in these regions, so sufficient matrix creep must have failed weak fibers in the region. These fiber breaks then acted as stress raisers, initiating cracks in the local area. Figure 4.28

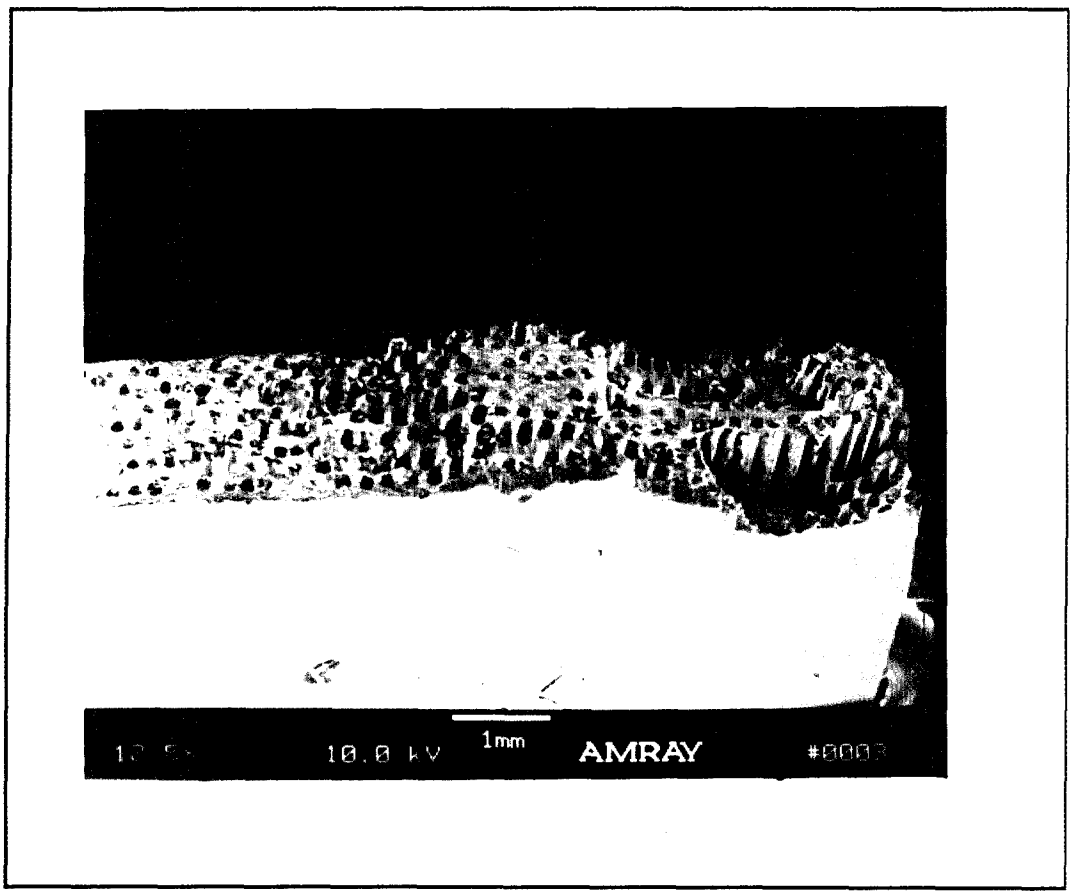

Figure 4.25 Fracture Surface. 800 MPa, 0.1 Hz, 427°C (12.5x)

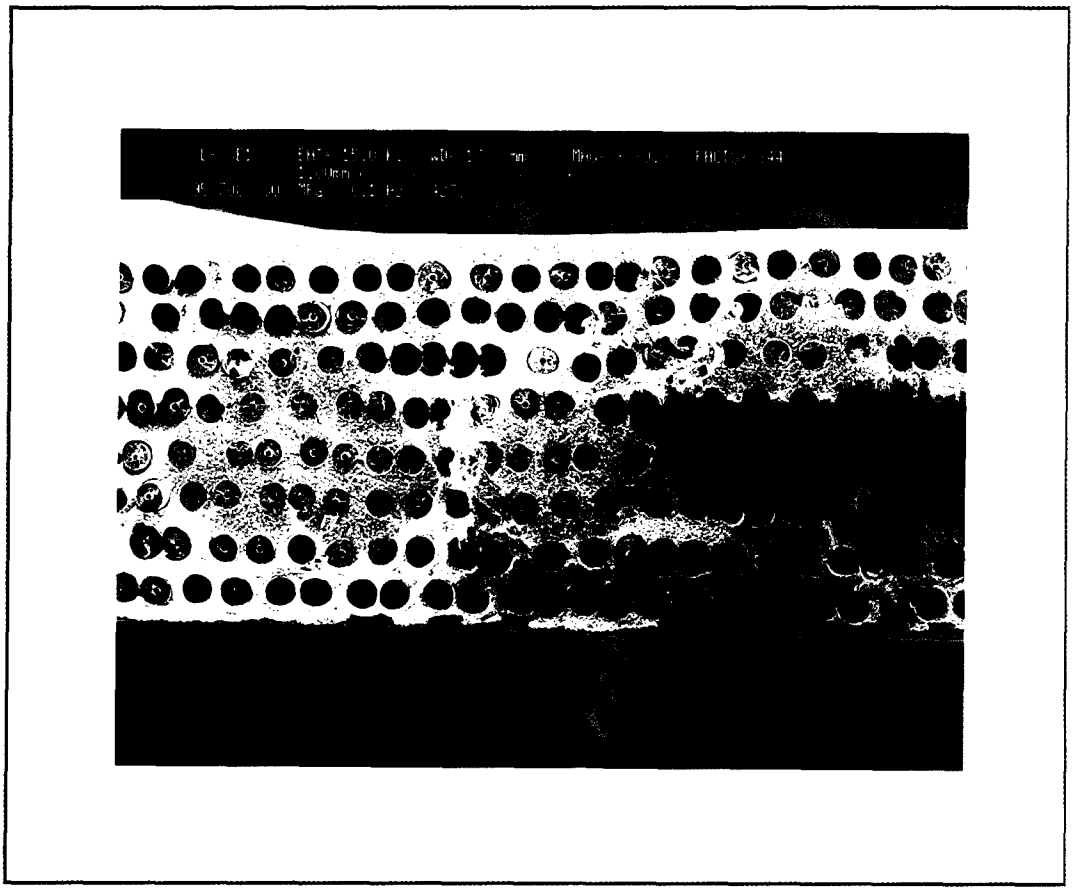

Figure 4.26 Interior Matrix Cracks. 800 MPa, 0.1 Hz, 427°C (30x)

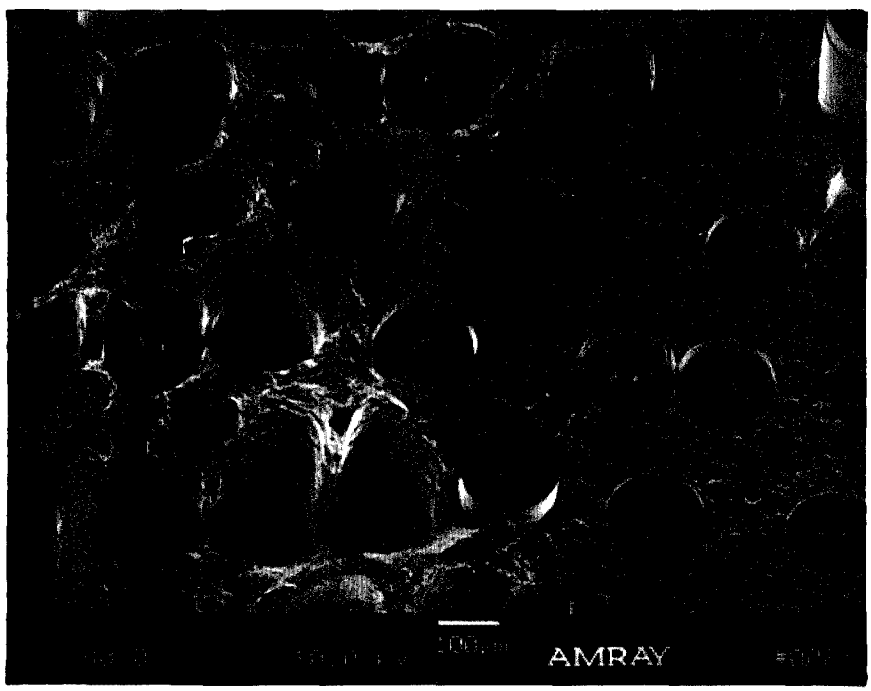

Figure 4.27 Transition from Ductility to Matrix Cracking.
800 MPa, 0.1 Hz, 427°C (80x)

shows one fiber in the center of an interior matrix crack region which appears to have a void in the silicon carbide that surrounds its core. This may be an example of a weak fiber that failed. No obvious fiber damage was apparent in either of the other two interior matrix crack regions.

Since the dominant matrix crack grew to only about one-third of the specimen's width, the mechanisms leading to fracture probably included both creep and matrix fatigue cracking. In the case of cracking, stresses relieved from the matrix were transferred to the fibers which fractured at or near the cracking plane. In the areas of the specimen where

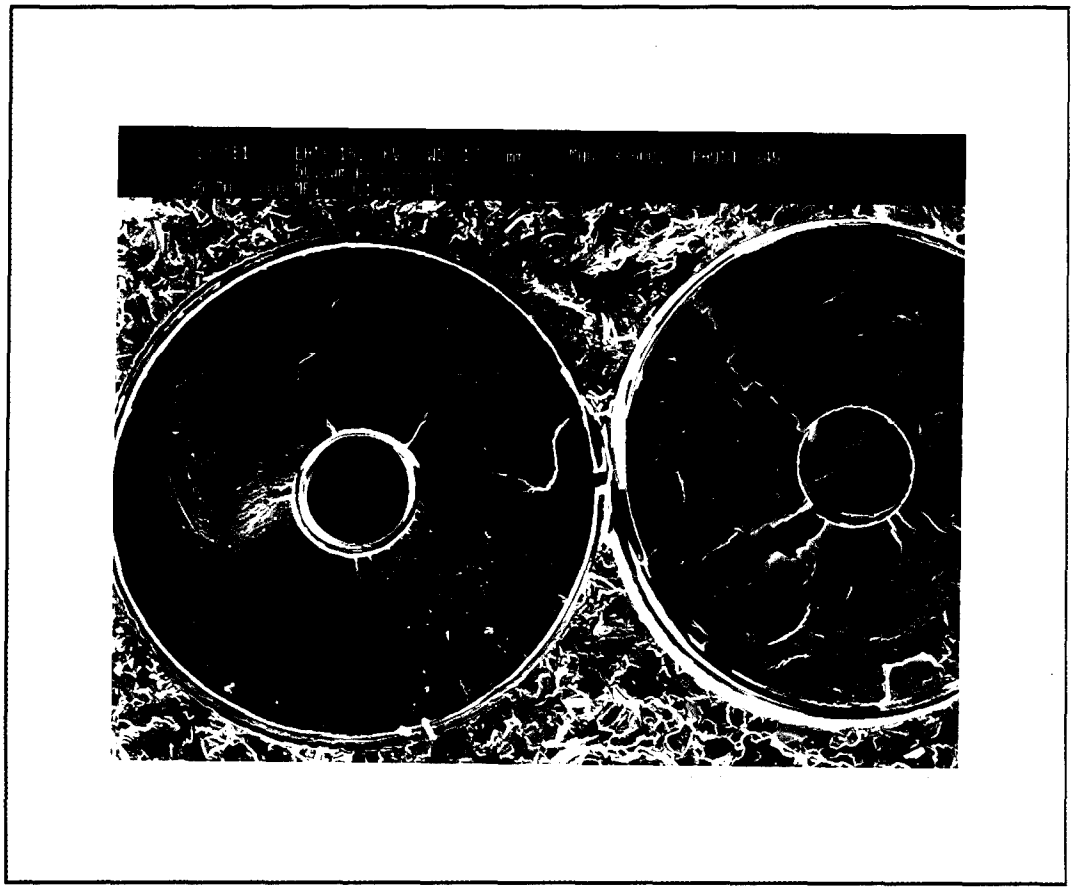

Figure 4.28 Damaged Fiber. 800 MPa, 0.1 Hz, 427°C (500x)

cracks did not initiate, the matrix experienced creep due to the high temperature and low frequency, and as the matrix relaxed, stress was transferred to the fibers. The fibers failed randomly (the weakest first) and then the matrix tore away. The interior crack growth further overloaded the fibers in the vicinity.

The lowest frequency test (0.01 Hz) was run at 900 MPa maximum stress. Macroscopic observations indicated that this specimen experienced almost as much matrix cracking damage as the specimen cycled at 10 Hz and 800 MPa maximum stress (Section 4.2.2). In fact, only two matrix cracks were observed on the fracture surface. Figure 4.29

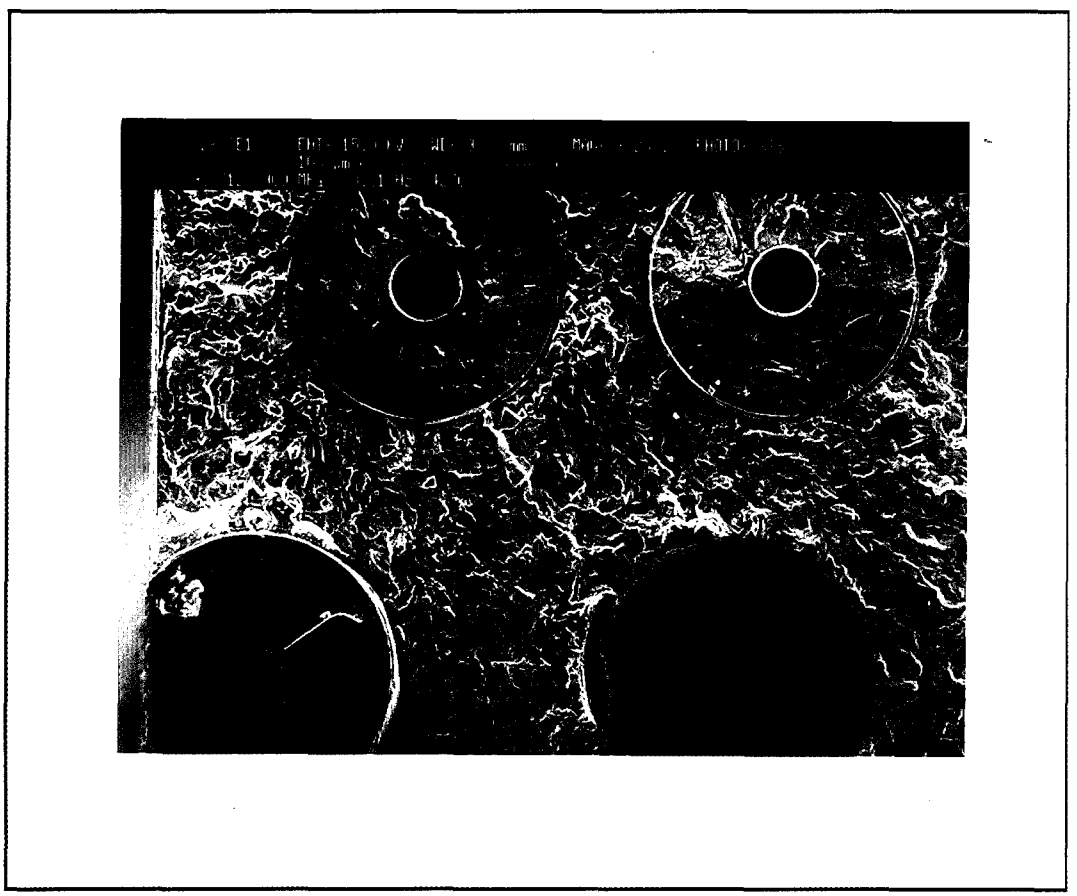

Figure 4.29 Burnt Fiber Cores in Edge Crack. 900 MPa, 0.01 Hz, 427°C (280x)

shows a damaged fiber on the specimen edge which may have initiated a crack that measured 0.8 mm into the specimen and about 1 mm in the thickness (edge) direction. The other crack was located in a corner and had the dimensions 1.6 mm along the specimen surface and 0.8 mm along the edge. Crack growth was only evident on 14% of the total fracture surface, while the remainder of the surface experienced ductile failure as evidenced by matrix necking, fiber pullout and dimpling. This suggests that fatigue behavior was dominated by matrix creep and fiber failure. Matrix cracks are often bridged by fibers, but Figure 4.29 shows oxidized carbon cores within an edge crack. This is evidence that these fibers broke early in the test, soon after the matrix around them cracked, and the 427°C heat burned away the carbon cores for the remainder of the test. The core diameter and amount of oxidation damage on the fiber surface indicates when (relatively) the fiber cracked. Neighboring the two fibers with burnt carbon cores were several with intact cores that probably failed late in the test.

The overall influence of frequency at the stress levels of 800 MPa and 900 MPa was a variation in the amount of matrix cracking. At the highest frequencies, matrix cracking was evident over the entire fracture surface, while the specimen cycled at 0.01 Hz exhibited matrix cracking on only 14% of the fracture surface. As frequency decreased from 10 Hz to 0.01 Hz, it appeared that laminate failure changed from highly matrix-dominated to highly fiber-dominated. This trend will also be reported in the next section, which presents mixed-mode fractography observations.

4.3.3 Mixed-Mode Failure (σ_{max} = 1050 MPa)

Next, fracture surfaces of specimens tested at a maximum stress of 1050 MPa and frequencies from 0.01 Hz to 10 Hz were observed. Each specimen seemed to experience less fatigue cracking than its counterpart at the low stress level, but the amount of cracking and ductility again varied with frequency.

Figure 4.30 shows one end of the fracture surface of the specimen cycled at 10 Hz, where the predominant matrix crack initiated in one corner but grew through the thickness about 1.7 mm into the width of specimen. A narrow, 0.8 mm long surface crack appeared

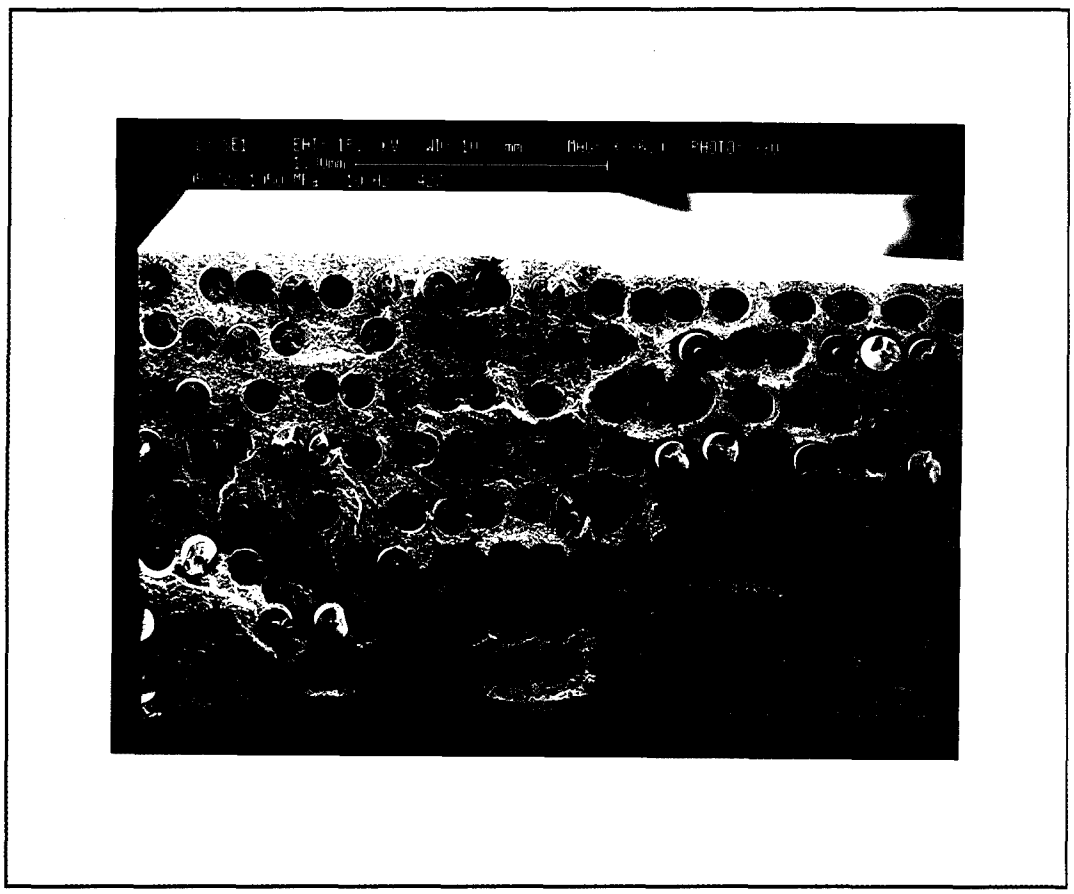

Figure 4.30 Fracture Surface. 1050 MPa, 10 Hz, 427°C (36x)

near the center of the specimen, and an edge crack on the opposite end that included both corners grew about 0.5 mm into the specimen. Therefore, the total through-the-thickness crack growth was about 30% of the total cross-sectional area. This approximates the 31% crack growth observed in the low stress specimen cycled at 0.1 Hz. The specimen probably failed because the matrix cracked enough to overload the reinforcing fibers. Examination of carbon cores revealed no burning, so it is likely that the fibers fractured late in the test.

Figure 4.31 shows a similar corner crack in the specimen cycled at 1 Hz, which

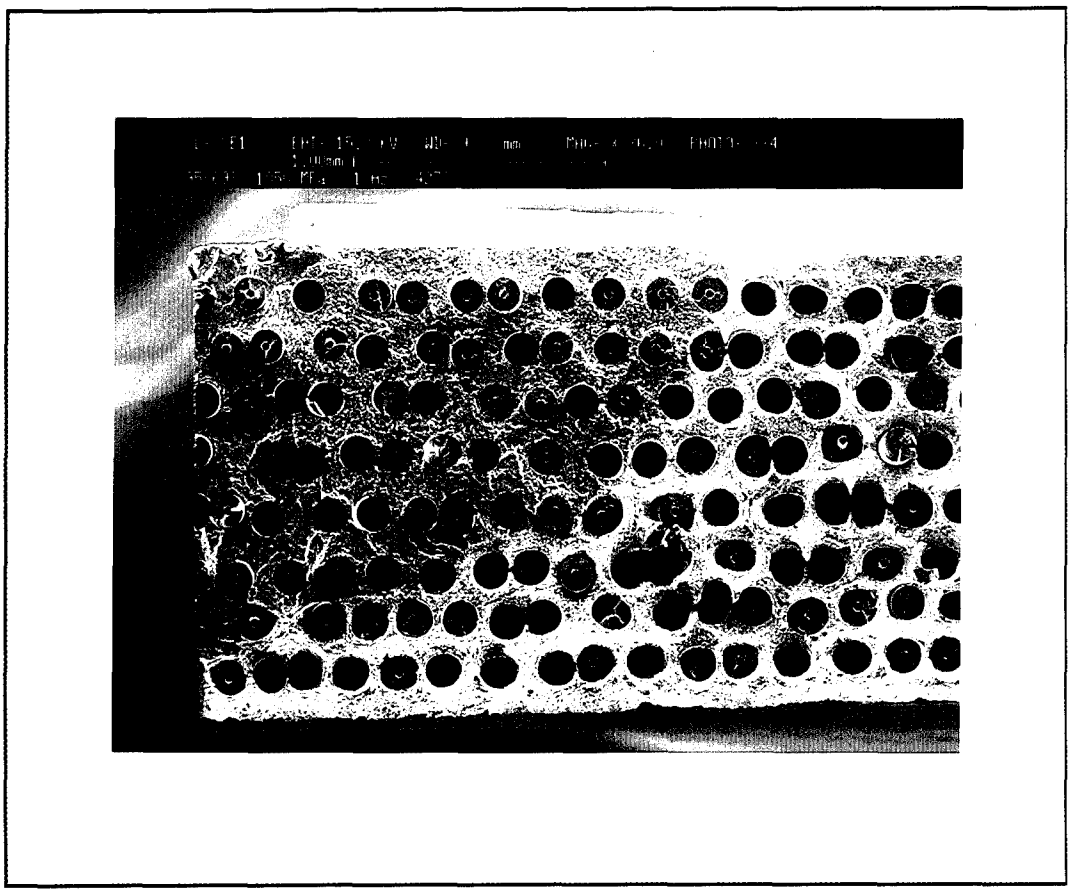

Figure 4.31 Fracture Surface. 1050 MPa, 1 Hz, 427°C (36x)

measured 1.9 mm in the surface direction and 1.7 mm in the edge direction. The only other crack was located on the opposite edge and grew roughly 0.3 mm, and the equivalent through-the-thickness crack growth was estimated to be 20% of its fracture surface. Most fiber cross-sections within the matrix crack region were clean, which indicated late fracture, but other fibers had oxidation damage. Figure 4.32 shows a clean, undamaged fiber in the cracked region (0.45 mm from the corner), while the fiber in Figure 4.33 exhibits oxide damage including flaking of the core (0.65 mm from the corner).

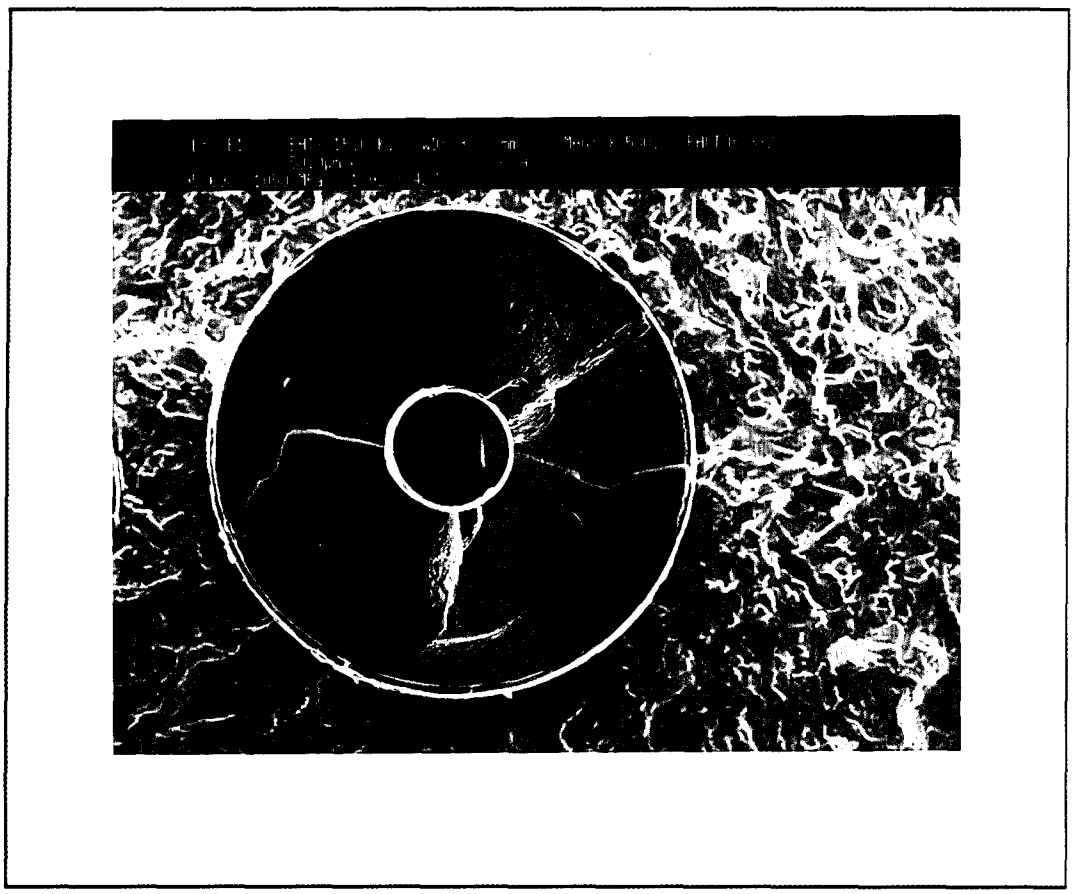

Figure 4.32 Clean, Undamaged Fiber. 1050 MPa, 1 Hz, 427°C (500x)

In the specimen cycled at the lower frequency of 0.1 Hz, fracture was dominated by matrix creep, which led to random fiber failure and ductile matrix failure. The largest matrix crack was a semicircular edge crack, and the equivalent through-the-thickness crack growth was about 6% of the fracture surface. Like the test at 800 MPa and the same frequency, this fracture surface also happened to contain a possible interior crack, as shown in Figure 4.34. The region was located near the mid-width, but very close to the

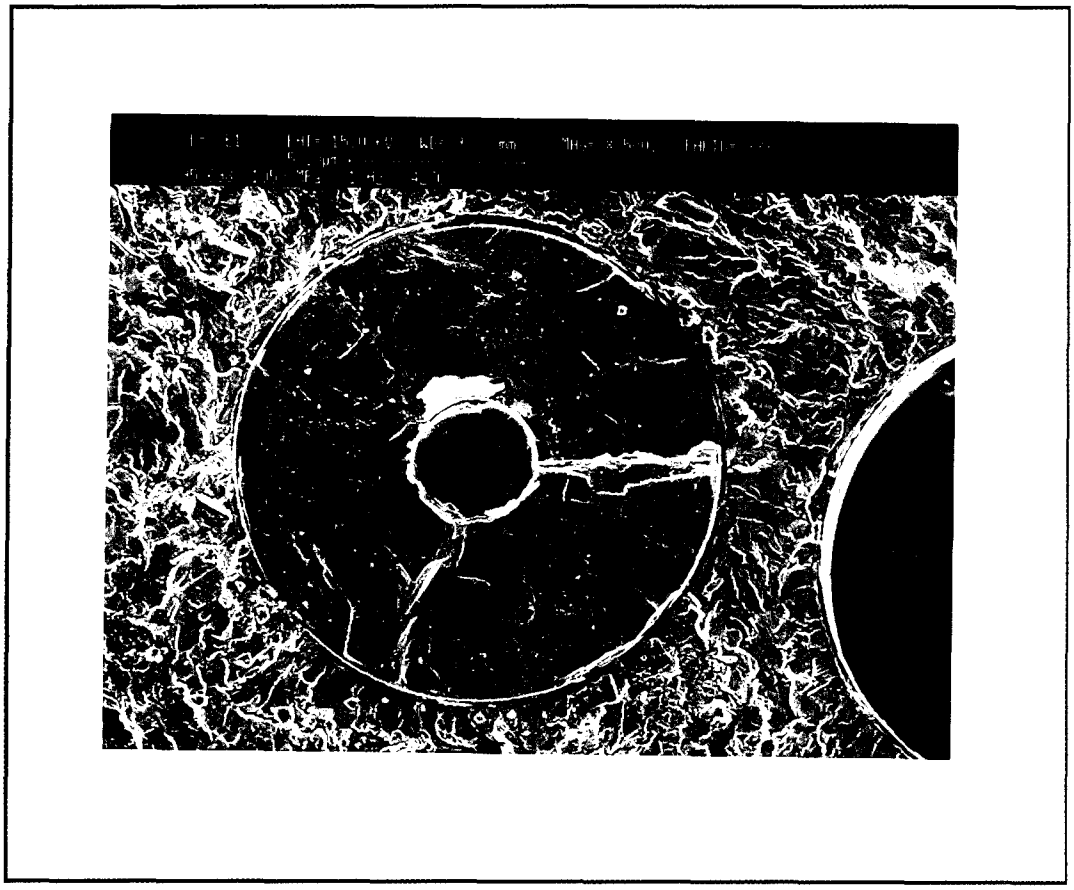

Figure 4.33 Oxide Damage on Fiber and Flaking of the Core.
1050 MPa, 1 Hz, 427°C (500x)

specimen surface. It was surrounded on three sides by ductility, but the fourth side was hidden by a "step" in the fracture surface. No cracks were visible on the specimen surface near the step, so it is likely that the crack originated within the specimen. Inspection of this region revealed that the core of the centermost fiber was partially pulled out. It also appeared that there was an air pocket on one side of the same fiber. This is not conclusive evidence, but cracking may have initiated at a break in this fiber.

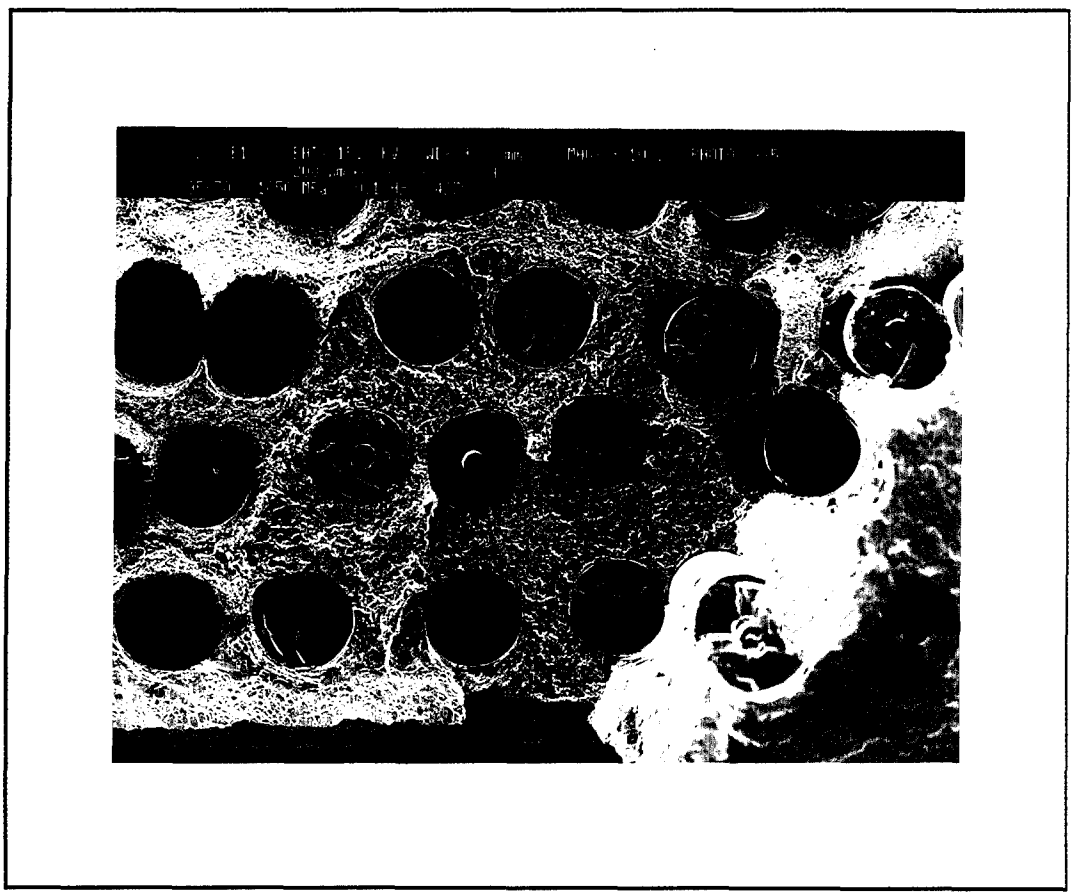

Figure 4.34 Possible Interior Matrix Crack. 1050 MPa, 0.1 Hz, 427°C (100x)

The most creep-dominated failure at this stress level occurred in the specimen cycled at 0.01 Hz. Figure 4.35 shows the only crack observed which was on a surface near one edge, which measured 0.8 mm in the edge direction and 1.3 mm in the surface direction. In addition to more matrix creep at this low frequency, the elevated temperature tended to embrittle the specimen, giving dominance to fewer cracks. About 7% of the surface exhibited matrix cracking.

Failure mechanisms in tests conducted at 1050 MPa maximum stress were highly dependent on frequency. The specimens cycled at 10 Hz and 1 Hz exhibited matrix

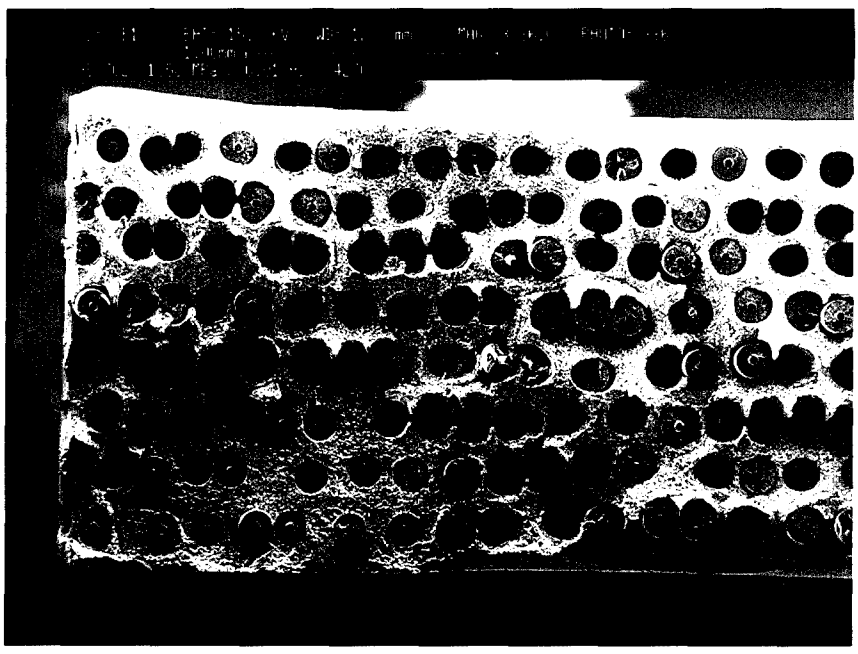

Figure 4.35 Fracture Surface. 1050 MPa, 0.01 Hz, 427°C (36x)

cracking on 20% to 30% of their surfaces, while cracking was limited to 6% and 7% in the specimens cycled at the lower frequencies. This clearly shows a shift from matrix- to fiber-dominated failure between the test frequencies of 1 Hz and 0.1 Hz.

4.3.4 Effects of Higher Test Temperature

It has been shown in the previous sections that increasing the stress level and decreasing the test frequency caused the SCS-6/Ti-6-4 composite to fracture with less matrix cracking and more creep-induced fiber failure. Two fractured specimens, tested at 538°C and cycled at 0.1 Hz, were examined to see the effects of higher test temperature on fracture mechanisms. The maximum stress levels for the two tests were 800 MPa and 1050 MPa.

The specimen tested at 800 MPa maximum stress failed under the mixed modes of matrix-cracking and ductile overload. The sole matrix crack grew 1.7 mm from the edge into the specimen (23% of the fracture surface). At the same maximum stress and frequency, 31% of the fracture surface of the specimen tested at 427°C exhibited matrix cracking. Observations of broken fibers in the crack plane showed oxidation damage. This damage was greatest near the specimen edge and decreased toward the center of the specimen. Burnt cores revealed that a few of the fibers cracked early in life, possibly at the same time the matrix crack was advancing. A high-magnification view of the cracked region showed cleaved grains, but the characteristics of intergranular decohesion were not apparent.

The specimen tested at a maximum stress of 1050 MPa exhibited a small edge crack on its fracture surface that measured 0.4 mm x 0.4 mm and an interior center crack that measured 0.4 mm x 0.5 mm. This evidence from cracking covered only about 2% of the fracture surface area. Like interior cracks in other specimens, it is likely that sufficient creep failed a fiber in that area which initiated matrix cracking. Figure 4.36 shows significant intergranular decohesion in the matrix cracking region, which further supports the conclusions of a creep-dominated response. Higher temperatures often lead to more oxidation which can embrittle the matrix, and therefore increase crack growth. However,

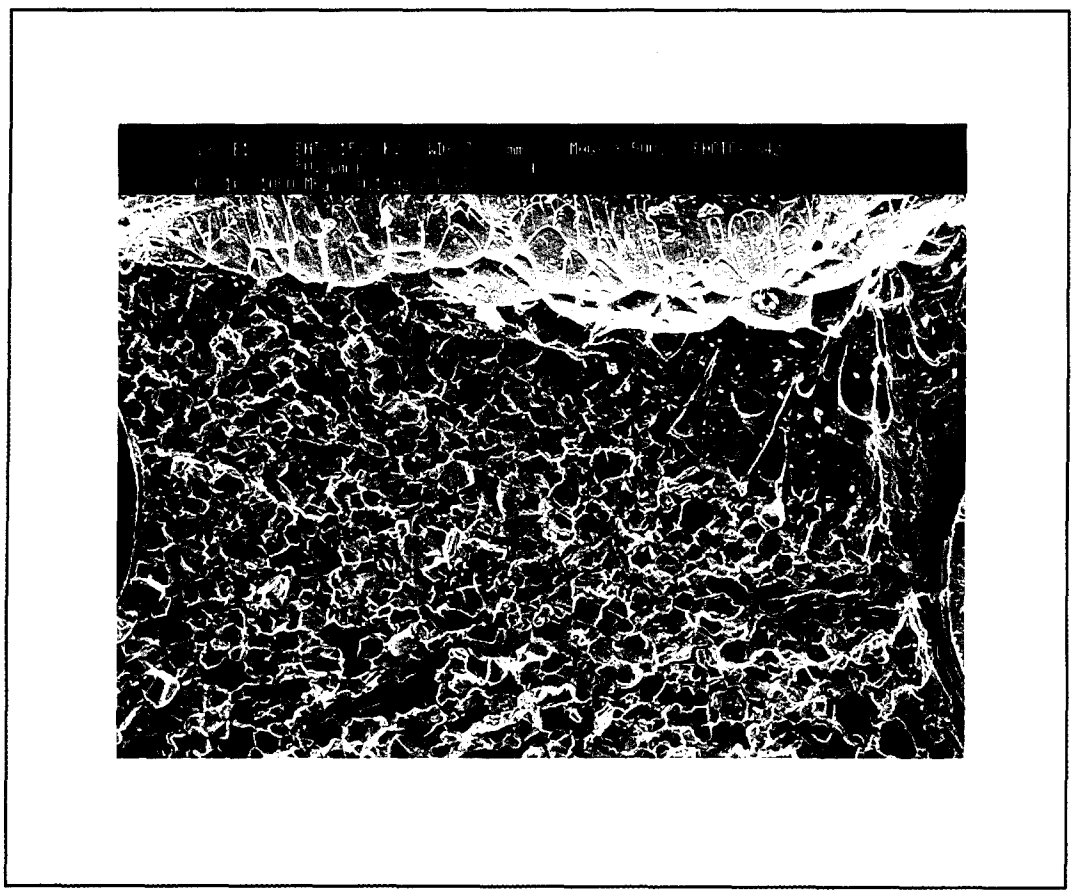

Figure 4.36 Intergranular Decohesion. 1050 MPa, 0.1 Hz, 538°C (500x)

both of these specimens showed that testing at 538°C increased the extent of ductile failure from creep and lessened matrix cracking.

4.3.5 Summary of Fractography Observations

The fracture mechanisms of SCS-6/Ti-6-4 were established from fracture surface observations of specimens tested at various frequencies and maximum stresses, and at temperatures of 427°C and 538°C. Close attention was paid to fracture surface features that evidenced brittle matrix cracking or ductile overload. The extent of matrix crack regions were compared so that the effects of cyclic frequency, maximum stress level, and temperature could be understood.

Brittle matrix crack regions were found on every fracture surface. A few matrix cracks originated on the specimen surface and grew into the thickness, but the majority originated at the corners of the fracture surface and at the specimen edges, and grew into the specimen width. In many cases cracks seemed to initiate at broken fibers or edge damage incurred from machining. These crack growth regions were characterized by flat surfaces where fibers broke at or near the plane of the matrix crack. The condition of the fiber cores suggested that most fibers bridged matrix cracks and fractured late in life. Observations under high magnification revealed that matrix cracking occurred mostly by transgranular cleavage; however, intergranular decohesion was evident in specimens that experienced more creep due to lower test frequencies, higher maximum stresses and higher temperatures.

Specimens tested at higher stresses exhibited ductile matrix failure throughout the fracture surface. Matrix cracks still existed on edges and in corners, but overall failure was fiber-dominated. The stress transferred from the relaxed matrix to the fibers which resulted in random cracking of the weakest fibers first, and eventually all other fibers. When a fiber broke early in the life of the specimen, a matrix crack sometimes initiated in the interior of the specimen. Intergranular cracking in these regions suggested the influence of creep. Once several fibers had broken, the unreinforced matrix pulled apart, leaving the characteristic ductile, dimpled surface with matrix necking and fiber pullout. Failure was fiber-dominated in specimens cycled at all frequencies, but the amount of matrix cracking increased as test frequency increased. Figure 4.37 shows the relationship between cyclic frequency and the amount of fatigue crack growth observed at each maximum stress level.

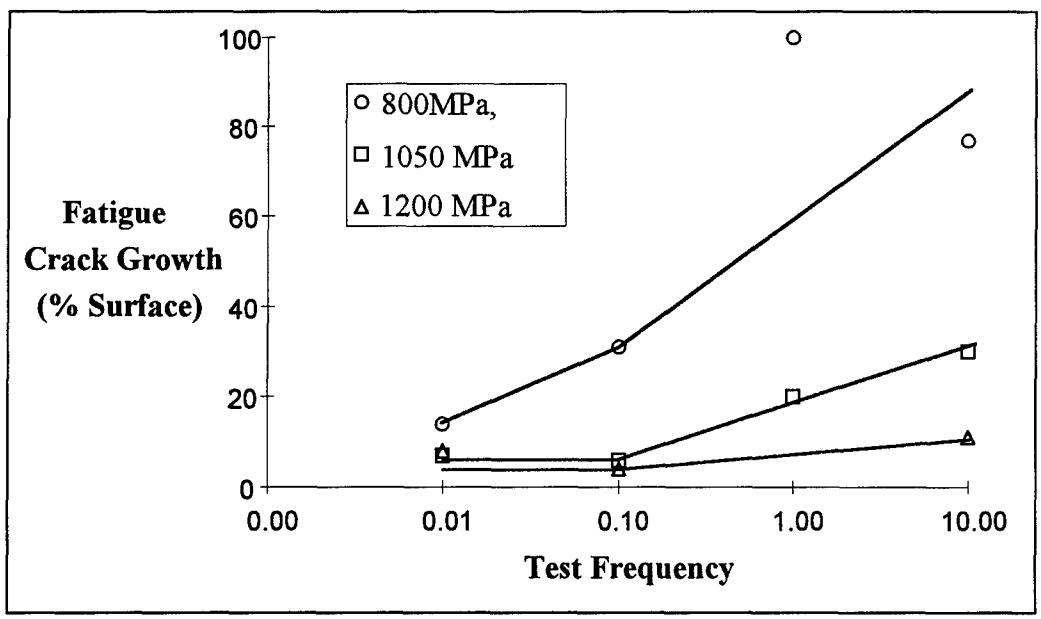

Figure 4.37 Fatigue Crack Growth vs. Test Frequency

Matrix cracking dominated the fracture of specimens at lower stress levels, but the amount of crack growth increased as frequency increased. When multiple cracks grew on different planes, regions of ductility were observed between the planes. Fibers apparently were overloaded and eventually broke as the matrix cracks advanced, leaving small areas of the specimen cross-section to bear the entire tensile load. Fibers in this region cracked under the load, and the weak matrix pulled apart in a ductile manner. These regions were easily identified by irregular surfaces with random fiber pull-out and matrix necking surrounding the fibers.

At the 1050 MPa maximum stress level, the dominant mechanism of failure depended on test frequency. Although all the fracture surfaces exhibited ductility, crack growth was observed on 20% to 30% of the surfaces of the specimens cycled at 1 Hz and 10 Hz, which indicated that the failure of these specimens was matrix-dominated. However, specimens cycled at the lower frequencies exhibited very little crack growth and so failure was dominated by random fiber failure.

Fracture surfaces of two specimens tested at 538°C, frequency of 0.1 Hz, and maximum stress levels of 800 MPa and 1050 MPa, revealed that increased temperature caused specimen failure to be more fiber-dominated. Crack growth at the 800 MPa maximum stress level was observed on 23% of the surface, compared with 31% on the surface of the specimen tested at 427°C, and crack growth at the 1050 MPa maximum stress level was observed on 2% of the surface, compared with 6% on the surface of the specimen tested at 427°C.

4.4 Microscopic Observations--Microscopy

Fracture surface observations provided the evidence for determining failure mechanisms, but microscopy revealed the condition of the fibers and matrix directly behind the fracture surface. Specimens were sectioned so that the face could be ground and polished down to the first layer of fibers. Each sample was about 1 cm long, and the width of the specimen.

Microscopy observations are again categorized by maximum stress levels that led to fiber-dominated, matrix-dominated and mixed-mode failure. A comparison of specimens fatigued at different frequencies at each stress level is presented and inferences of fatigue response and failure mechanisms are discussed. All microscopic observations were performed on specimens tested at 427°C, and several photographs of laminate damage are included.

4.4.1 Fiber-Dominated Failure Mode (σ_{max} = 1200 MPa)

In general, more fiber cracking than matrix cracking was observed at the 1200 MPa maximum stress level, but the amount of fiber/matrix interface damage varied with frequency. The sample of the specimen cycled at 10 Hz revealed fiber/matrix interface damage throughout the specimen. This damage was indicated by dark gaps between the fiber and matrix constituents. No fibers were broken completely, but small fiber cracks appeared randomly throughout the sample. Figure 4.38 shows a matrix crack found in the center of the sample. The crack was bridged by two fibers, and one fiber had a longitudinal crack that connected two transverse cracks. It is likely that damage in this

fiber initiated the interior matrix crack. No other matrix cracks were found in this specimen.

No matrix cracks were found in the 0.1 Hz sample, but one interior fiber was fractured. Figure 4.39 shows this fractured fiber and the initiation of a crack in the matrix bonded to the fiber, which again is evidence that interior matrix cracks often result from fractured fibers. Like the specimen observed at 10 Hz, this sample contained interfacial damage on most fibers across its width, but the cracking was less extensive. Interestingly, little interfacial damage was found near the one observed fiber crack.

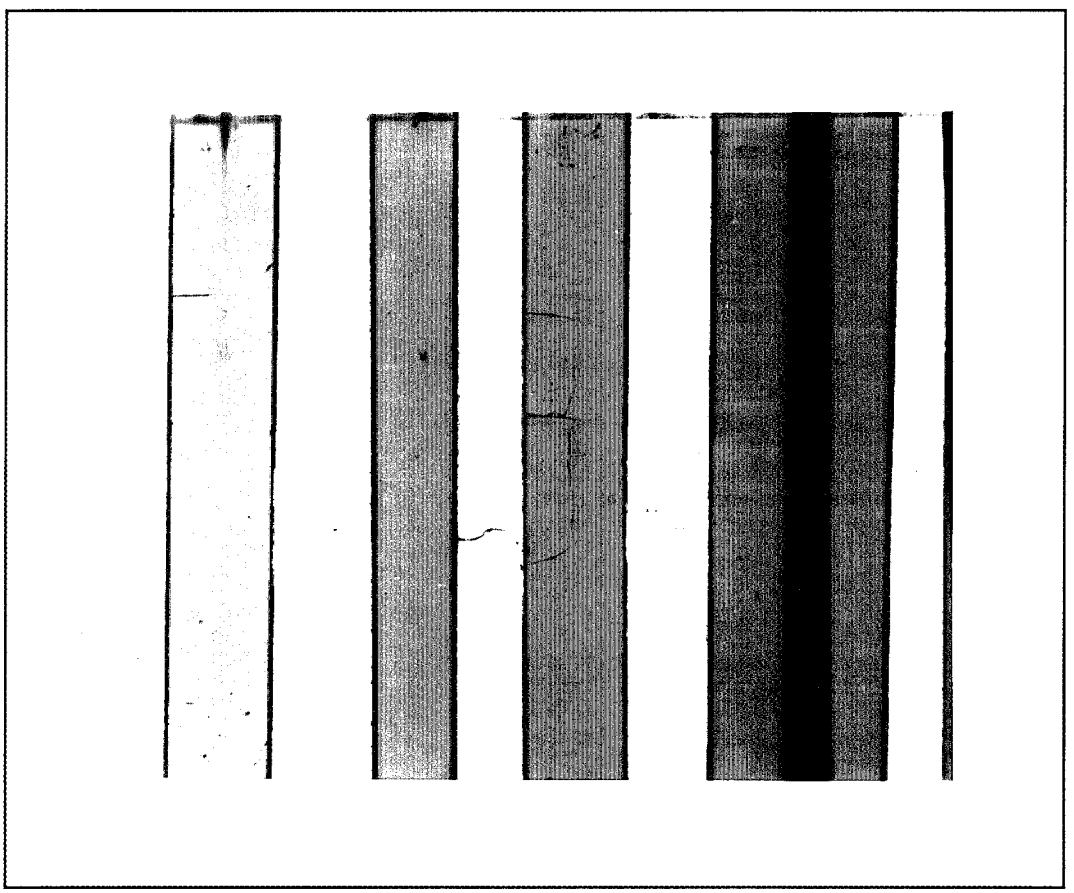

Figure 4.38 Interior Matrix Crack. 1200 MPa, 10 Hz, 427°C (100x)

The maximum extent of fiber damage was observed in the specimen tested at 0.01 Hz and 1200 MPa maximum stress, where small cracks were found in almost every fiber but very little interfacial damage was observed. Figures 4.40 and 4.41 show that matrix cracks initiated where fiber damage was greatest, and Figure 4.42 indicates that some fibers cracked because of matrix voids between them.

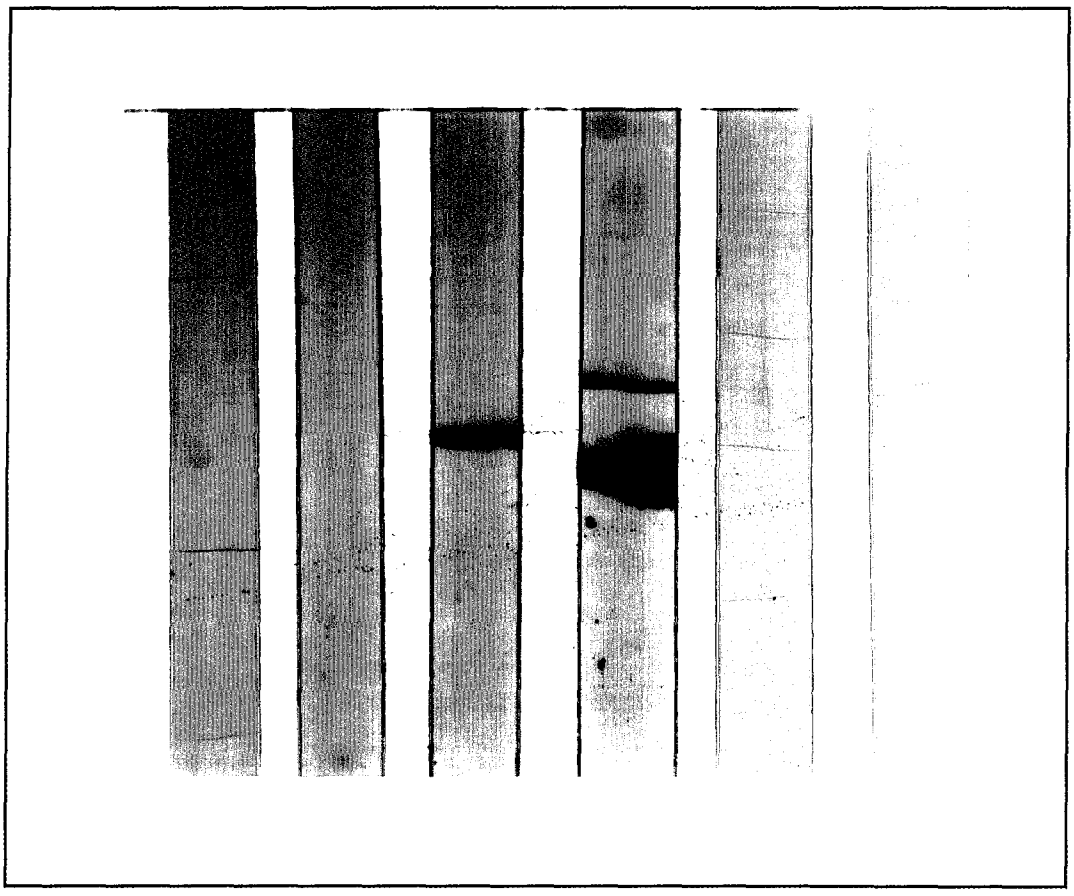

Figure 4.40 Fiber Fracture and Matrix Cracking. 1200 MPa, 0.01 Hz, 427°C (100x)

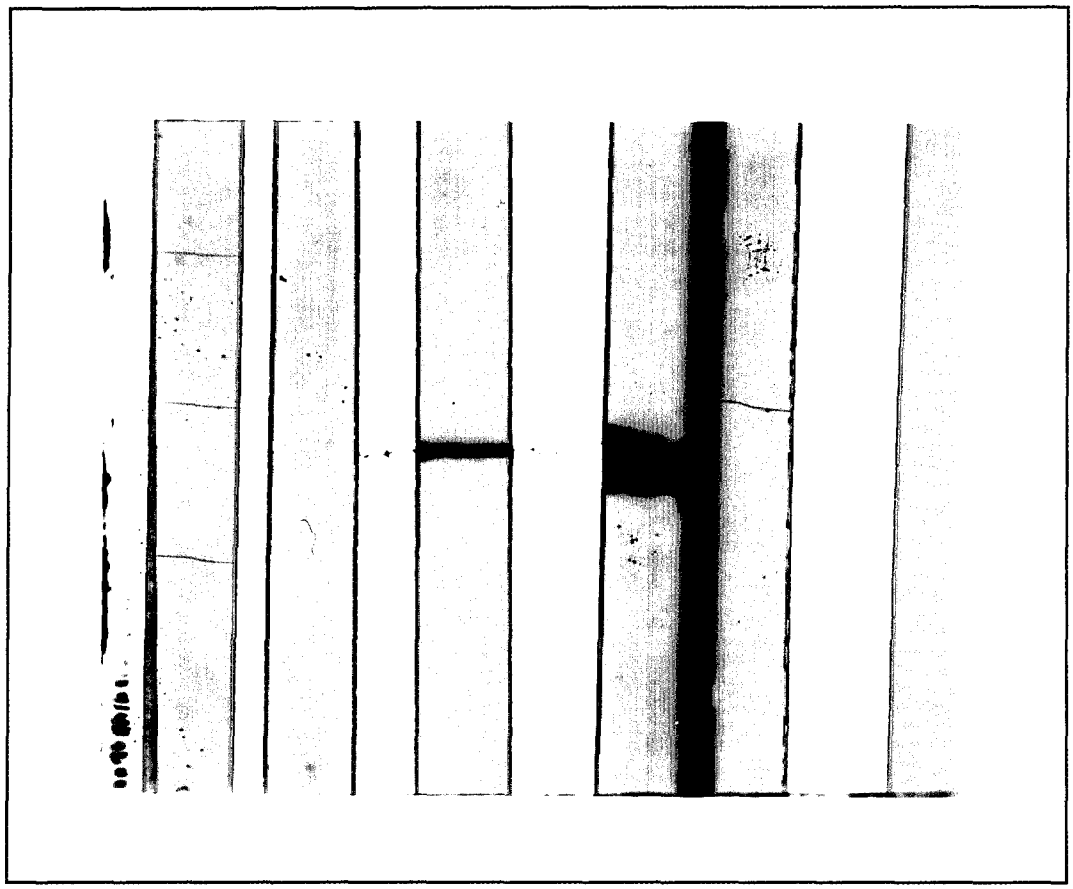

Figure 4.41 Fiber Fracture and Matrix Cracking. 1200 MPa, 0.01 Hz, 427°C (100x)

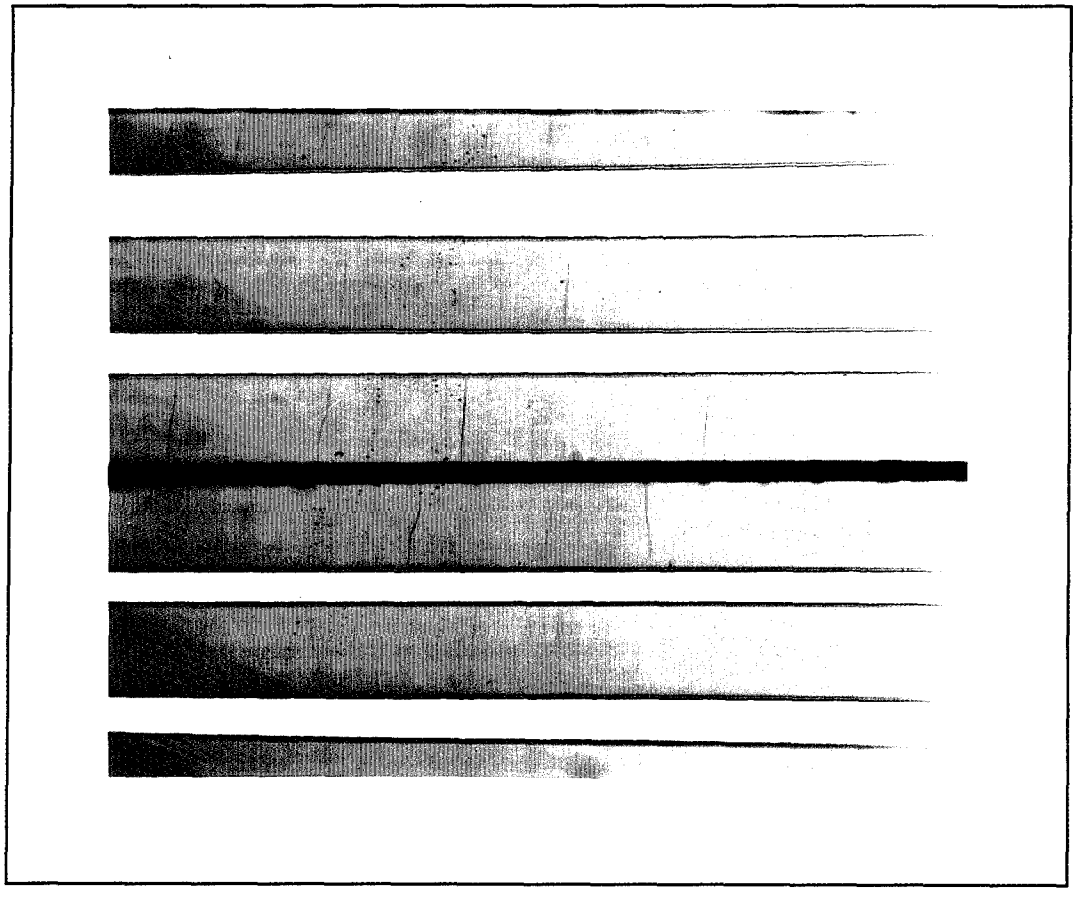

Figure 4.42 Matrix Void and Fiber Cracks. 1200 MPa, 0.01 Hz, 427°C (100x)

4.4.2 Matrix-Dominated Failure Mode (σ_{max} = 800, 900 MPa)

Of all the specimens, the most matrix cracking was evident in the one cycled at 10 Hz and 800 MPa maximum stress. There were five cracks in the matrix on one side of the sample that all originated at damage sites on the edge of the specimen. These cracks propagated perpendicular to the loading direction, each crossing, but not cracking, five to eight fibers. Figure 4.43 shows two such matrix cracks. Fiber bridging was also noted by Sanders and Kraabel in similar tests of the SCS-6/Ti-15-3 composite [15,26]. The fibers

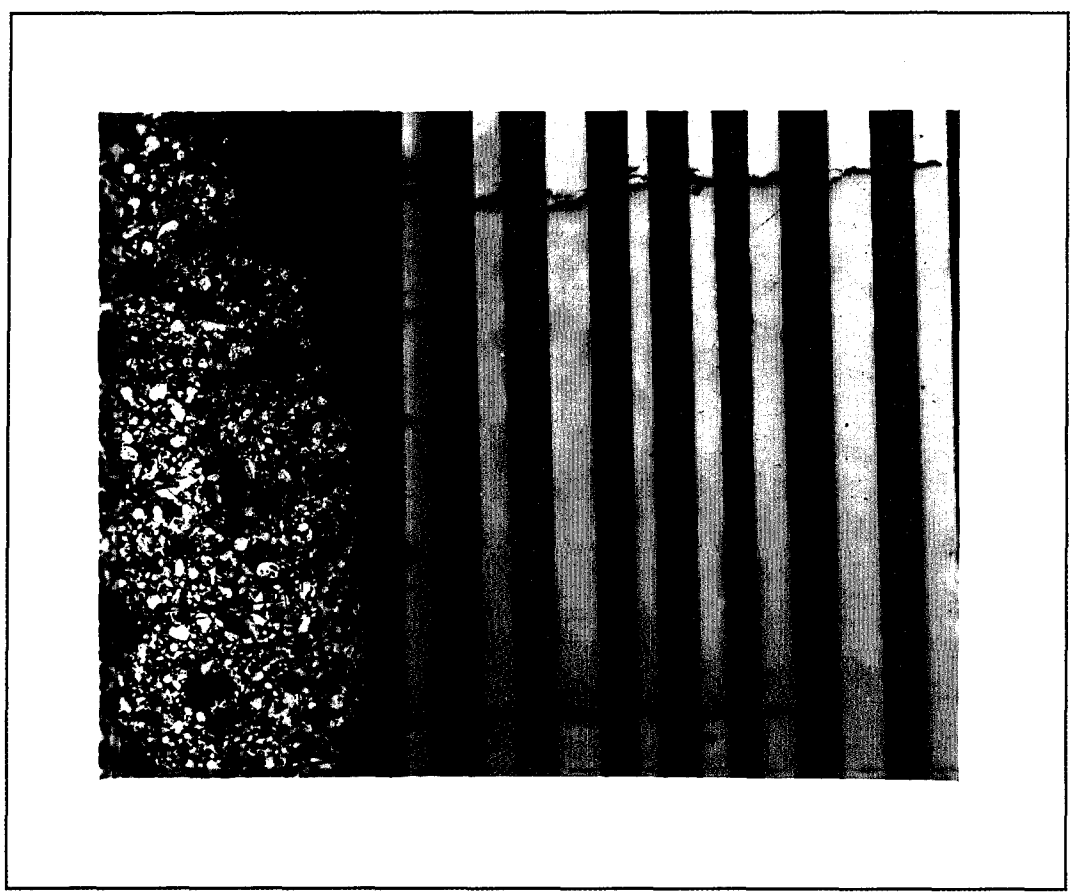

Figure 4.43 Fiber Bridging and Extensive Interface Damage.
800 MPa, 10 Hz, 427°C (50x)

intersected by the matrix cracks were much stronger than the matrix in which the cracks were growing, and as the crack progressed around the fiber, the weak and brittle fiber/matrix interface often cracked. In most cases of matrix cracking dominated fatigue response, matrix cracks continue to grow and load is transferred to the fibers. When the fibers can no longer withstand the increased stress, they fracture in a brittle manner. An interior crack shown in Figure 4.44 that seemed to originate from one or two broken fibers, grew to span eighteen fibers. Figure 4.45 is a photo of one of the damaged fibers within the interior crack. It is likely that this fiber failed first, causing fiber/matrix interface damage and the initiation of the matrix crack.

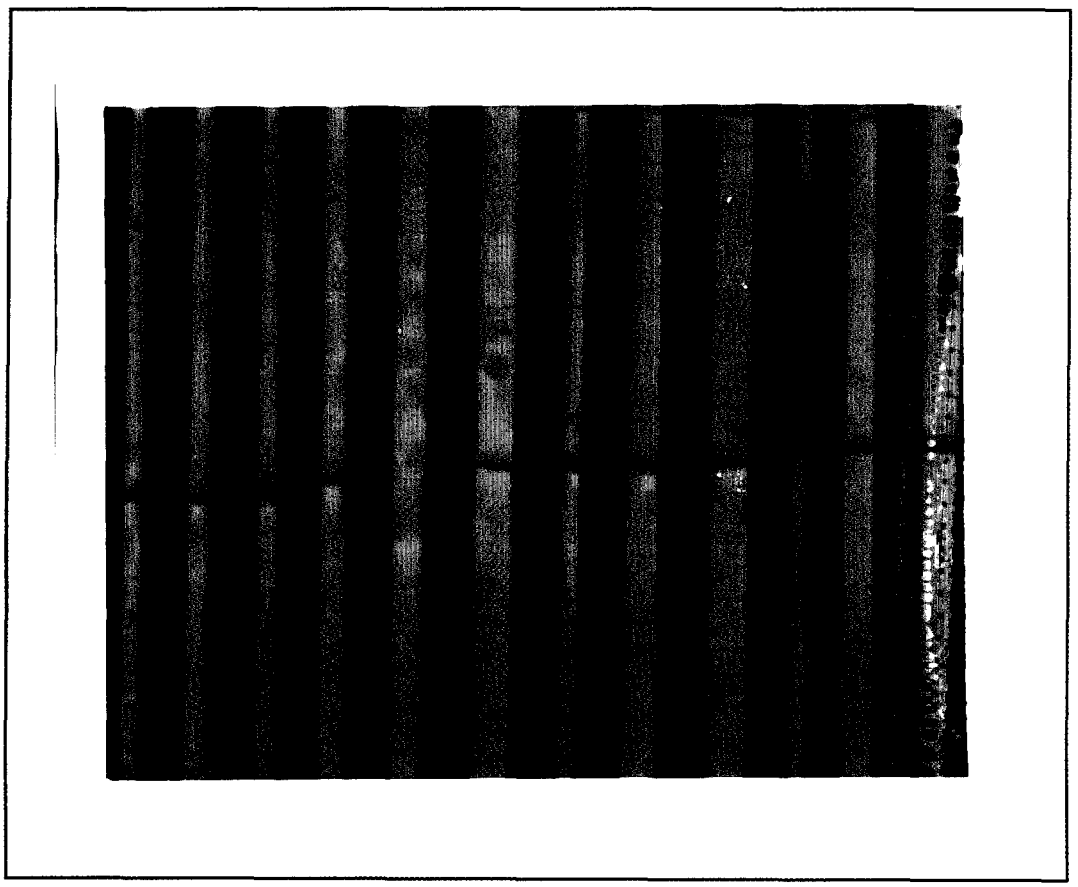

Figure 4.44 Interior Crack and Fiber Damage. 800 MPa, 10 Hz, 427°C (50x)

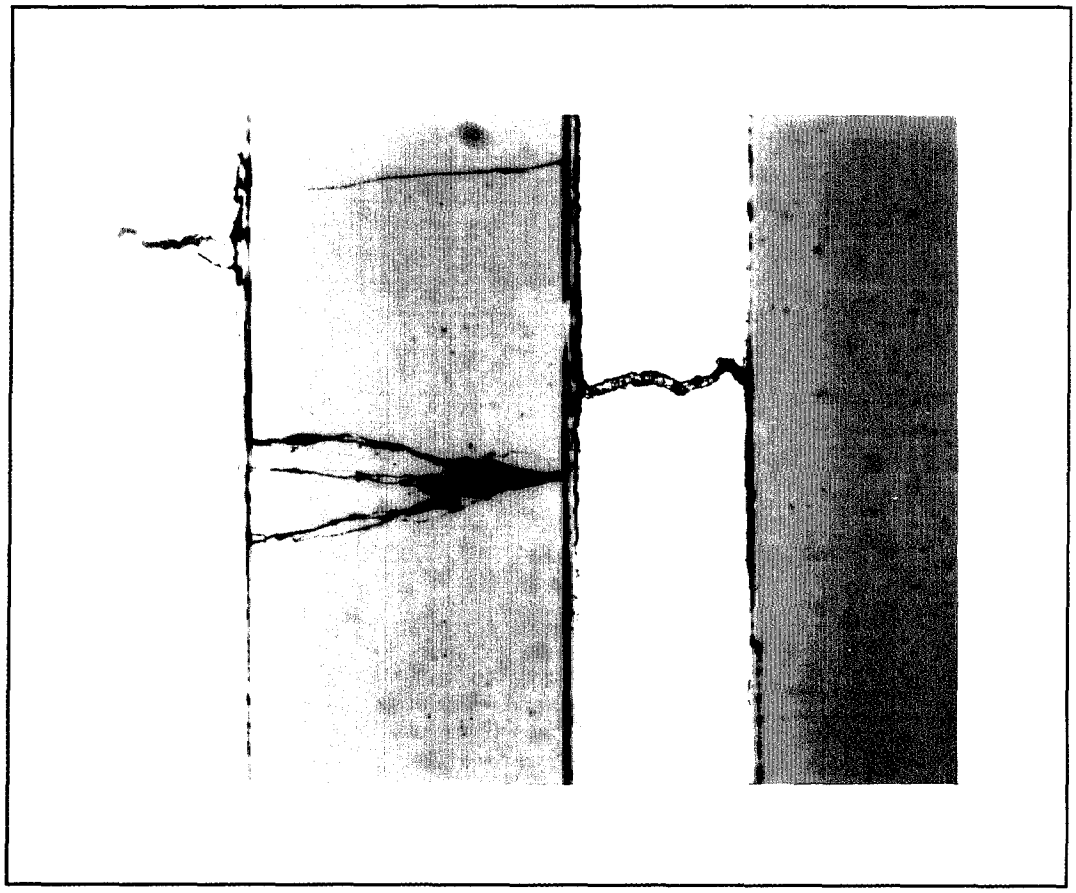

Figure 4.45 Damaged Fiber. 800 MPa, 10 Hz, 427°C (400x)

Microscopy observation of the specimen cycled at 1 Hz revealed only two edge cracks, one bridged by a single fiber and the other by six fibers. Figure 4.46 shows one of the larger of the two edge cracks, and Figure 4.47 shows how the matrix crack caused damage to the fiber/matrix interface. A fine fiber crack is also visible in this figure that was possibly caused by the stress concentration in the area. Interface debonding was observed on fibers throughout the sample.

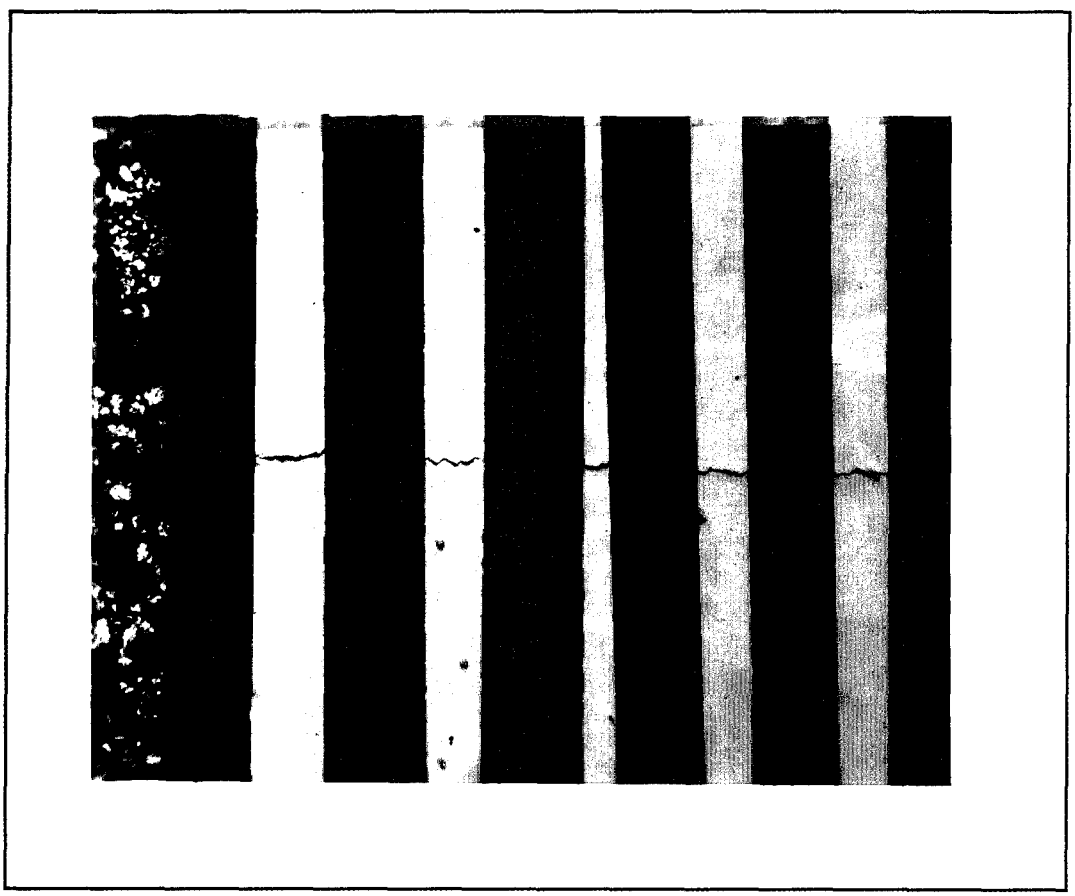

Figure 4.46 Matrix Crack Initiated at Damaged Edge.
800 MPa, 1 Hz, 427°C (100x)

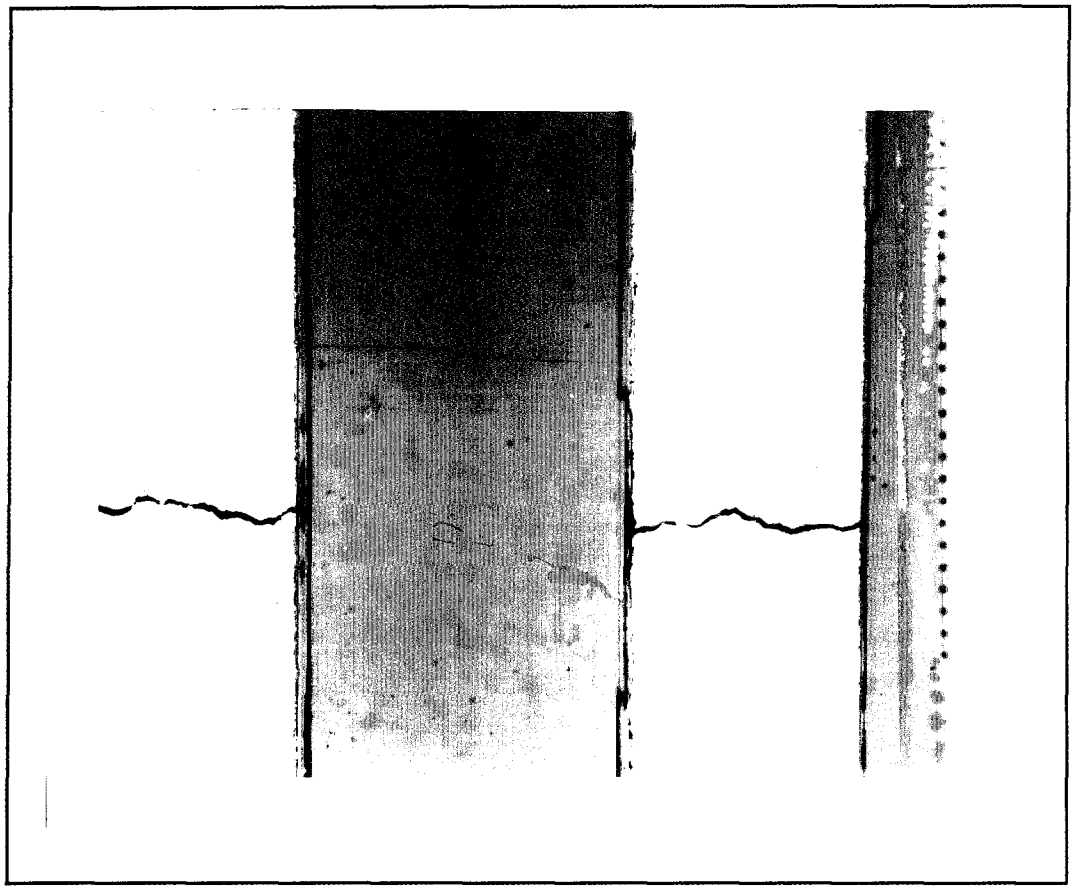

Figure 4.47 Matrix Cracking Causing Interface Damage.
800 MPa, 1 Hz, 427°C (400x)

Figure 4.48 shows extensive interface damage in the specimen tested at 0.01 Hz and 900 MPa maximum stress. Gaps were widest and most extensive near one edge, and damage decreased on fibers closer to the center of the specimen, but little interface damage was observed near the other edge of the sample. A damaged fiber visible on the edge of the specimen was fractured, but no matrix cracks were initiated and none appeared on the sample, which suggests the lower cyclic frequency either hampered matrix cracking in general or promoted the growth of a single crack. Macroscopic analysis and fractography observations revealed that the fatigue response included both matrix cracking

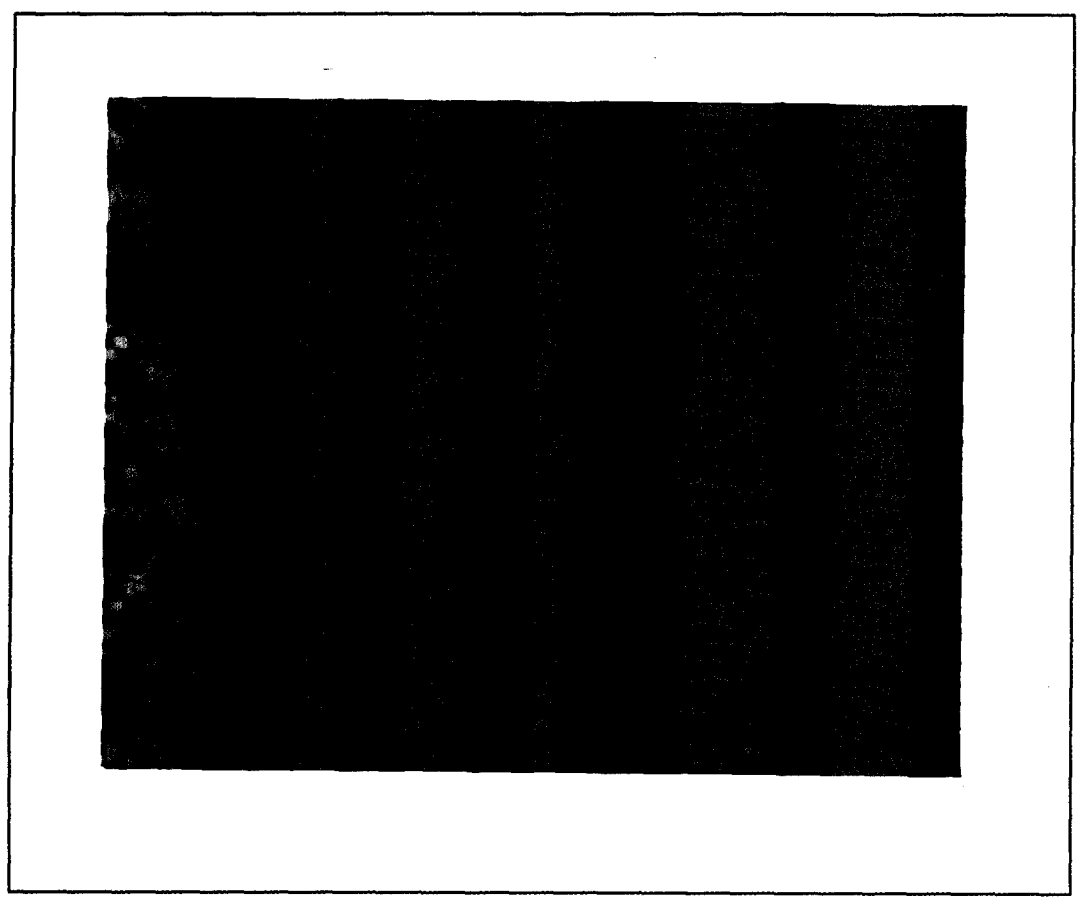

Figure 4.48 Extensive Interface Damage. 900 MPa, 0.01 Hz, 427°C (100x)

(the fracture surface contained an extensive crack) and creep-induced matrix relaxation, leading to fiber failure.

4.4.3 Mixed-Mode Failure (σ_{max} = 1050 MPa)

There were fewer matrix cracks observed in samples of specimens tested at the medium stress level (1050 MPa) than those tested at the lower stress level, but cyclic frequency influenced the extent of matrix cracking and fiber fracture. Figure 4.49 depicts the sample's edge of the specimen cycled at 10 Hz, where fiber damage from machining initiated a matrix crack which grew two fibers into the specimen. Figure 4.50 shows a

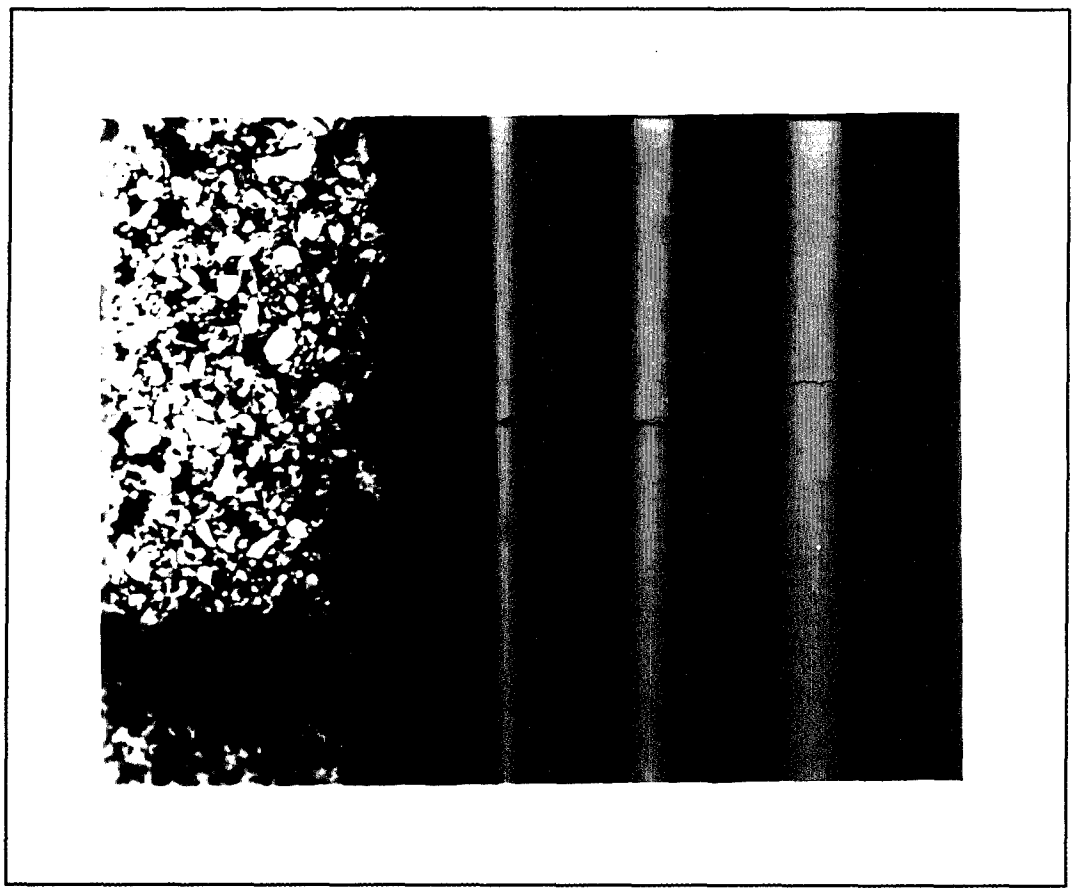

Figure 4.49 Edge Damage. 1050 MPa, 10 Hz, 427°C (100x)

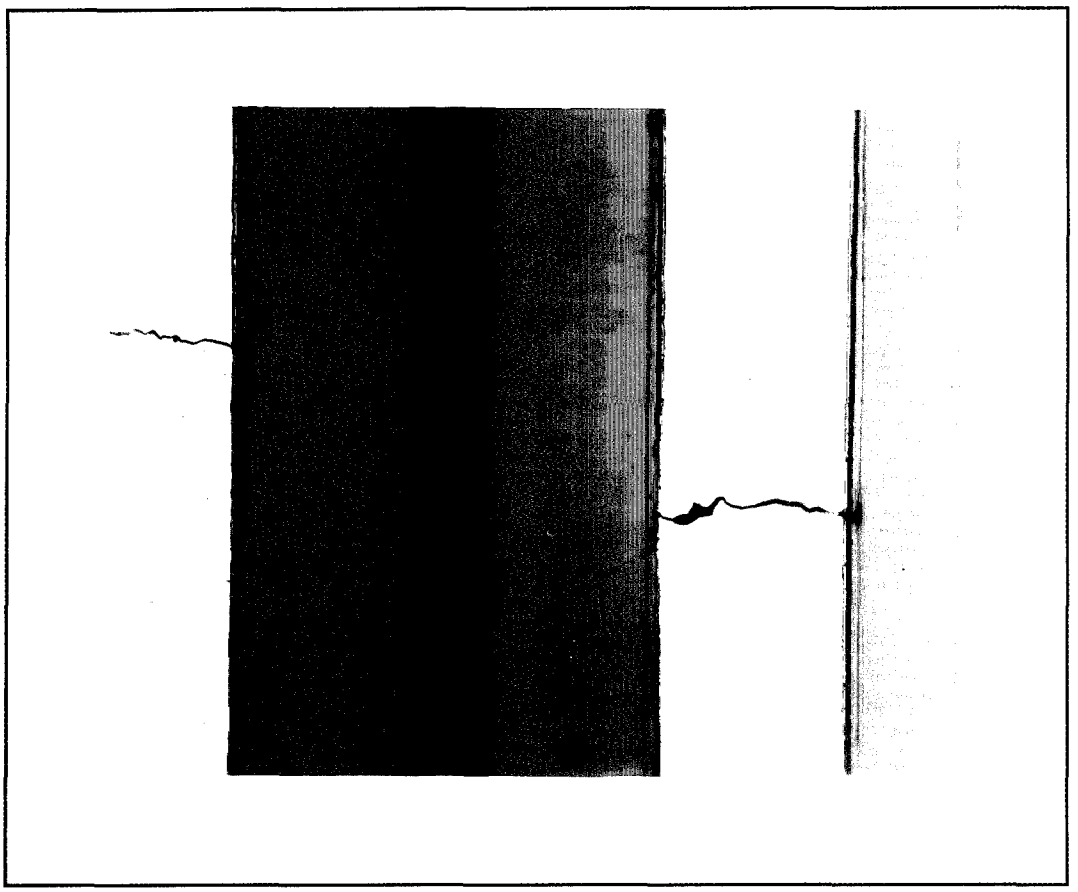

Figure 4.50 Matrix Crack Damaging Interface. 1050 MPa, 10 Hz, 427°C (400x)

matrix crack beginning to damage the interfaces of bridging fibers, and Figure 4.51 indicates that fiber cracking occurred where cores were absent and where edge machining damaged fibers. The cores of the interior fibers may have detached during the polishing procedure.

Figure 4.52 shows the single matrix crack observed in the specimen tested at 1 Hz, which initiated at one edge and was bridged by six fibers. Several fibers contained cracks initiated either where the matrix crack met the fiber or at locations offset from the growing crack. Figure 4.53 depicts the interface damage in these areas of fiber bridging. Interface

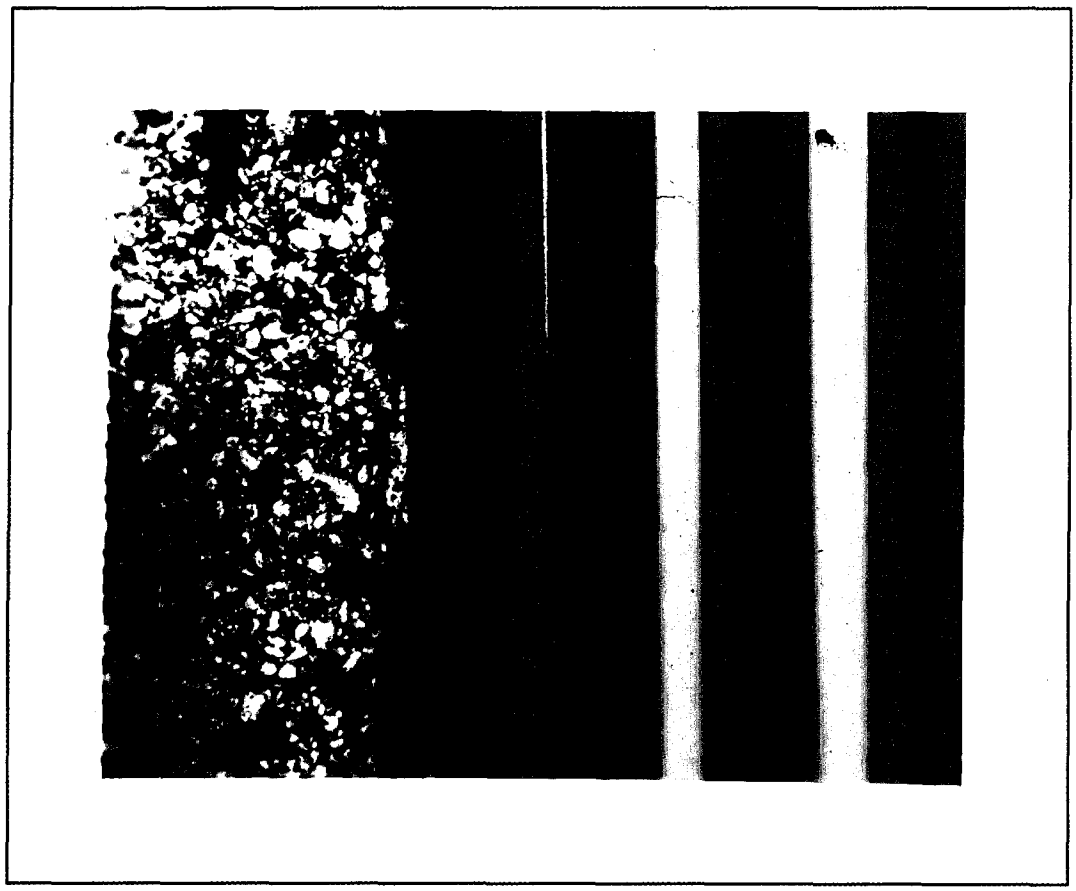

Figure 4.51 Absent Cores Cause Fiber Damage. 1050 MPa, 10 Hz, 427°C (100x)

damage was evident around ten fibers on one side of the sample, which comprised one-third of the specimen's width.

No matrix crack growth was visible in the samples of the specimens cycled at 0.1 Hz and 0.01 Hz. The specimen cycled at 0.1 Hz contained broken fibers in several places along its edge and two edge cracks were arrested by the first fiber. Fiber/matrix interface debonding extended only two or three fibers into the specimen width. The sample of the specimen cycled at 0.01 Hz revealed fiber pullout along the sectioned edge, but no fiber cracks were observed in the specimen's interior. Little interfacial damage was present.

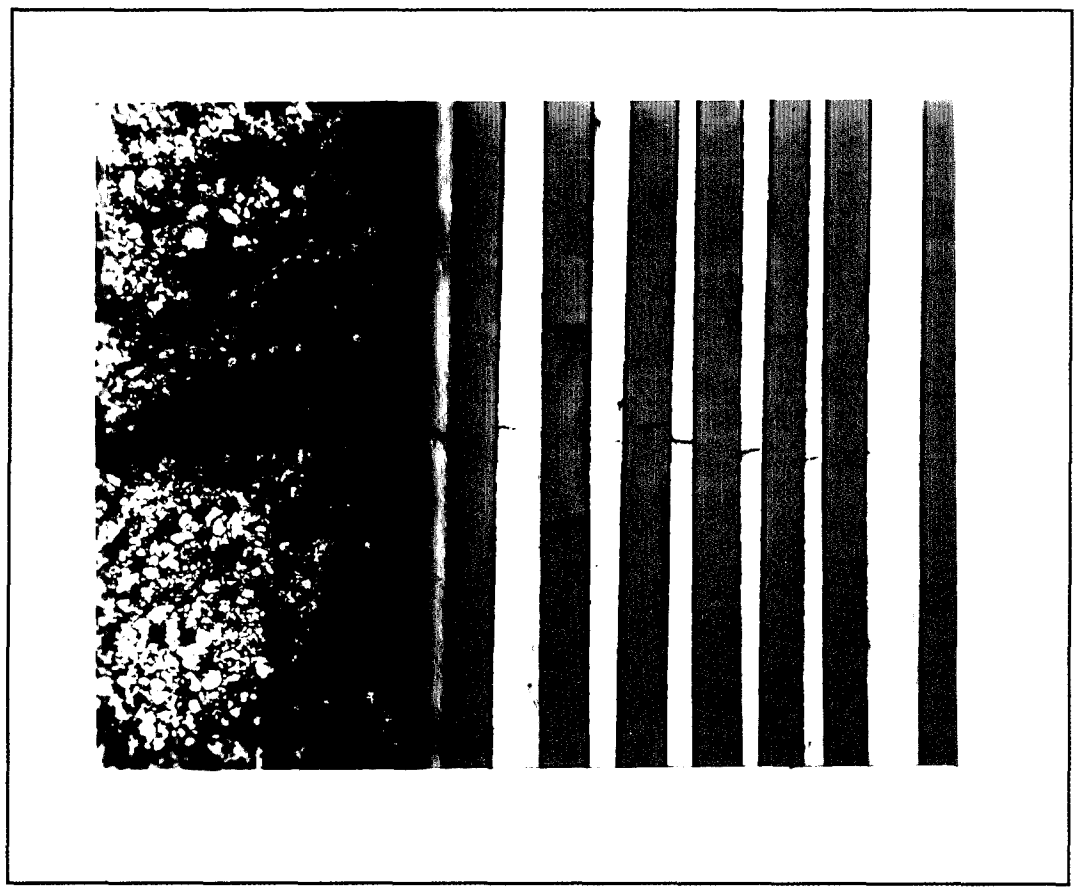

Figure 4.52 Fiber Cracks at Points of Fiber Bridging.
1050 MPa, 1 Hz, 427°C (50x)

Figure 4.53 Extensive Interface Damage. 1050 MPa, 1 Hz, 427°C (100x)

4.4.4 Summary of Microscopy Observations

Microscopic examination of the first lamina in each test specimen showed that damage and fracture mechanisms differed for specimens tested at the three different stress levels and four different test frequencies. Matrix cracking was found to be most dominant at the highest frequencies and lowest stress levels, while random fiber failure dominated the damage in specimens tested at lower frequencies and higher stresses.

At the 1200 MPa stress level, matrix cracks did not develop but fiber damage was extensive, especially in the sample cycled at the lowest frequency. Random fiber cracks

were visible throughout the samples, and a few complete fiber fractures initiated small matrix cracks. The fiber/matrix interfaces were damaged throughout these specimens. Matrix cracks were evident in all samples at the low stress level, but the number and length of cracks decreased as test frequency decreased. Matrix cracks almost always initiated at the specimen edges, at sites of fiber damage due to machining. In a few cases, however, cracks initiated from fiber/matrix interface failure, caused either by interfacial defects or damaged fibers. Matrix cracks at this stress level were always bridged by fibers. Rarely were the fibers damaged, but the interfacial zone often cracked at the points of bridging. The presence of fewer matrix cracks at lower frequencies indicated that one or two cracks dominated and grew quickly, not allowing other cracks to mature.

At medium stress levels, very few fiber and matrix cracks were found, but interfacial damage was prevalent. Fractographic analysis showed that both matrix creep and cracking caused final fracture. This stress level was great enough to crack interfacial zones without the aid of stress raisers from advancing crack tips, but few fibers cracks were observed. Several matrix cracks appeared in samples cycled at the higher frequencies but none in samples tested at the lower frequencies. The amount of interfacial damage did not appear to be frequency dependent.

5 Fatigue Life Analysis and Comparisons

The macroscopic and microscopic observations presented in Chapter 4 revealed the behavior of the SCS-6/Ti-6-4 composite under isothermal fatigue. The mechanisms of deformation and damage over the life of the specimen as well as the nature of final fracture were discussed for a test matrix where stress level, test frequency and temperature were varied. It is also important to understand how frequency variations affect fatigue life of the composite. This chapter examines such effects, primarily at 427°C but also at other temperatures. Table 5.1 is presented to give the actual number of cycles to failure for each test. All experiments were performed under the load-control mode with R = 0.05 in a laboratory environment.

5.1 Frequency Effects on Fatigue Life

Several tools are helpful to illustrate frequency effects on fatigue life. One is the Wholer (or S-N) diagram, where the maximum applied stress is plotted against the number of cycles the specimen endured before failure. A variation of this diagram plots maximum applied stress against the duration of the test (time). A third tool illustrates whether fatigue life is primarily cycle-dependent, primarily time-dependent or whether an interdependence exists. This diagram plots cycles to failure against test frequency, where each series of data represents a particular stress level and temperature.

Figure 5.1 shows the composite's fatigue life as a function of cycles to failure for specimens tested at 427°C. Readily apparent is the near linear correlation of maximum stress level with the log of the number of cycles to failure. Sanders found that the scatter band for data in this region is approximately a factor of two [26]. That is, a repeated test could last anywhere from half the duration to twice the duration of the original test.

Table 5.1 Fatigue Life Results

Temperature (°C)	Frequency (Hz)	Maximum Stress (MPa)	Cycles to Failure
21	10	800	411562
21	10	1050	95634
370	1	800	134467
370	1	1050	33120
370	10	800	327666
370	10	1050	22131
370	10	1050	33802
427	0.01	900	10827
427	0.01	1050	2889
427	0.01	1200	1747
427	0.1	800	90434
427	0.1	1050	13620
427	0.1	1200	10700
427	1	800	130707
427	1	1050	23096
427	10	800	163029
427	10	900	81199
427	10	1050	26252
427	10	1200	12911
538	0.1	800	22704
538	0.1	1050	2624
538	10	800	96643
538	10	1050	11260
427	0.01	1050	* >3975
427	1	800	** 92501

* Invalid Test

** Invalid Test, R=0.1

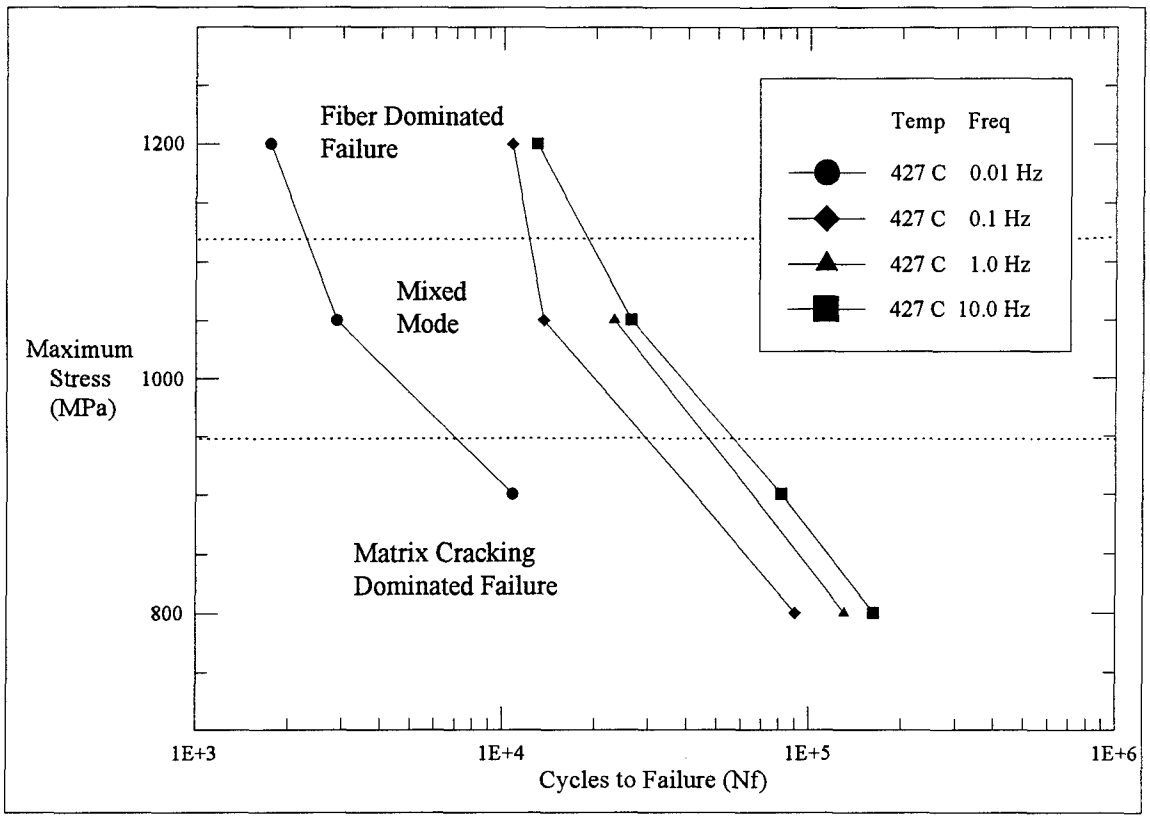

Figure 5.1 S-N Diagram, Frequency Comparisons at 427°C

Despite the possibility of scatter, there appears to be a trend of lines of constant frequency shifting to the left as frequency is reduced tenfold. Little difference in fatigue life exists between tests at the higher two frequencies: the specimens tested at 1 Hz endured about 15% fewer cycles than the 10 Hz specimens. However, the 0.1 Hz tests withstood about 36% fewer cycles than the 1 Hz tests, and the specimens tested at 0.01 Hz endured almost 80% fewer cycles than the specimens tested at 0.1 Hz. Apparently, stress level does not affect this fatigue life shift due to frequency since the lines are close to parallel. If failure of the composite were purely dependent on the number of fatigue

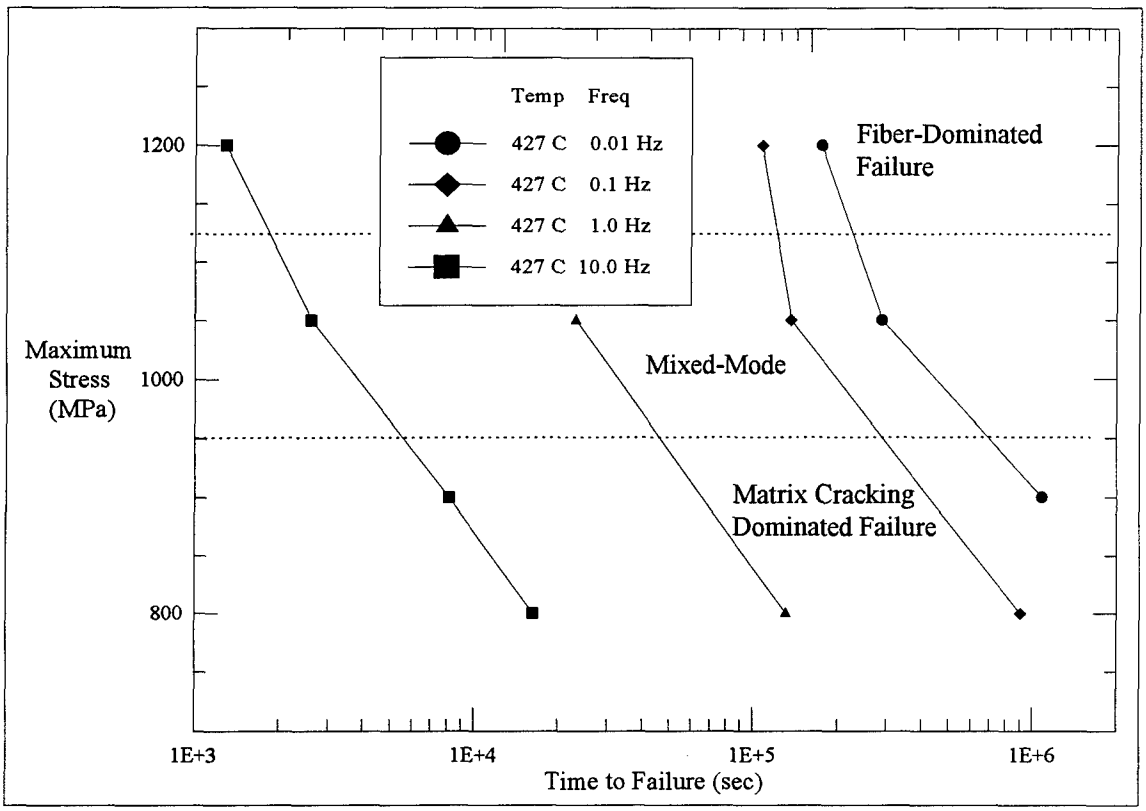

Figure 5.2 S-t Diagram, Frequency Comparisons at 427°C

cycles, each of the lines of constant frequency would be coincident. For SCS-6/Ti-6-4, it is evident that as frequency decreases, life becomes less cycle-dependent.

Another way to view the same information is to plot the maximum stress against time to failure, as in Figure 5.2. This plot illustrates the degree to which final fracture of the composite is dependent on the duration of the test. Figure 5.2 shows that as cyclic frequency decreases, the lines of constant frequency shift to the right, yet there is less of a shift for each tenfold frequency reduction. The fatigue tests at 1 Hz lasted eight to nine times longer than those at 10 Hz, because the life at these high frequencies was nearly cycle-dependent (as shown in Figure 5.1). However, the tests at 0.1 Hz lasted only six to

seven times longer than those at 1 Hz, and the tests at 0.01 Hz lasted only about twice as long as those at 0.1 Hz. Again, for a purely cycle-dependent phenomenon, each decade decrease in frequency would result in a decade increase in lifetime duration. This suggests that the environment also had an effect on fatigue life.

The N-f diagram (number of cycles to failure plotted against test frequency) is another useful tool to show the degree to which fatigue life is cycle- or time-dependent. Figure 5.3 is one such diagram for tests conducted at 427°C. It is important to note that the slopes of the lines at constant maximum stress are all positive at the lowest frequencies, but then level off to almost zero at higher frequencies (slopes for 800 MPa

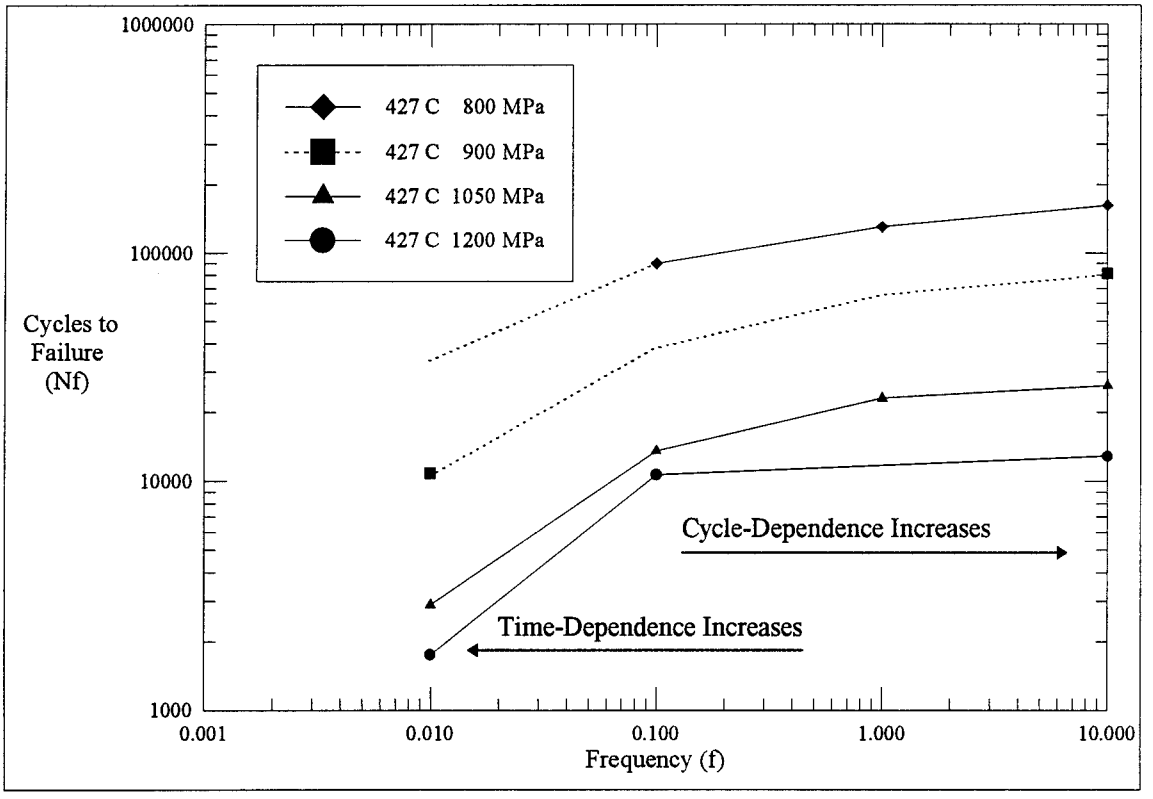

Figure 5.3 N-f Diagram, 427°C

and 900 MPa have been estimated with dashed lines based on the relative positions of data points). In fact, the slopes of the lines in the 0.01 Hz to 0.1 Hz range are nearly equal to one decade of cycles to failure for each decade change in frequency which indicates that fatigue life is almost purely time-dependent. The near-zero slopes of the lines of constant stress for the data between 0.1 Hz and 10 Hz show that the number of cycles to failure is almost independent of test frequency, i.e., fatigue life is nearly cycle-dependent.

The macroscopic and microscopic observations of specimens cycled at 1 Hz and 10 Hz revealed damage dominated by matrix cracking. This is typical of high-frequency fatigue, where cracks advance with each cycle, generally independent of rate. Failure of a specimen occurs when crack growth reaches a critical length, so it is therefore dependent on the number of cycles it received.

There are two probable reasons for the shift from cycle- to time-dependence at lower frequencies. During slower cycles, the specimen is exposed to the high temperature environment for a much longer duration. Oxidation, which embrittles the titanium matrix, may promote crack initiation and accelerate crack propagation, and lead to a reduced fatigue life. In addition to experiencing greater oxidation, specimens fatigued at lower frequencies experience much more creep, as was evident in the macroscopic and microscopic observations of Chapter 4. During a true creep test, the stress on a specimen is held constant and the specimen is allowed to "creep" until failure. The low frequency fatigue test could be considered an inefficient creep test, where few cracks develop and propagate, and the specimen fails after being stressed for a certain length of time. Thus it

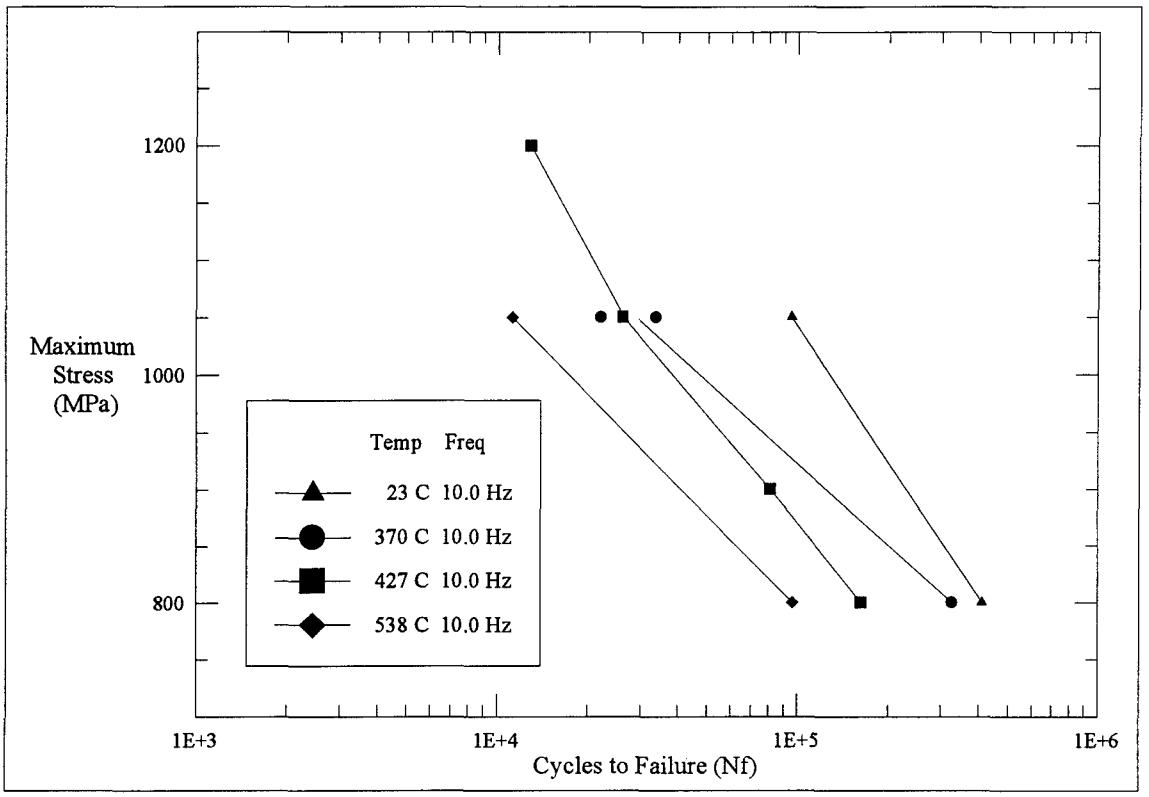

Figure 5.4 S-N Diagram, Temperature Comparisons at 10 Hz

appears that the influences of both creep and oxidation may contribute to the time-dependent character of fatigue life at low frequencies.

5.2 The Influence of Temperature on Frequency Effects

To study whether or not the above stated frequency effects are dependent on temperature, several tests were run at temperatures other than 427°C. The final diagram that will be used in this chapter plots cycles to failure against test temperature. First, Figure 5.4 shows how fatigue life varied with test temperature. These tests were run at 10 Hz, with temperatures ranging from 23°C to 538°C. This S-N diagram shows that fatigue

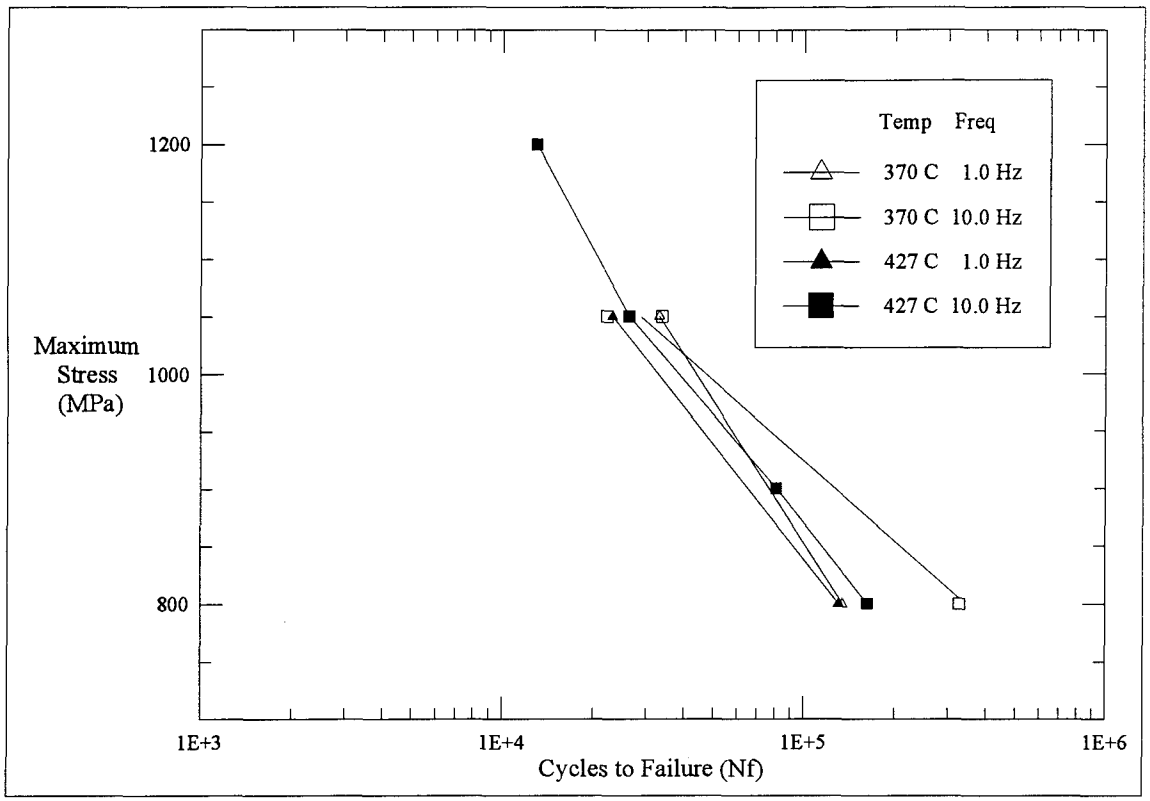

Figure 5.5 S-N Diagram, 370°C and 427°C Comparison

life definitely decreased with increasing test temperature. This was due to the lower material modulus, more thermal strain and greater effects of oxidation and matrix relaxation at higher temperature, which resulted in higher strain for the same stress levels.

Figures 5.5 and 5.6 are S-N diagrams that compare tests conducted at 370°C and 538°C with tests conducted at 427°C. Figure 5.5 shows little, if any, influence of reduced temperature on frequency effects at 1 Hz and 10 Hz, but fatigue life appeared to be primarily cycle-dependent at both temperatures. This was expected since the diagram compared tests at the higher two test frequencies. In Figure 5.6, comparison of tests conducted at 427°C and 538°C (0.1 Hz and 10 Hz) shows a different trend. The diagram

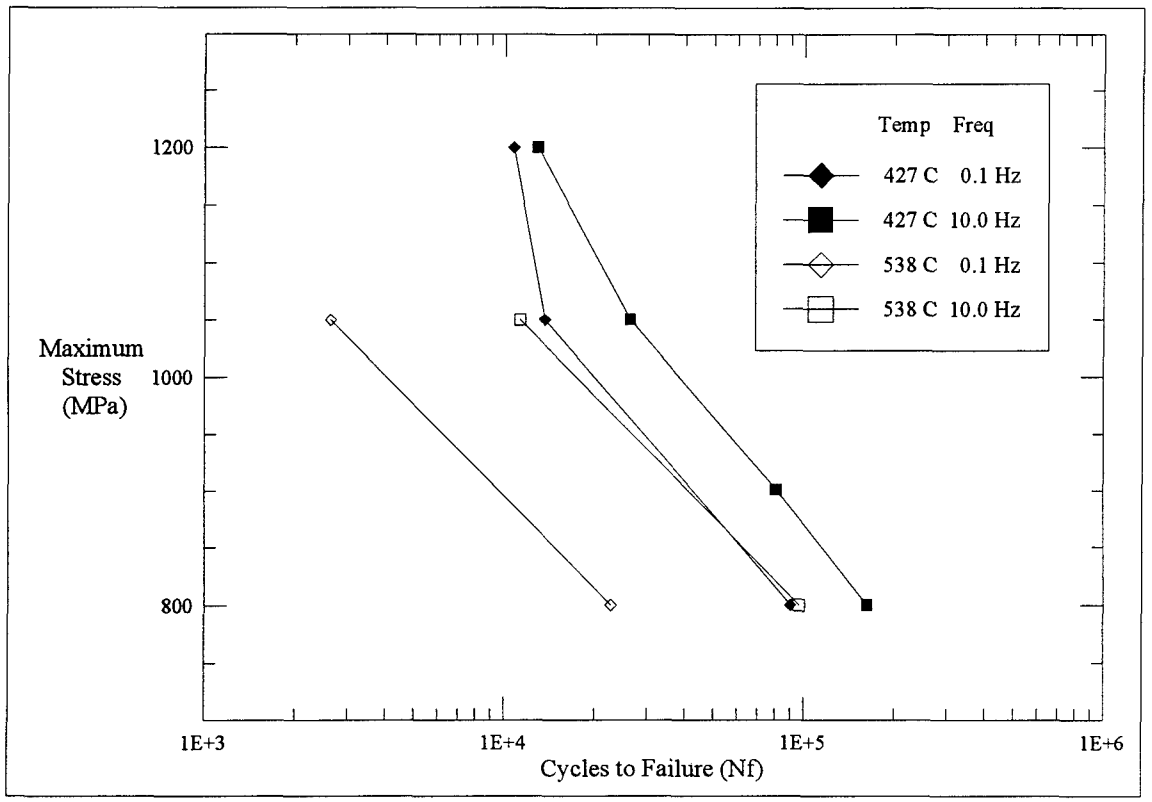

Figure 5.6 S-N Diagram, 427°C and 538°C Comparison

shows that the fatigue lives at 538°C were much shorter than those at 427°C. Also, the shift from 0.1 Hz to 10 Hz was much greater at the higher temperature. At 538°C, the 10 Hz tests endured four times more cycles than the 0.1 Hz tests endured, while at 427°C the 10 Hz tests withstood only twice the number of cycles experienced at 0.1 Hz. This reveals that the environment (elevated temperature in laboratory air) significantly influences the shift to time-dependent failure with decreasing frequency.

Figure 5.7 illustrates this transition from cycle- to time-dependence for the composite tested at 427°C and 538°C (dashed lines estimate the trends between the data points at the higher temperature). The slopes of the 538°C constant maximum stress lines

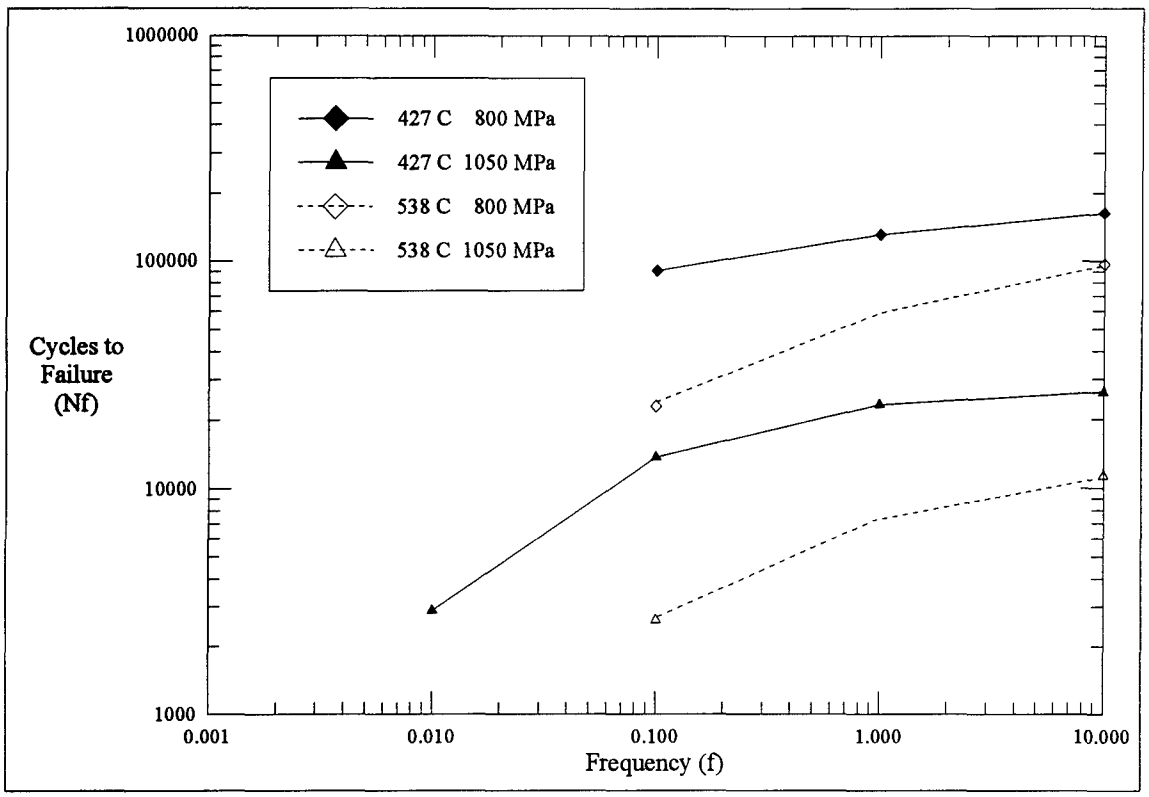

Figure 5.7 N-f Diagram, 427°C and 538°C Comparison

are slightly steeper than the those at 427°C. Despite the limited data set, this indicates that testing at higher temperature introduced more time-dependence in fatigue lives.

One final way to evaluate this data is to view a temperature-life diagram (Figure 5.8), which indicates the general effects of temperature on fatigue life. As temperature increased to 538°C, there existed a mild trend of shortened life, but no dramatic drop. Again, it is apparent that at 538°C there is a much greater gap between the 0.1 Hz and 10 Hz fatigue lives at each stress level than there is at 427°C.

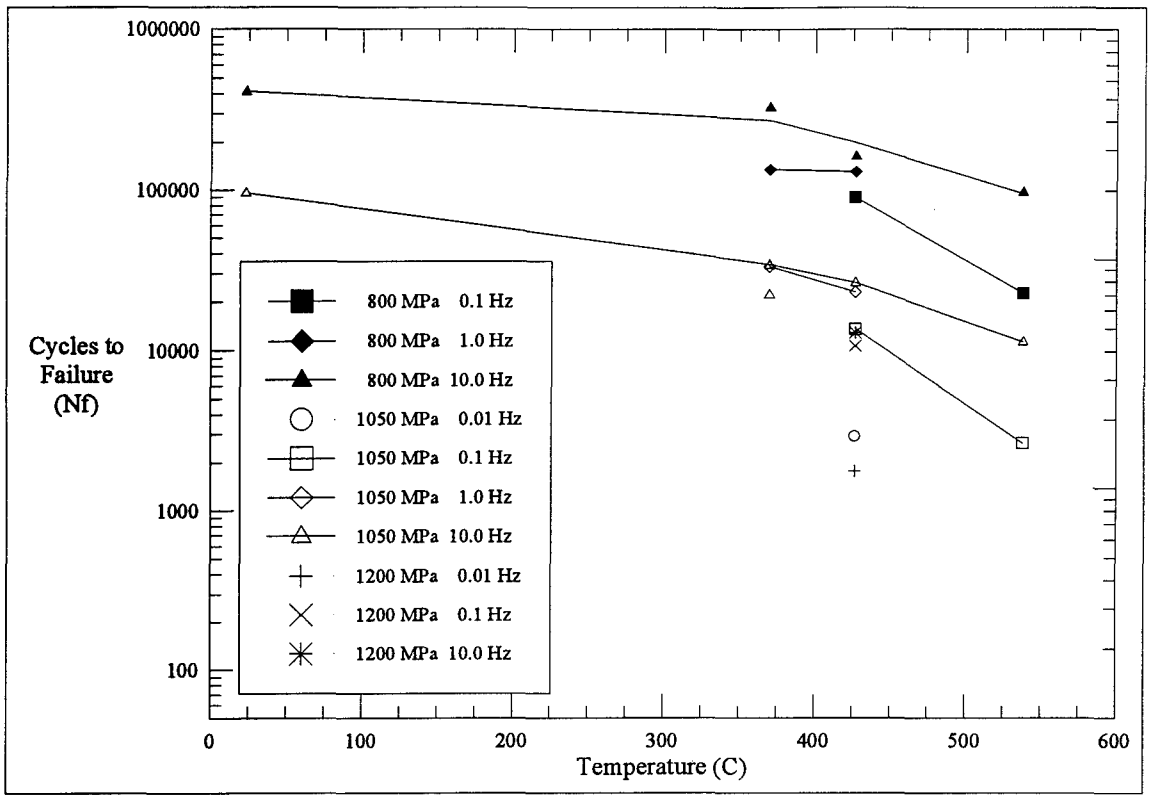

Figure 5.8 N-T Diagram

5.3 Summary of Fatigue Life Observations

This chapter has shown several clear trends in fatigue life data for the SCS-6/Ti-6-4 composite system. For all tests conducted at 427°C, the S-N relationships at constant frequencies on the fatigue life curve were relatively linear and parallel. There appeared to be a gradual transition from cycle-dependence to time-dependence as frequency changed from 10 Hz to 0.01 Hz. Comparison of these tests to their counterparts at 370°C and 538°C showed that these frequency effects were magnified as temperature increased: lower frequency tests at 538°C exhibited greater time-dependence than tests at 427°C.

This was caused by poorer creep and environmental resistance at the higher temperature. Finally, a diagram of fatigue life versus temperature showed that life decreased with increasing temperature up to 538°C, but not dramatically.

6 Conclusions and Recommendations

The goal of this research was to explore the impact that cyclic frequency has on the fatigue behavior and life of the unidirectional SCS-6/Ti-6-4 composite laminate. While titanium-alloy composites have undergone extensive testing in recent years, frequency effects have not received much attention. Far from being a trivial matter, the rate of cyclic fatigue significantly influences the composite's response and failure mechanisms.

Twenty-two load-controlled isothermal fatigue tests were performed at four frequencies and four temperatures. Modulus and strain histories, as well as stress-strain data during cycling provided macroscopic evidence of various fatigue mechanisms, while microscopic physical observations identified primary and secondary causes of specimen failure. Tests conducted at the 1200 MPa maximum stress level exhibited fiber-dominated fatigue responses: there appeared to be little damage from matrix crack growth, and fracture was caused by random fiber failure. Strain histories also showed that these specimens experienced much more matrix creep than specimens at lower maximum stress levels. However, at the lower stress levels of 800 MPa and 900 MPa, the fatigue response was largely dominated by progressive matrix cracking which led to final fracture. At these stress levels, higher test frequencies intensified matrix cracking while lower frequencies increased matrix creep and the resulting effects. The response at the intermediate stress level of 1050 MPa was determined by test frequency, and was found to be either matrix- or fiber-dominated.

Oxide deposits on matrix grains and damage to fibers were observed on fracture surfaces of specimens tested at elevated temperatures. Instead of increasing the amount of laminate damage due to matrix cracking, raising the test temperature generally seemed to lower crack growth and induce matrix creep, evidenced by increasing strain histories and more ductile failure on the fracture surfaces. This trend had its exceptions, however, so further experimentation at various temperatures, frequencies and stress levels should be performed in order to establish causative correlations.

After evaluating the impact of frequency on fatigue response, a second goal of the study was to examine how fatigue life was altered. A common assumption in MMC fatigue testing is that the life of a specimen is mainly dependent on stress (or strain) range, test temperature and specimen geometry. Holding these variables constant, a specimen will fail after a certain number of cycles, since each cycle advances matrix cracks by a certain distance and matrix crack length usually determines failure. The present investigation showed that this is a valid postulate for fatigue testing at high frequencies and for cases where frequency variation is minimal.

Results from this study show that frequency effects must be considered when the anticipated fatigue rate of the composite's application is low (tens of seconds per cycle) or when it is expected to vary considerably. In fact, at the lowest frequencies (0.01 Hz and 0.1 Hz), fatigue life at elevated temperatures was found to be largely time-dependent. Just as lower frequencies greatly impacted fatigue response, the number of cycles to failure was reduced by as much as a factor of six when test frequency changed from 0.1 Hz to

0.01 Hz. Wholer diagrams as well as plots of cycles to failure versus frequency were used to determine when fatigue life became less cycle-dependent and more time-dependent.

It was also shown that the increased effects of oxidation and creep at higher test temperatures caused the time-dependent nature of MMC fatigue life at lower frequencies to become more pronounced. The dominant cause of this increased time-dependence could be determined by running similar tests in a vacuum or inert environment to isolate the influence of creep on reduction of fatigue life. Such research would bring closure the study of frequency effects in the isothermal fatigue of titanium matrix composites.

Appendix A - Additional Macroscopic Comparisons

Comparisons of modulus and mean strain histories are presented below. Modulus is normalized by the specimen's initial modulus and cycle count is normalized by the number of cycles to failure. Fatigue responses from tests of varying frequency are compared first, and then responses of tests of varying temperature are compared.

A.1 Effects of Varying Test Frequency

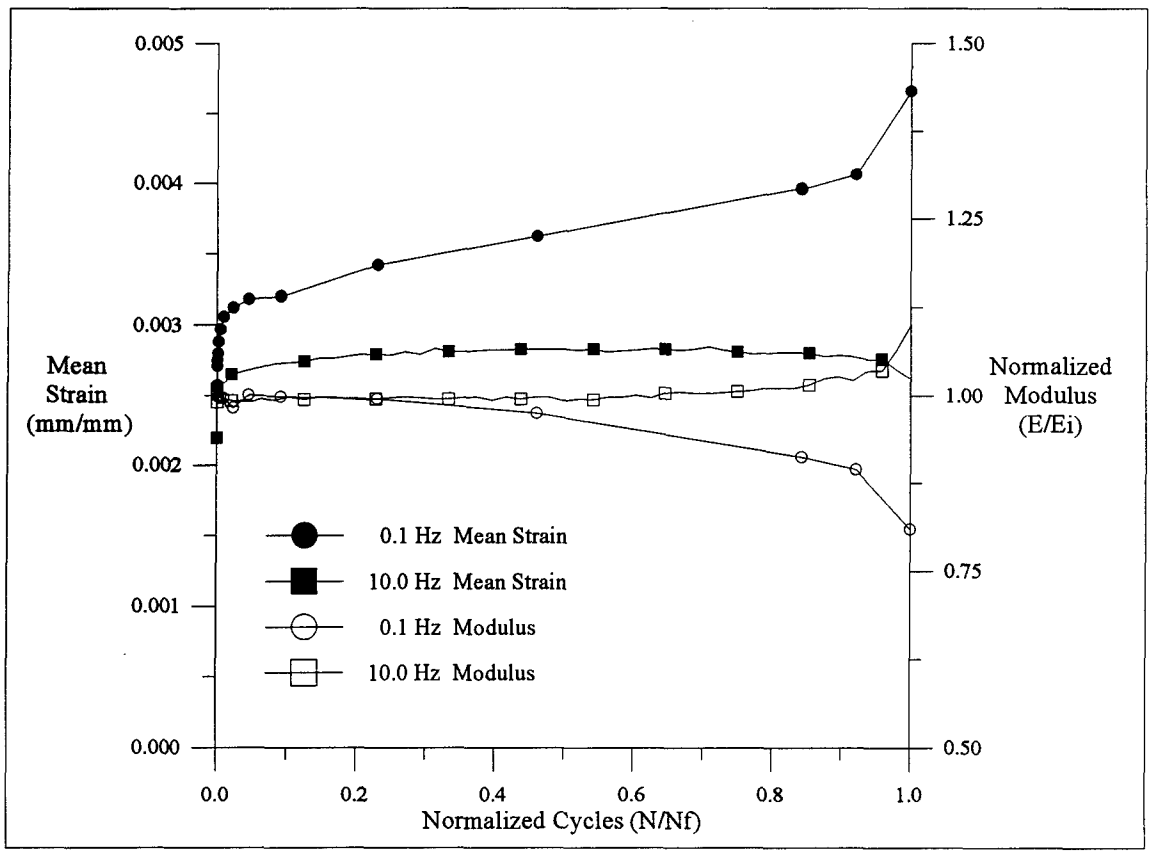

Figure A.1 Strain and Modulus History Comparisons (800 MPa, 538C)

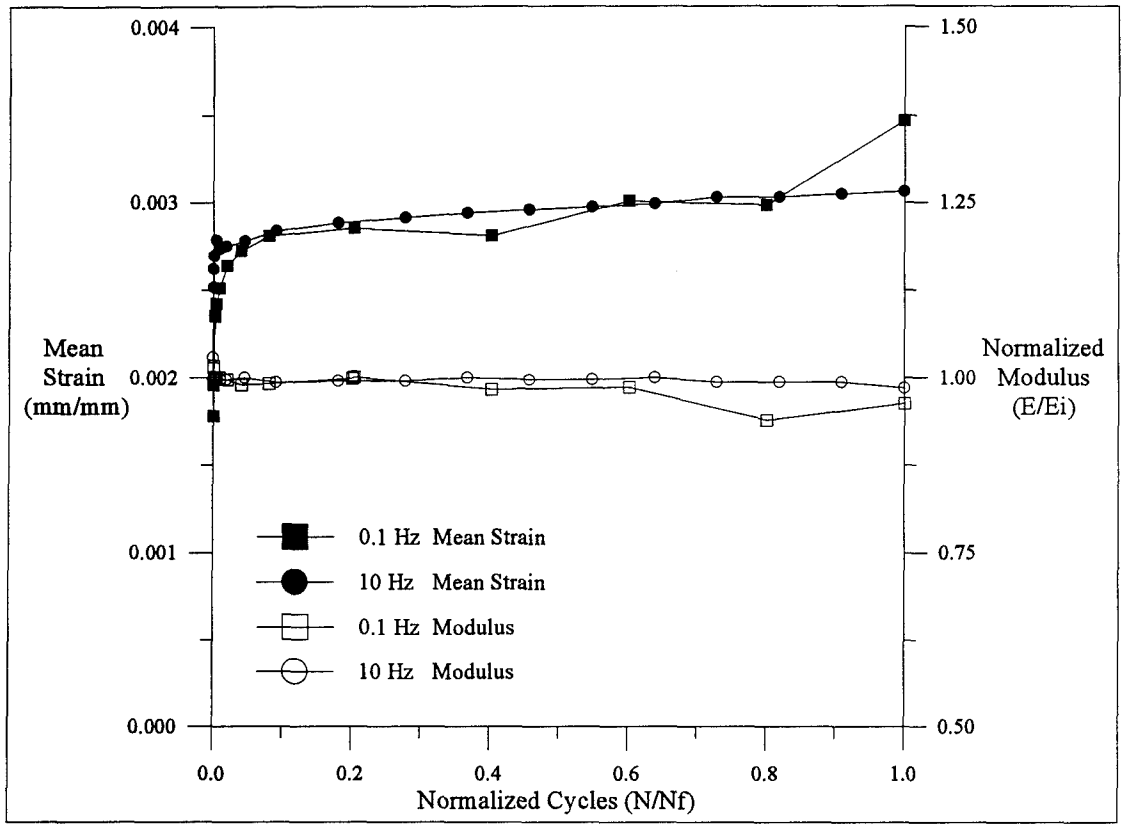

Figure A.2 Strain and Modulus History Comparisons (1050 MPa, 538°C)

A.2 Effects of Varying Test Temperature

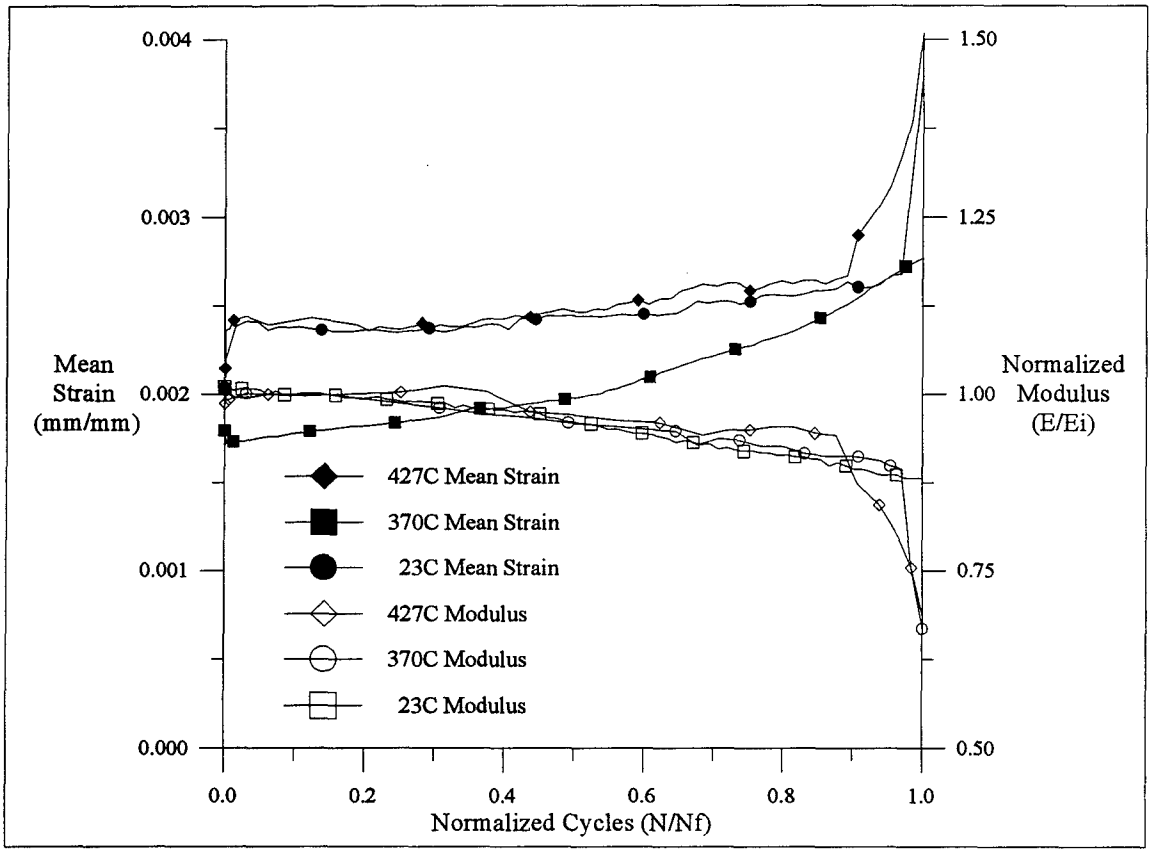

Figure A.3 Strain and Modulus History Comparisons (800 MPa, 10 Hz)

Appendix B - LISOL Analysis

B.1 Background

The Laminated comosite Inelastic Solver developed by Robertson [24] models the nonlinear behavior of MMC laminates. It uses the Bodner and Partom unified viscoplastic theory to model the matrix material and treats the fiber as thermoelastic. The program used temperature dependent material properties of the Ti-6-4 matrix and the SCS-6 fibers, and ten-cycle loading profiles for several isothermal tests. Each profile began at zero stress and 815°C, and was then cooled to room temperature (to simulate high-temperature processing). Next, the profile ramped the temperature to 427°C (test temperature), and the loading cycle began. Table B.1 presents is a sample loading cycle for a test at 1200 MPa maximum stress and 0.01 Hz cyclic frequency. The cycle begins at the fifth step.

Table B.1 LISOL Loading Cycle

Δt (sec)	T (°C)	σ_x	σ_y	τ_{xy}	increment
0.001	815.	0.	0.	0.	1
1000.	23.	0.	0.	0.	5
180.	427.	0.	0.	0.	60
0.0125	427.	60.	0.	0.	5
0.0125	427.	345.	0.	0.	5
0.0125	427.	630.	0.	0.	5
0.0125	427.	915.	0.	0.	5
0.0125	427.	1200.	0.	0.	5
0.0125	427.	915.	0.	0.	5
0.0125	427.	630.	0.	0.	5
0.0125	427.	345.	0.	0.	5
0.0125	427.	60.	0.	0.	5

B.2 Results

The following figures plot the maximum microstresses for the fiber and matrix constituents of four tests. The tests at the 800 MPa and 1200 MPa maximum stress levels, and 10 Hz and 0.1 Hz frequencies were selected.

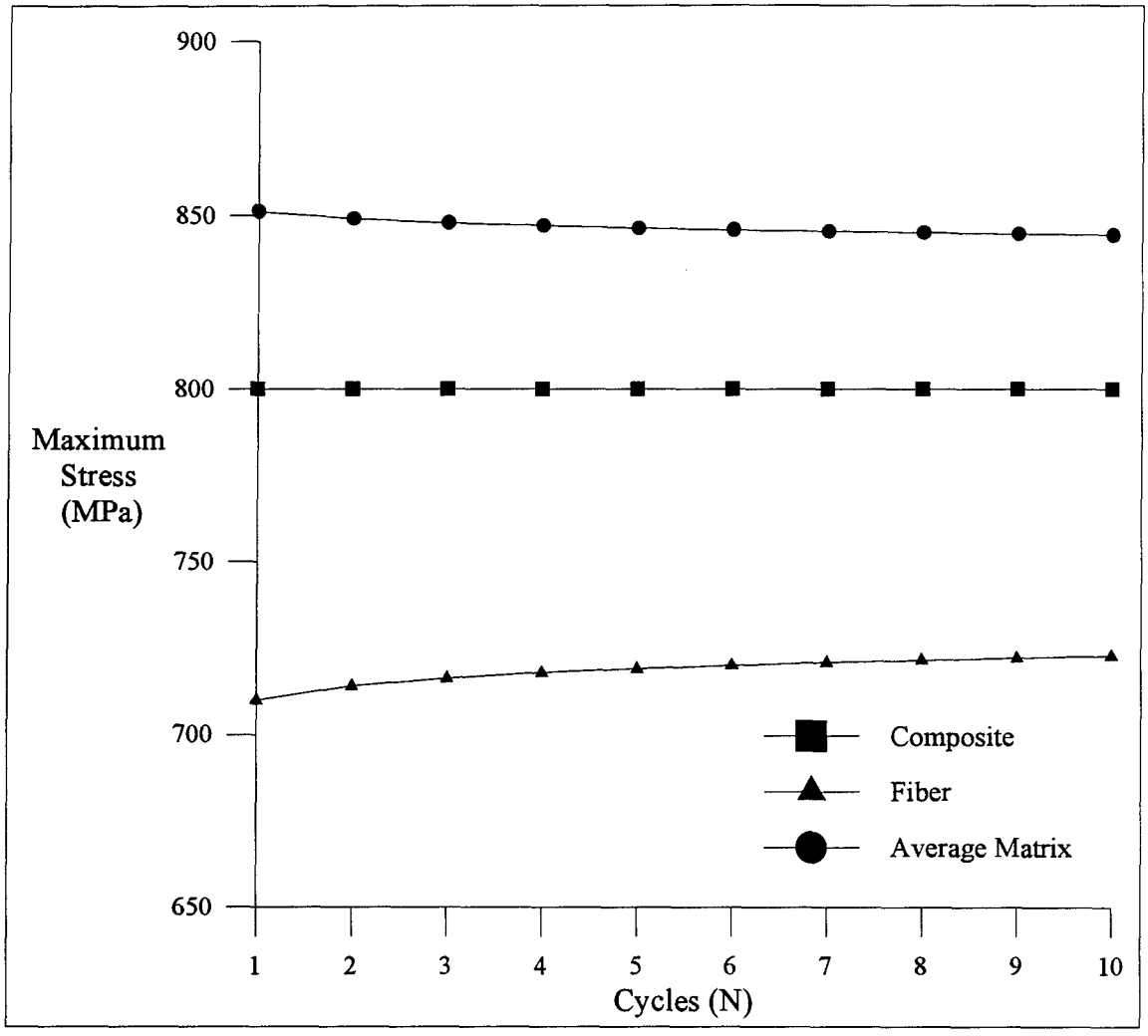

Figure B.1 Microstresses (10 Hz, 800 MPa, 427°C)

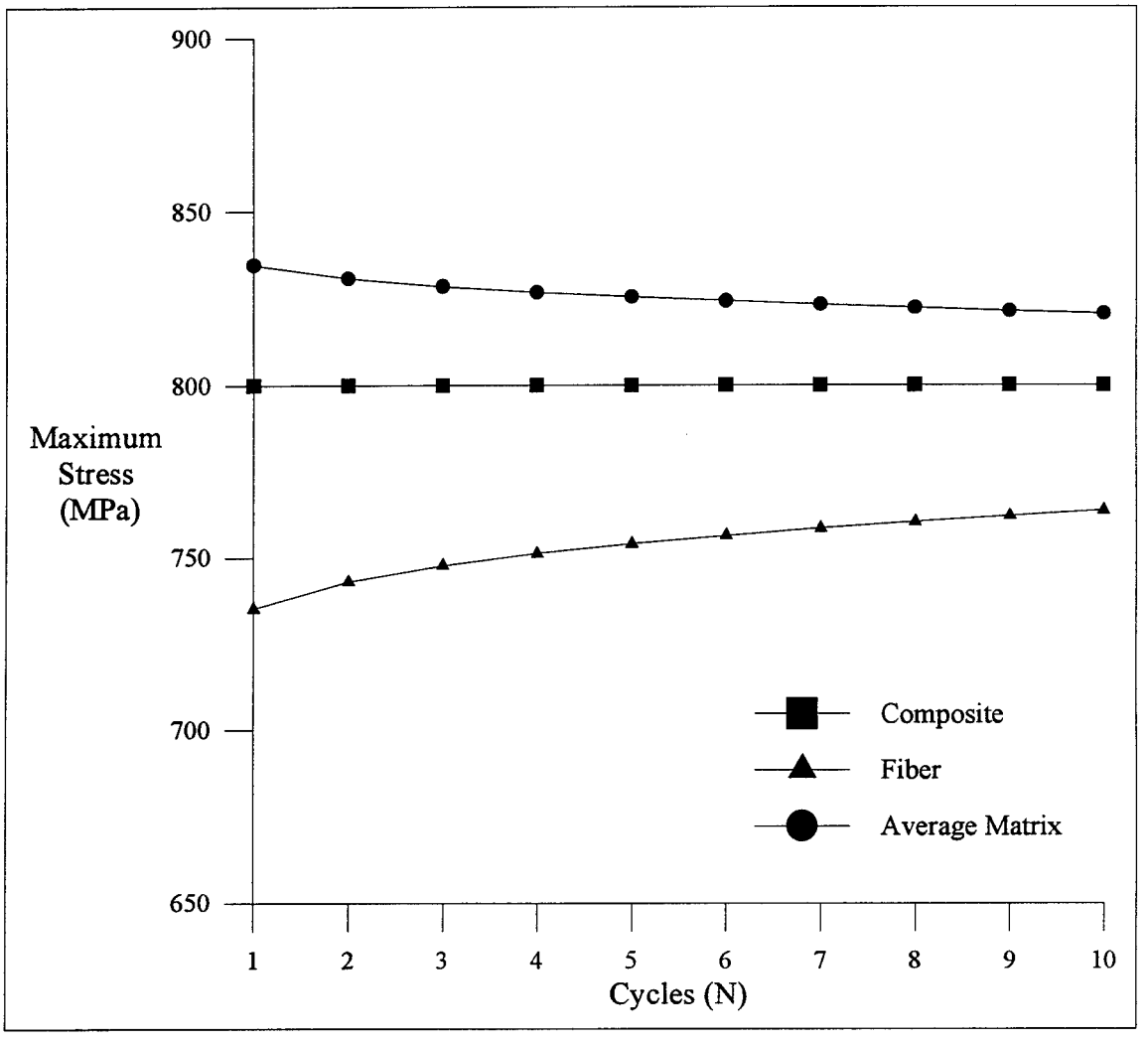

Figure B.2 Microstresses (0.1 Hz, 800 MPa, 427°C)

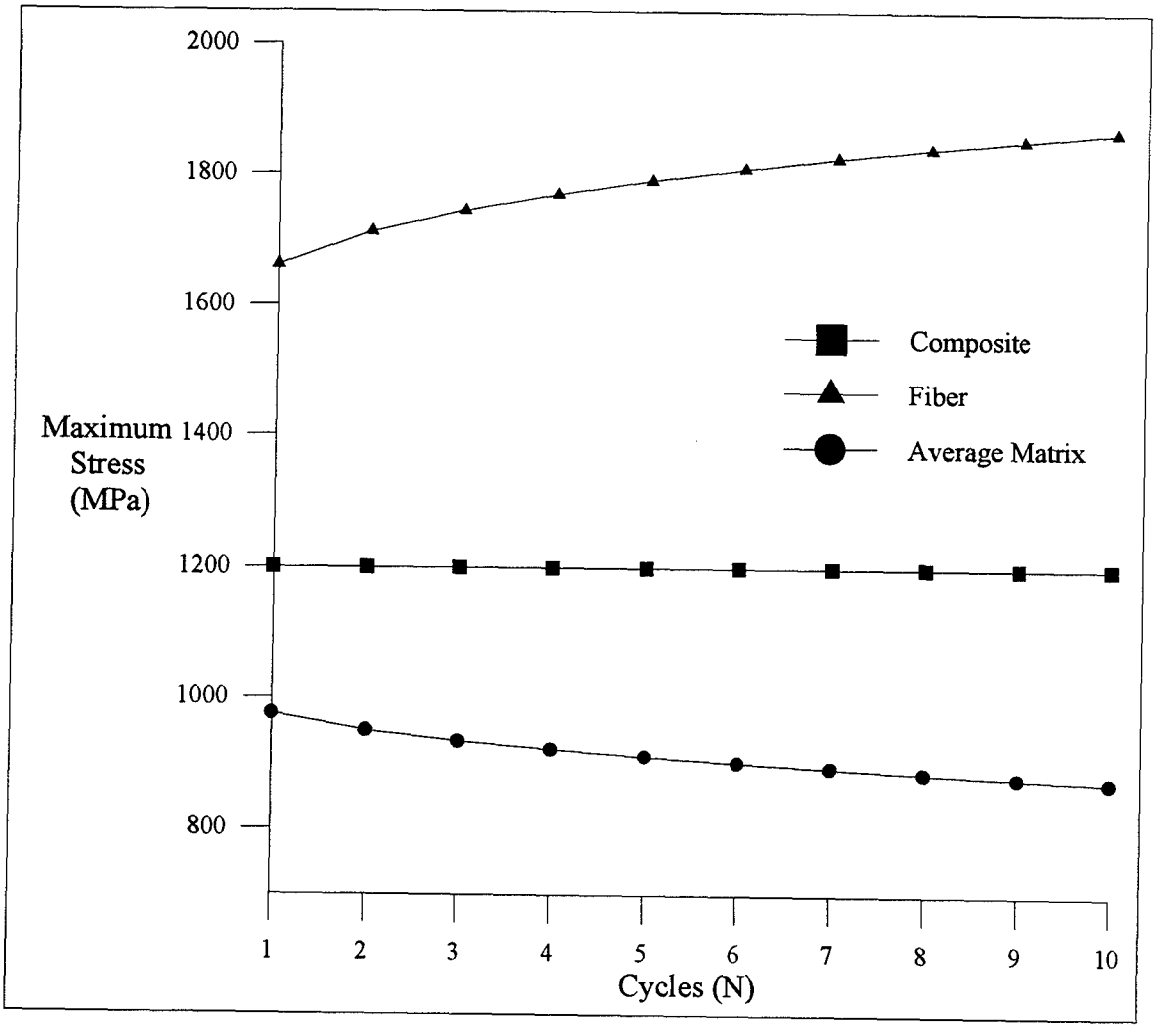

Figure B.3 Microstresses (10 Hz, 1200 MPa, 427°C)

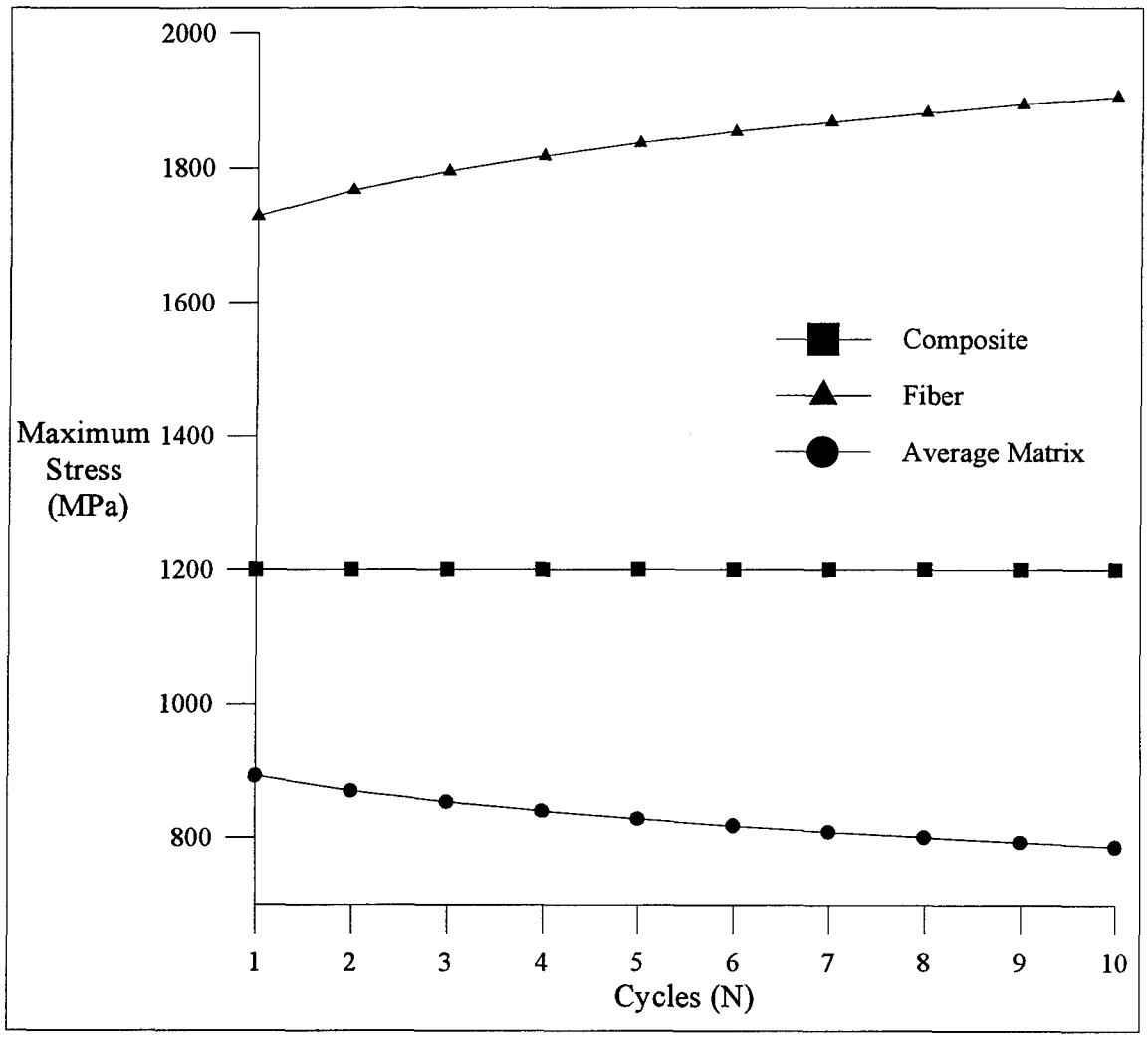

Figure B.4 Microstresses (0.1 Hz, 1200 MPa, 427°C)

Appendix C - Additional Photographs of Fractured Specimens

Photographs of all fractured specimens are presented below. Table 4.2 of Section 4.2 lists specimens that failed outside the 12.7 mm test section.

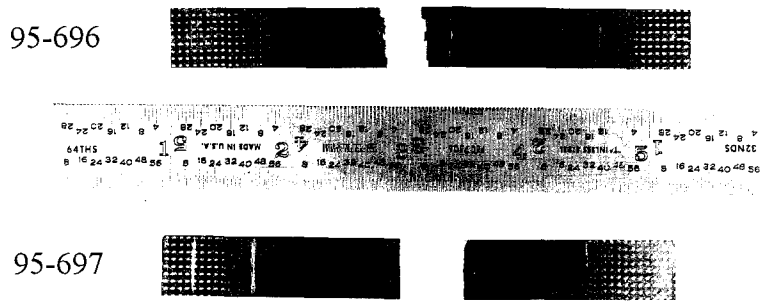

Figure C.1 Specimen Nos. 95-696 and 95-697

95-698

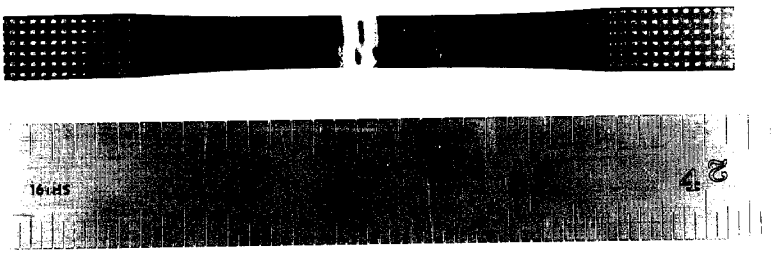

Figure C.2 Specimen No. 95-698

95-699

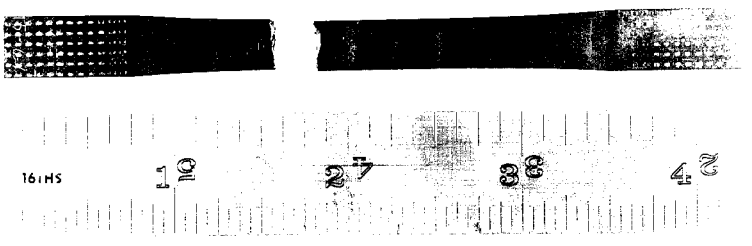

Figure C.3 Specimen No. 95-699

95-700

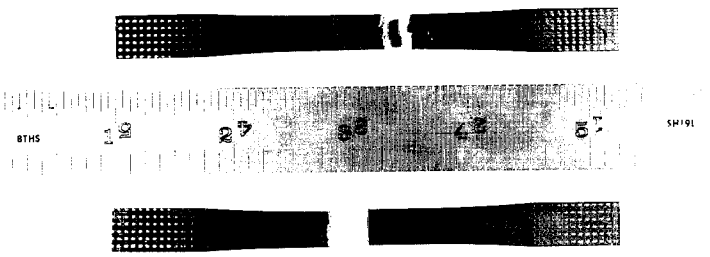

95-702

Figure C.4 Specimen Nos. 95-700 and 95-702

95-701

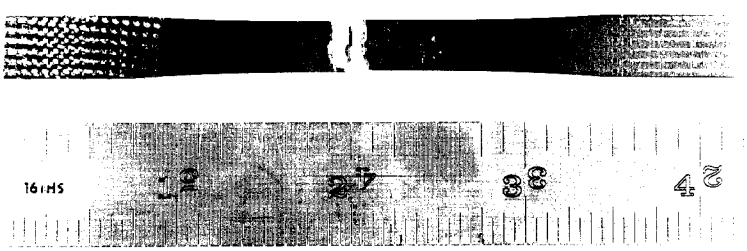

Figure C.5 Specimen No. 95-701

95-710

95-711

Figure C.6 Specimen Nos. 95-710 and 95-711

95-722

95-723

95-724

95-725

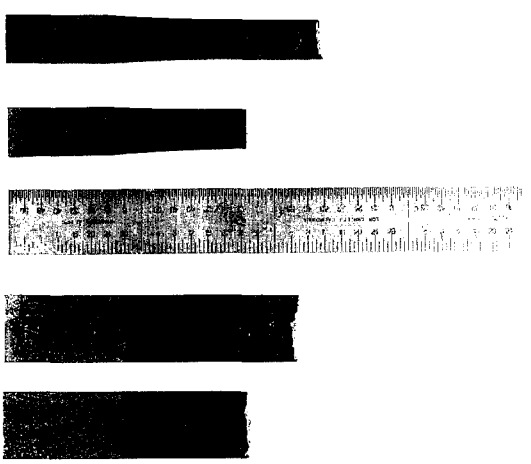

Figure C.7 Specimen Nos. 95-722, 95-723, 95-724, and 95-725

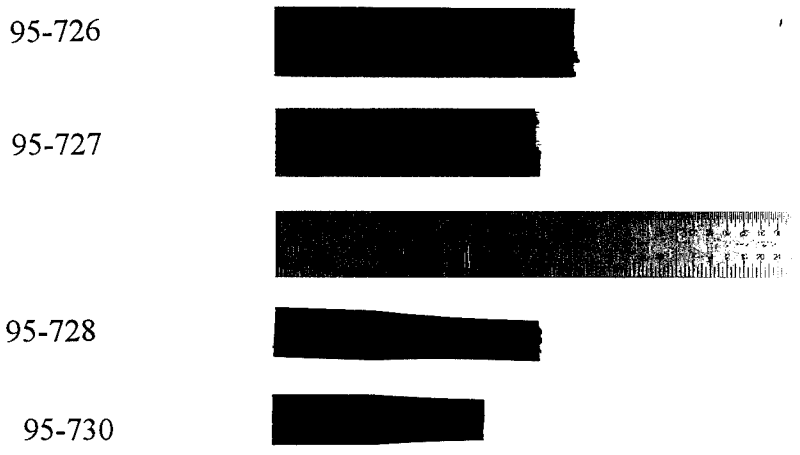

Figure C.8 Specimen Nos. 95-726, 95-727, 95-728, and 95-730

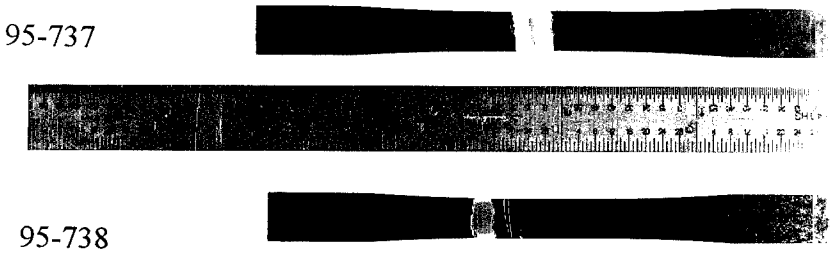

Figure C.9 Specimen Nos. 95-737 and 95-738

Bibliography

1. Bhatt, R. T. and Grimes, H. H., "Fatigue Behavior of SiC Reinforced Ti(6Al-4V) at 650 °C," *Metallurgical Transactions A*, Vol. 13A, November 1982, pp. 1933-1938.

2. Bhatt, R. T. and Grimes, H. H., *Fatigue of Fibrous Composite Materials, ASTM STP 723*, American Society for Testing and Materials, Philadelphia, 1979, pp. 274-290.

3. Boyam, E. A., "Investigation of Tension-Compression Fatigue of a Cross-Ply $[0/90]_{2s}$ Metal Matrix Composite at Room and Elevated Temperature," MS Thesis, AFIT/GAE/ENY/93D-06, Graduate School of Engineering, Air Force Institute of Technology (AU), Wright-Patterson AFB, OH, December 1993.

4. Broek, D., *Elementary Engineering Fracture Mechanics* (Fourth Revised Edition), Kluwer Academic Publishers, Boston, 1991.

5. Castelli, M. G. et al., "Thermomechanical Testing Techniques for High-Temperature Composites: TMF Behavior of SiC(SCS-6)/Ti-15-3," NASA TM-103171, 1990.

6. Dennis, L. B., "Fatigue Behavior of a Cross-Ply Metal Matrix Composite at Elevated Temperature Under Strain Controlled Mode," MS Thesis, AFIT/GAE/ENY/94D-07, Graduate School of Engineering, Air Force Institute of Technology (AU), Wright-Patterson AFB, OH, December 1993.

7. El-Soudani, S. M. and Gambone M. L., "Strain-controlled Fatigue Testing of SCS-6/Ti-6Al-4V Metal-Matrix Composite," *Fundamental Relationships Between Microstructures and Mechanical Properties of Metal Matrix Composites*, P. K. Liaw and M. N. Gungor, Eds., The Minerals, Metals and Materials Society, 1990, pp. 669-704.

8. Gabb, T. P. et al., "Isothermal and Nonisothermal Fatigue Behavior of a Metal Matrix Composite," *Journal of Composite Materials*, Vol. 24, June 1990, pp. 667-686.

9. Jeng, S. M. et al., "Damage Mechanisms of SCS-6/Ti-6Al-4V Composite Under Thermal-mechanical Fatigue," *Materials Science and Engineering*, Vol. A156, 1991, pp. 117-124.

10. Jeng, S. M. et al., "Fracture Mechanisms of Fiber-reinforced Titanium Alloy Matrix Composites: Part I: Interfacial Behavior," *Materials Science and Engineering*, Vol. A138, 1991, pp. 155-167.

11. Jeng, S. M. et al., "Fracture Mechanisms of Fiber-reinforced Titanium Alloy Matrix Composites: Part II: Tensile Behavior," *Materials Science and Engineering*, Vol. A138, 1991, pp. 169-180.

12. Jeng, S. M. et al., "Fracture Mechanisms of Fiber-reinforced Titanium Alloy Matrix Composites: Part III: Toughening Behavior," *Materials Science and Engineering*, Vol. A138, 1991, pp. 181-190.

13. Jeng, S. M. et al., "Fracture Mechanisms of Fiber-reinforced Titanium Alloy Matrix Composites: Part IV: Low Cycle Fatigue," *Materials Science and Engineering*, Vol. A148, 1991, pp. 67-77.

14. Johnson, W. S., "Fatigue Testing and Damage Development in Continuous Fiber Reinforced Metal Matrix Composites," *Metal Matrix Composites: Testing, Analysis, and Failure Modes*, W. S. Johnson, Ed., American Society for Testing and Materials, Philadelphia, 1989.

15. Kraabel, D. L., "Investigation of Tension-Compression Fatigue Behavior of a Unidirectional Metal Matrix Composite at Elevated Temperature," MS Thesis, AFIT/GAE/ENY/94D-16, Graduate School of Engineering, Air Force Institute of Technology (AU), Wright-Patterson AFB, OH, December 1993.

16. Lerch, B. A. et al., "Heat Treatment Study of the SiC/Ti-15-3 Composite System," NASA TP-2970, January 1990.

17. Majumdar, B. S. and Newaz, G. M., "Inelastic Deformation of Metal Matrix Composites: Plasticity and Damage Mechanisms," *Philosophical Magazine*, Vol. 66, No. 2, 1992, pp.187-212.

18. Mallick, P. K., *Fiber-reinforced Composites: Materials, Manufacturing, and Design* (Second Edition), Michael Dekker, Inc., New York, 1993.

19. Mall, S. and Portner, B., "Characterization of Fatigue Behavior in Cross-Ply Laminate of SCS-6/Ti-15-3 Metal Matrix Composite at Elevated Temperature," *Journal of Engineering Materials and Technology*, Vol. 114, October 1992, pp. 409-415,

20. Mall, S. and Ermer, P. G., "Thermal Fatigue Behavior of a Unidirectional SCS-6/Ti-15-3 Metal Matrix Composite," *Journal of Composite Materials*, Vol. 25, December 1991, pp. 1668-1686.

21. Nicholas, T. et al., "Frequency and Stress Ratio Effects on Fatigue of Unidirectional SCS-6/Ti-24Al-11Nb Composite at 650°C," *Fatigue 93*, Vol. 2, J. -P. Bailon and J. I. Dickson, Eds., EMAS, 1993, pp. 995-1000.

22. Nimmer, R. et al., "Micromechanical Modeling of Fiber/Matrix Interface Effects in Transversely Loaded SiC/Ti-6-4 Metal Matrix Composites," *Journal of Composites Technology & Research*, Vol. 13, No. 1, Spring 1991, pp. 3-13.

23. Portner, B. D., "Investigation of Fatigue Damage Mechanisms in a Metal Matrix Composite Under Elevated Temperature," MS Thesis, AFIT/GAE/ENY/90D-20, Graduate School of Engineering, Air Force Institute of Technology (AU), Wright-Patterson AFB, OH, December 1993.

24. Robertson, D. D., "A Nonlinear Three-Dimensional Micromechanics Model for Fiber-Reinforced Laminated Composites," Ph.D. Dissertation, AFIT/DS/AA/93-3, Graduate School of Engineering, Air Force Institute of Technology (AU), Wright-Patterson AFB, OH, November 1993.

25. Saff, C. R. et al., "Damage Initiation and Growth in Fiber-Reinforced MMCs," *Journal of Metals*, November 1988, pp. 58-63.

26. Sanders, B. P. and Mall, S., "Longitudinal Fatigue Response of a Metal Matrix Composite Under Strain Controlled Mode at Elevated Temperature," *Journal of Composites Technology & Research*, Vol. 16, No. 4, October 1994, pp. 304-313.

27. Schoutens, J. E. and Tempo, K., *Introduction to Metal Matrix Composite Materials*, MMCIAC Tutorial Series, DoD Metal Matrix Composites Information Analysis Center, June 1982.

28. Sun, C. T. et al., "Mechanical Characterization of SCS-6/Ti-6-4 Metal Matrix Composite," *Journal of Composite Materials*, Vol. 24, October 1990, pp. 1029-1059.

29. Suresh, S. et al., Eds., *Fundamentals of Metal Matrix Composites*, Butterworth-Heinemann, Boston, 1993.

30. Taljera, R., *Fatigue of Composite Materials*, Technomic Publishing Company, Lancaster, PA, 1987.

Vita

Lieutenant Robert N. Pittman [redacted]

He graduated from Chittenango High School, Chittenango, NY in 1988 and entered the United States Air Force Academy that summer. In 1992, Lieutenant Pittman was commissioned as a Second Lieutenant and received a Bachelor of Science in Engineering Sciences. His first tour of duty was at the National Air Intelligence Center, Wright-Patterson AFB, OH, where he served as an Air Launched Missile Engineer. He entered the Graduate School of Engineering of the Air Force Institute of Technology in May 1994.

[redacted]

REPORT DOCUMENTATION PAGE

Form Approved
OMB No. 0704-0188

1. AGENCY USE ONLY *(Leave blank)*	2. REPORT DATE	3. REPORT TYPE AND DATES COVERED
	December 1995	Master's Thesis

4. TITLE AND SUBTITLE
FREQUENCY EFFECTS ON FATIGUE BEHAVIOR OF A UNIDIRECTIONAL METAL MATRIX COMPOSITE AT ELEVATED TEMPERATURE

5. FUNDING NUMBERS

6. AUTHOR(S)

Robert N. Pittman, 1st Lt, USAF

7. PERFORMING ORGANIZATION NAME(S) AND ADDRESS(ES)

Air Force Institute of Technology
2750 P Street
WPAFB, OH 45433-6583

8. PERFORMING ORGANIZATION REPORT NUMBER
AFIT/GAE/ENY/95D-20

9. SPONSORING/MONITORING AGENCY NAME(S) AND ADDRESS(ES)

WL/MLLN
Dr T. Nicholas
2230 Tenth Street, Ste 1
WPAFB, OH 45433-7817

10. SPONSORING/MONITORING AGENCY REPORT NUMBER

11. SUPPLEMENTARY NOTES

12a. DISTRIBUTION/AVAILABILITY STATEMENT

Approved for public release, distribution unlimited

12b. DISTRIBUTION CODE

13. ABSTRACT *(Maximum 200 words)*

The fatigue response and life of a unidirectional SCS-6/Ti-6-4 metal-matrix composite were examined under tension-tension, load-controlled conditions at elevated temperatures and different frequencies. Composite specimens were fatigued at frequencies of 0.01, 0.1, 1 and 10 Hz, and at three stress levels. Plots of cycles to failure versus maximum stress and test frequency showed that fatigue life was more cycle-dependent at higher frequencies and more time-dependent at lower frequencies. Comparisons of tests at 427°C with their counterparts at 370°C and 538°C showed that these frequency effects were magnified as temperature increased: lower frequency tests at 538°C exhibited greater time-dependence than tests at 427°C, which was due to poorer creep and environmental resistance at the higher temperature. Macroscopic analysis of tests conducted at lower stress levels and higher frequencies revealed decreasing laminate stiffness with cycling, typical of matrix-dominated responses, while increasing strain and constant modulus histories during fatigue indicated that tests conducted at higher stress levels and lower frequencies were fiber-dominated. Microscopic observations revealed that the extent of matrix cracking increased at lower stress levels and higher frequencies.

14. SUBJECT TERMS
Metal-matrix composites (MMCs), Frequency Effects, SCS-6/Ti-6-4, Isothermal Fatigue, Fiber Cracks, Matrix Cracks, Creep, Cycle-dependent, Time-dependent

15. NUMBER OF PAGES
145

16. PRICE CODE

17. SECURITY CLASSIFICATION OF REPORT	18. SECURITY CLASSIFICATION OF THIS PAGE	19. SECURITY CLASSIFICATION OF ABSTRACT	20. LIMITATION OF ABSTRACT
Unclassified	Unclassified	Unclassified	UL

GENERAL INSTRUCTIONS FOR COMPLETING SF 298

The Report Documentation Page (RDP) is used in announcing and cataloging reports. It is important that this information be consistent with the rest of the report, particularly the cover and title page. Instructions for filling in each block of the form follow. It is important to ***stay within the lines*** to meet ***optical scanning requirements***.

Block 1. Agency Use Only *(Leave blank)*.

Block 2. Report Date. Full publication date including day, month, and year, if available (e.g. 1 Jan 88). Must cite at least the year.

Block 3. Type of Report and Dates Covered. State whether report is interim, final, etc. If applicable, enter inclusive report dates (e.g. 10 Jun 87 - 30 Jun 88).

Block 4. Title and Subtitle. A title is taken from the part of the report that provides the most meaningful and complete information. When a report is prepared in more than one volume, repeat the primary title, add volume number, and include subtitle for the specific volume. On classified documents enter the title classification in parentheses.

Block 5. Funding Numbers. To include contract and grant numbers; may include program element number(s), project number(s), task number(s), and work unit number(s). Use the following labels:

C	- Contract	**PR**	- Project
G	- Grant	**TA**	- Task
PE	- Program Element	**WU**	- Work Unit Accession No.

Block 6. Author(s). Name(s) of person(s) responsible for writing the report, performing the research, or credited with the content of the report. If editor or compiler, this should follow the name(s).

Block 7. Performing Organization Name(s) and Address(es). Self-explanatory.

Block 8. Performing Organization Report Number. Enter the unique alphanumeric report number(s) assigned by the organization performing the report.

Block 9. Sponsoring/Monitoring Agency Name(s) and Address(es). Self-explanatory.

Block 10. Sponsoring/Monitoring Agency Report Number. *(If known)*

Block 11. Supplementary Notes. Enter information not included elsewhere such as: Prepared in cooperation with...; Trans. of...; To be published in.... When a report is revised, include a statement whether the new report supersedes or supplements the older report.

Block 12a. Distribution/Availability Statement. Denotes public availability or limitations. Cite any availability to the public. Enter additional limitations or special markings in all capitals (e.g. NOFORN, REL, ITAR).

- **DOD** - See DoDD 5230.24, "Distribution Statements on Technical Documents."
- **DOE** - See authorities.
- **NASA** - See Handbook NHB 2200.2.
- **NTIS** - Leave blank.

Block 12b. Distribution Code.

- **DOD** - Leave blank.
- **DOE** - Enter DOE distribution categories from the Standard Distribution for Unclassified Scientific and Technical Reports.
- **NASA** - Leave blank.
- **NTIS** - Leave blank.

Block 13. Abstract. Include a brief *(Maximum 200 words)* factual summary of the most significant information contained in the report.

Block 14. Subject Terms. Keywords or phrases identifying major subjects in the report.

Block 15. Number of Pages. Enter the total number of pages.

Block 16. Price Code. Enter appropriate price code *(NTIS only)*.

Blocks 17. - 19. Security Classifications. Self-explanatory. Enter U.S. Security Classification in accordance with U.S. Security Regulations (i.e., UNCLASSIFIED). If form contains classified information, stamp classification on the top and bottom of the page.

Block 20. Limitation of Abstract. This block must be completed to assign a limitation to the abstract. Enter either UL (unlimited) or SAR (same as report). An entry in this block is necessary if the abstract is to be limited. If blank, the abstract is assumed to be unlimited.